

Synthesis and characterization of hybrid polymers as new functional coating materials

DOCTORAL THESIS

submitted in fulfillment of the requirements
of the degree Doctor rer. nat. of the Department of Chemistry,
Faculty of Sciences, University of Hamburg

by Natalie Wagner

Hamburg, 03.03.2016

The present work was conducted under the supervision of Prof. Dr. Patrick Théato
from September 2011 to September 2015
at the Institute for Technical and Macromolecular Chemistry of the University of Hamburg.

1. Adviser:	Prof. Dr. Patrick Théato
2. First Assessor:	Prof. Dr. Patrick Théato
3. Second Assessor:	Prof. Dr. Wolfgang Maison
Date of Defense:	06.05.2016

I. List of Publications

Installation of Zwitterionic α -Amino Phosphoric Acid Moieties on Surfaces via a Kabachnik-Fields Post-Polymerization Modification, N. Wagner, L. Schneider, M. Michelswirth, K. Küpper, P. Theato, *Macromolecular Chemistry and Physics* **216**, 783-793 (2015)

Impact Factor of 2.62 (2015)

Investigation of Antifouling Properties of Surfaces Featuring Zwitterionic α -Aminophosphonic Acid Moieties, N. Wagner, P. Zimmermann, P. Heisig, F. Klitsche, W. Maison, P. Theato *Macromolecular Bioscience* **15**, 1673-1678 (2015)

Impact Factor of 3.85 (2015)

Reactive Coatings in Glass Capillaries: Preparation of Temperature- and Light-Responsive Surfaces and Accurate Determination of Wettability Switching,

N. Wagner, D. Kessler, P. Theato, *Macromolecular Chemistry and Physics* Early view (2015)

Impact Factor of 2.62 (2015)

Review Article

Light-induced wettability changes on polymer surfaces, N. Wagner, P. Theato, *Polymer* **55**, 3436-3453 (2014)

Impact Factor of 3.56 (2014)

II. Table of contents

1	Summary.....	1
2	Zusammenfassung.....	2
3	Introduction.....	4
4	Polymeric Materials.....	5
4.1	<i>Free radical polymerization.....</i>	5
4.2	<i>Controlled radical polymerization.....</i>	6
4.2.1	<i>Atom Transfer Radical Polymerization (ATRP).....</i>	6
4.2.2	<i>Reversible Addition Fragmentation Chain Transfer Polymerization (RAFT).....</i>	7
5	Hybrid materials.....	10
5.1	<i>Stimuli-responsive hybrid polymers.....</i>	14
	Thin film characterization.....	19
6.1	<i>X-ray photoelectron spectroscopy (XPS).....</i>	19
6.2	<i>Atomic Force Microscopy (AFM).....</i>	20
6.3	<i>ATR-FTIR spectroscopy.....</i>	22
6.4	<i>Contact angle measurements.....</i>	23
6.5	<i>Surface free energy measurements.....</i>	25
6.6	<i>Calculation of the equilibrium contact angle from the meniscus height.....</i>	26
7	Aim of work.....	27
8	Publications.....	28
9	Results und discussion.....	55
9.1	<i>Synthesis of Inorganic-Organic Hybrid Polymers.....</i>	56
9.1.2	<i>Hybrid Polymer Synthesis Using RAFT.....</i>	57
9.2	<i>General Coating Properties.....</i>	61
9.2.1	<i>Temperature- and Light-Responsive Capillaries.....</i>	63
9.2.2	<i>Zwitterionic α-Aminophosphonic Acid Moieties on Surfaces.....</i>	66
9.2.3	<i>Investigation on Antifouling Properties of Zwitterionic α-Aminophosphonic Acid Moieties on Surfaces.....</i>	66
10	References.....	68
	Appendix	
	Chemicals	
	Acknowledgements	

III. List of Abbreviation

A	ampere
a.u.	arbitrary units
AFM	atomic force microscopy
AIBN	azobisisobutyronitrile
ATR	attenuated total reflectance
ATRP	atom transfer radical polymerization
BPO	benzoyl peroxide
br	broad peak in NMR spectrum
CA	contact angle
CDCl ₃	chloroform, deuterized
CFU	colony forming units
CTA	chain transfer agent
δ	chemical shift (NMR spectroscopy)
d	duplet (splitting in NMR spectroscopy)
DMF	dimethylformamide
EDX	energy dispersive X-ray
eV	electron volt
FTIR	Fourier transform infrared spectroscopy
GPC	gel permeation chromatography
h	hours
Hz	Hertz
KFR	Kabachnik-Fields-reaction
LCST	lower critical solution temperature
m	multiplet (splitting in NMR spectroscopy)
MA	methacrylate
MCRs	multi-component reactions
MMA	methylmethacrylate
M_n	molecular weight (number average)
MTMS	methyltrimethoxysilane
M_w	molecular weight (weight average)

n	refractive index
NBD	7-nitro-2,1,3-benzoxadiazole
NIPAM	<i>N</i> -isopropylacrylamide
NMP	nitroxide mediated polymerization
NMR	nuclear magnetic resonance
OD	optical density
O_{1s}	energy level
P_{2p} , $P_{2p3/2,1/2}$	energy level
<i>PDI</i>	polydispersity index (M_w/M_n)
PDMA	poly(decylmethacrylate)
PDMS	poly(dimethylsiloxane)
PEG	poly(ethylene glycol)
PEHA	poly(ethylhexylacrylate)
PPFPA	poly(pentafluorophenylacrylate)
PPFPVB	poly(pentafluorophenyl vinylbenzoate)
PMA	poly(methylacrylate)
PMMA	poly(methylmethacrylate)
PMSSQ	poly(methylsilsesquioxane)
PNIPAM	poly(<i>N</i> -isopropylacrylamide)
ppm	parts per million (NMR spectroscopy)
PPSSQ	poly(phenylsilsesquioxane)
PSSQ	poly(silsesquioxane)
q	quartet (splitting in NMR spectroscopy)
θ_a	advancing contact angle
θ_r	receding contact angle
RAFT	reversible addition fragmentation chain transfer
rpm	rounds per minute
RT	room temperature
s	singlet (splitting in NMR spectroscopy)
t	triplet (splitting in NMR spectroscopy)
TEOS	tetraethyl-orthosilicate
TGA	thermogravimetric analysis

THF	tetrahydrofuran
TMOS	tetramethyl-orthosilicate
UV/Vis	ultraviolet/visible light
V	volt
wt%	weight percent
XPS	X-ray photoelectron spectroscopy

1 Summary

In the present thesis, the synthesis of hybrid polymers based on the efficient modification chemistry of poly(methylsilsesquioxanes)-poly(pentafluorophenylacrylate) is described, yielding various substrate surfaces with different properties, such as anti-fouling and thermo- or light-responsive behavior. For this purpose, the new hybrid polymers poly(methylsilsesquioxane)-poly(4-vinyl benzaldehyde) (PMSSQ-PStCHO) and light- and temperature-responsive polymers were synthesized.

First, it was demonstrated an effective two-step approach to integrate zwitterionic α -aminophosphonic acids onto substrate surfaces, which were shown to provide antifouling effects.

Thereafter, silicon surfaces were functionalized with poly(methylsilsesquioxane)-poly(4-vinyl benzaldehyde) in THF. Subsequently, α -aminophosphonates were introduced on surfaces via Kabachnik–Fields post-polymerization modification (*sur*-KFR), by employing various combinations of amines and dialkyl phosphonates. The successful Kabachnik-Fields reaction of aldehyde functionalized surfaces with amines and dialkyl phosphonates was proven by precise analysis of the obtained surfaces, which included infrared, energy-dispersive X-ray and X-ray photoelectron spectroscopy measurements, confirming a practically quantitative conversion of aldehydes without any detectable structural defects. After subsequent deprotection reaction of dialkyl phosphonates, the obtained zwitterionic surfaces were characterized by various techniques, such as infrared spectroscopy, contact angle measurements and surface energy measurements. Additionally, bacterial cell adhesion assays and blood adsorption assays were conducted to prove antifouling properties of the resulting films. It was found that the obtained zwitterionic-functionalized polymer substrates exhibited a low protein adsorption in PBS buffer and showed reduced adhesion properties against *S. epidermidis* cells.

Then, different methods to generate of temperature- and light-responsive coatings on the surfaces were investigated. Therefore, new thermo- and light-responsive copolymers were synthesized, that are derived from alkylamines, yielding a thermo-responsive behavior with an amino-spiropyran as the corresponding photochromic group. To prepare the temperature- and light responsive coatings, two complementary approaches were explored. In the first approach, the reactive hybrid polymer is modified prior to deposition on a surface. Alternatively, a reactive hybrid polymer coating is deposited on a surface and

subsequently functionalized via a post-modification route yielding the respective responsive surfaces.

In the present thesis, the synthesis of hybrid polymers is described based on the efficient modification chemistry of poly(methylsilsesquioxanes)-poly(pentafluorophenylacrylate) yielding various substrate surfaces that exhibit a thermo- or light-responsive behavior. Furthermore, the reversible isomerization of spiropyran moieties in the copolymers, which was induced by irradiation with UV light, had an influence on the water wettability behavior. First, different temperature-responsive coatings were prepared by surface-modification reactions inside the capillary and the accessible temperature-controlled switching range of the contact angles was directly measured using water with different temperatures. The obtained values are comparable to the results obtained by the sessile drop method but the error range is much smaller, which allows a more accurate determination of the equilibrium contact angles. This convenient method of reactive coatings inside glass capillaries may find further application in searching for other poly(acrylamide)-based stimuli-responsive coatings which may not be limited to temperature or light as a stimulus.

The results of this work show the versatility and the high potential of inorganic-organic hybrid polymers which are suitable for the preparation of various applications in different areas of life, such as medicine, microbiology, microelectronics and many others.

2 Zusammenfassung

In dieser wissenschaftlichen Arbeit wurde die Synthese neuartiger Hybridpolymere basierend auf PMSSQ-PPFPA-Chemie beschrieben, die zur Herstellung von Antifouling-Oberflächen sowie licht- und temperaturschaltbaren Oberflächenbeschichtungen verwendet werden können. Dafür wurden neue Hybridpolymere, wie zum Beispiel Poly(methylsilsesquioxane)-poly(4-vinyl benzaldehyde) (PMSSQ-PStCHO) und Temperatur- und lichtsichtbare hergestellt.

Zunächst, wird eine Zwei-Schritt-Methode zur Einführung von zwitterionischen α -Aminophosphonsäuren an den Substratoberflächen vorgestellt, die einen Antifouling-Effekt aufweisen.

Des Weiteren wurden die Siliziumwafer mit Hybridpolymer-Lösung in THF funktionalisiert und die α -Aminophosphonat-Gruppen mit Hilfe der *sur*-KFR unter Verwendung

verschiedener Amine und Dialkylphosphonate. Die erhaltenen Aldehyd-funktionalisierten Siliziumwafer wurden mit Hilfe von Infrarotspektrometrie, energiedispersiver Röntgenspektroskopie und Photoelektronenspektroskopie charakterisiert. Die Untersuchungen zeigen eine quantitative Umwandlung der Aldehyd-Gruppen ohne nachweisbare Strukturfehler.

Abschließend wurde die Entschützung der Dialkylphosphonate durchgeführt und die resultierenden zwitterionischen Oberflächen wurden mittels Infrarotspektroskopie, Kontaktwinkelmessungen und Oberflächenenergiemessungen untersucht.

Zusätzlich wurden bakterielle Zelladhäsion-Tests und Blutadsorption-Assays durchgeführt, um die Antifouling-Eigenschaften der resultierenden Beschichtungen zu testen. Die Zwitterion-funktionalisierten Oberflächen weisen nach dem Waschen mit PBS-Puffer eine sehr niedrige Abscheidung der Biomaterie sowie reduzierte Hafteigenschaften gegen *S. epidermidis*-Zellen auf.

Ferner wurden verschiedene Verfahren zur Erzeugung von temperatur- und lichtschtbaren Oberflächenbeschichtungen untersucht. Hierzu wurde ein neues thermo- und lichtschtbares Copolymer synthetisiert, in welchem die thermische Schaltbarkeit auf einem Alkylamin sowie auf der photochromen Gruppe des Spiropyran funktionalisierten Amins basiert. Es existieren zwei komplementäre Ansätze zur Herstellung der temperatur- und lichtschtbaren Beschichtungen. Bei dem ersten Ansatz kann das reaktive Hybridpolymer vor der Abscheidung auf der Oberfläche modifiziert werden. Alternativ wird eine Hybrid-reaktive Polymerbeschichtung an der Oberfläche abgeschieden und anschließend einer Modifikationsreaktion unterzogen, wobei entsprechend funktionalisierte Oberflächen entstehen.

In der vorliegenden Arbeit wird die Synthese von Hybridpolymeren basierend auf der Modifikation der reaktiven Ester-Gruppen des poly(methylsilsesquioxanes)-poly(pentafluorophenylacrylats), was zu Oberflächenbeschichtungen mit thermisch- und lichtschtbaren Eigenschaften führt, beschrieben.

Darüber hinaus konnten die Wasserbenetzbarkeits-Eigenschaften der resultierenden Filme durch die reversible Isomerisation von Spiropyran-Einheiten des Copolymers bei UV-Licht-Einstrahlung beeinflusst werden.

Zuerst wurden temperaturschtbare Beschichtungen mit Hilfe der Oberflächenmodifizierung der Innenwand der Glaskapillare durchgeführt. Danach wurde der

Wasserkontaktwinkel bei verschiedenen Temperaturen gemessen, um den möglichen temperaturkontrollierten Schaltbereich zu untersuchen. Die erhaltenen Kontaktwinkelwerte stimmen mit den Ergebnissen der Kontaktwinkelmessungen am statischen Tropfen überein. Allerdings ist der Fehlerbereich viel kleiner, was eine genauere Bestimmung des Gleichgewichts-Kontaktwinkels ermöglicht. Ferner kann diese Methode der Beschichtung von Innenwänden der Glaskapillaren bei der Untersuchung anderer Poly(acrylamid)-basierenden, stimuliresponsiven Beschichtungen verwendet werden, die nicht nur durch Temperatur bzw. Lichteinstrahlung angeregt werden können.

Die Ergebnisse dieser Arbeit zeigen die Vielseitigkeit und das große Potential der anorganisch-organischen Hybridpolymere, die für viele verschiedene Anwendungen in unterschiedlichen Bereichen unseres Lebens geeignet sind, z. B. in der Medizin, der Marine, der Mikroelektronik und in vielen anderen Bereichen.

3 Introduction

In the past years, the defined functionalization of micrometer surfaces has gained increasing interest, both in the microelectronic and in the automotive industry as well as in the building sector. Many different approaches of surface coatings have been tested and investigated. Particularly interesting are reactive polymer coatings which are applied from the solution and allow the tailoring of surfaces with versatile properties.

Recently, synthetic stimuli-responsive polymer films have gained great interest for the monitoring of reversible and nonreversible wetting properties. The use of different chemical and physical stimuli such as solvent, temperature or mechanical strength and the use of environmentally friendly chemicals can lead to a change in wettability behavior. Generally, external stimuli, such as solvents, light irradiation, temperature, pH value and electrical potential, can change the surface properties followed by a change in surface behavior.^{1,2,3,4,5,6}

4 Polymeric Materials

Functional polymers have gained enormous importance in recent years in many different areas such as the fabrication of electronic devices, medical and biomedical products, marine equipment and in nanoscience because of their versatile and unique properties.

Different polymeric materials with different architectures or functionalities usually require different polymerization techniques such as step-growth polymerization (polyaddition and polycondensation reactions) or chain-growth polymerization (radical polymerization, anionic or cationic polymerization). The most important polymerization techniques for the generation of functional surface coatings are free radical and controlled radical polymerization.

The free radical polymerization is the most commonly used technique to produce synthetic polymers due to the radical initiation of the polymerization reaction of many different monomers which occurs despite inert reaction conditions and impurities.

The controlled radical polymerization has the ability, besides controlling the molecular weight and obtaining a narrow molecular weight distribution, to build up polymers with specific architectures. Moreover, it shows tolerance towards a broad range of functional groups, for example, reactive esters, such as pentafluorophenyl esters. Furthermore, the controlled radical polymerization combined with a post-polymerization modification step allows the preparation of reactive surface coatings which exhibit high stability and reactivity. Usually, the coated substrate with reactive groups on the surface will be modified by dipping into a solution containing the desired functionalized molecule.

These two types of radical polymerization approaches will be explained below.^{1,7}

4.1 Free radical polymerization

Free radical polymerization starts by the reaction of an initiator (Figure 1) and a vinylic compound followed by propagation and termination reactions (Scheme 1).⁷

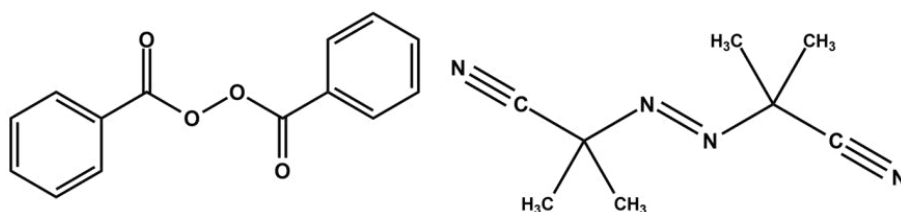
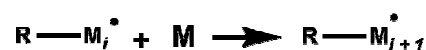
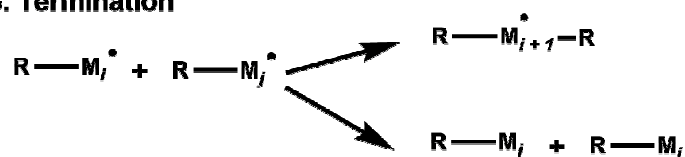


Figure 1 Initiators BPO and AIBN.⁷

1. Initiator**2. Propagation****3. Termination**

Scheme 1 Mechanism of free radical polymerization, where I = Initiator, R = radical, M = monomer.⁷

4.2 Controlled radical polymerization

In earlier times, the production of polymers with similar molecular weight was only possible by anionic and cationic polymerization. This changed with the invention of the controlled radical polymerization techniques. The biggest advantage of controlled radical polymerization is the possibility to predetermine the molecular weight of obtained polymers by the ratio of monomer to chain transfer agent and subsequent conversion. Due to their very narrow polydispersity, the obtained polymers can be used for chain extension polymerization which leads to block copolymers.^{1,2,3,4,5}

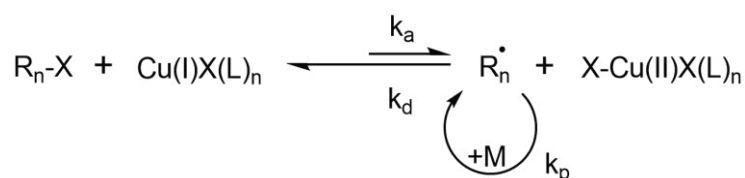
The most important techniques of controlled radical polymerization are the nitroxide-mediated polymerization (NMP), the atom transfer radical polymerization (ATRP) and the reversible addition-fragmentation chain transfer (RAFT) polymerization. ATRP and RAFT polymerizations are extremely versatile control polymerization reaction methods.^{6,7,8}

4.2.1 Atom Transfer Radical Polymerization (ATRP)

The Atom Transfer Radical Polymerization is the metal catalyzed polymerization reaction, which is initiated by the alkyl halides R-X and the metal complexes $Mt^nX_nL_m$, where X = halide, L = ligand. As catalysts, different transition-metal-salts can be used, for example, copper (I) salts, ruthenium, iron, cobalt and rhodium salts.^{9,10,11,12}

The polymerization reaction which is started by the addition of monomer by the radical R^\bullet occurs until it undergoes the reversible halogen transfer reaction, which in turn leads again

The polymerization reaction which is started by the addition of monomer by the radical R^\bullet occurs until it undergoes the reversible halogen transfer reaction, which in turn leads again to the corresponding polymer chain with a halogenic end group (RM_nX) and $Mt^nX_nL_m$. This reversible activation reaction of the growing chain end results in a low concentration of free radicals which helps to reduce the rate of termination during the polymerization reaction.¹³ After reversible halid atom transfer reaction and so-called “one-electron-oxidation-process”, a radical R^\bullet and the corresponding higher oxidation state metal complex with the coordinated halide anion $Mt^{n+1}X_{n+1}L_m$ will be formed. The radical R^\bullet is, on the one hand, in an equilibrium with $R-X$, but on the other hand, it can react with the monomer M , with other monomers or with $Mt^{n+1}X_{n+1}L_m$ (Scheme 2).



Scheme 2 Mechanism of copper-catalyzed ATRP.

In summary, the ATRP polymerization technique allows the creation of defined architectures such as polymer brushes and block-copolymers, enabling a good control of the molecular weight and narrow molecular weight distributions.^{13,14,15}

4.2.2 Reversible Addition Fragmentation Chain Transfer Polymerization (RAFT)

The reversible addition fragmentation chain transfer polymerization is one of the most effective methods to perform a controlled radical polymerization.^{7,8,16} RAFT is started by common radical initiators, like AIBN or BPO. RAFT is conducted in the presence of a chain transfer agent (CTA), such as dithioesters, trithiocarbonates, dithiocarbamates or xanthogenates, whose addition to the growing chain leads to a radical intermediate. Thiocarbonyl thioester derivatives are most commonly used as CTA reagent (Figure 2).^{17,18,19} The formation of stable thiocarbonyl thio radical intermediates is strongly influenced by the Z group, which provides both the stabilization and the proper fragmentation of R. Strong stabilizing groups activate the C=S bond, thus enhancing the radical addition that leads to the formation of the radical intermediate. At the same time, R should be a better leaving

group than the propagating chain P_n and a good re-initiation group towards the monomer.^{20,21}

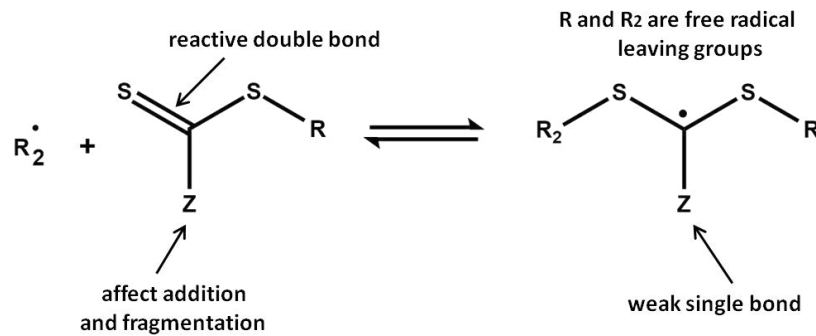
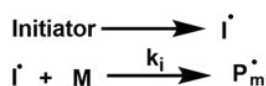


Figure 2 Molecular structure of chain transfer agents and the corresponding radical intermediate.²²

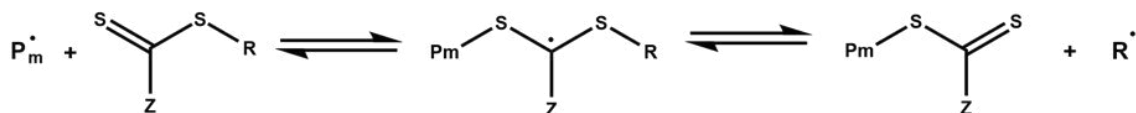
Schema 3 shows the general mechanism of the reversible addition fragmentation chain transfer polymerization. Firstly, the CTA radical intermediate is formed by addition of the propagating chain (P_n) to the CTA. Secondly, the formed CTA radical intermediate releases the remaining R. Subsequently, R reversibly transfers the polymerization to another chain (P_m) reversibly.

To sum it up, the “living”-character of this type of polymerization technique is assured by the continuous addition-fragmentation equilibrium.^{23,24}

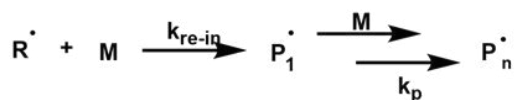
1. Initiator



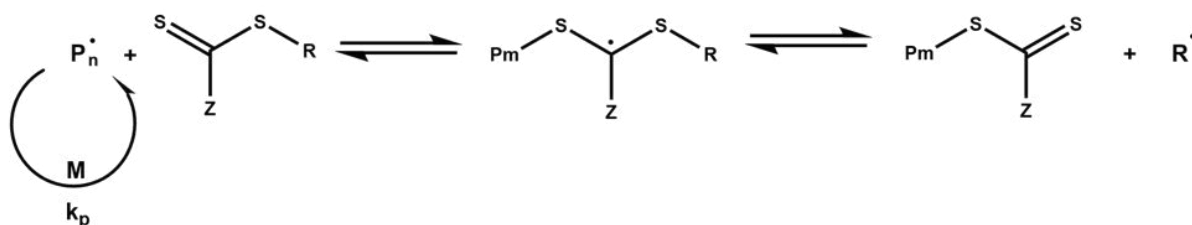
2. Initial equilibrium



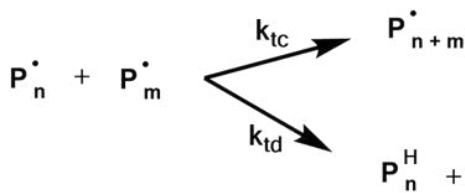
3. Reinitiation



4. Main equilibrium



5. Termination



Scheme 3 Mechanism of the RAFT-polymerization. ^{11,19,21}

In summary, both ATRP and RAFT polymerization techniques allow a good control of the molecular weight by conversion and narrow molecular weight distributions. However, RAFT polymerization is more preferable due to a wide monomer applicability and absence of transition metal element like copper (I), which requires additional purification steps to remove the toxic metal.^{21,23}

5 Hybrid materials

Hybrid materials include inorganic and organic species which have been known since the Maya epoch for example, Maya blue, which was a hybrid of indigo and clay. Such materials combine the unique features of ceramics and organic materials, such as hardness, thermal stability, bioactivity or elasticity, hydrophobicity and chemical activity. This makes hybrid materials suitable not only for biomedical applications, such as fully biocompatible implants, but also for many different application fields, such as electronics, mechanics, sensors etc.²⁵

Depending on the composition and structure of organic and inorganic components hybrid polymers can be categorized into matrix and building blocks. But the most frequently used classification is based on the interaction between inorganic and organic components. Within this category, hybrid materials can be divided into two groups, on the one hand, systems with non-covalent bonds, such as van-der-Waals or hydrogen interaction, and on the other hand, strong chemical bonds between inorganic and organic components, for example covalent or Lewis acid-based bonds (Figure 3).²⁶

Not only the bonding characteristics, but also the structural properties can be used to differentiate between the various hybrid materials. For example, phenyltrialkoxysilanes are organic compounds which contain a functional group that allowing an attachment to the inorganic network via the trialkoxysilane group. Thereby, the organosilica network is modified with functional groups which are not undergoing further chemical reactions with the material formed. In case of a hybrid network with integrated inorganic part, the organic moieties are modified with many anchor groups. If a reactive functional group is incorporated into the system, it is called a network functionalizer. Figure 4 summarizes the described systems.

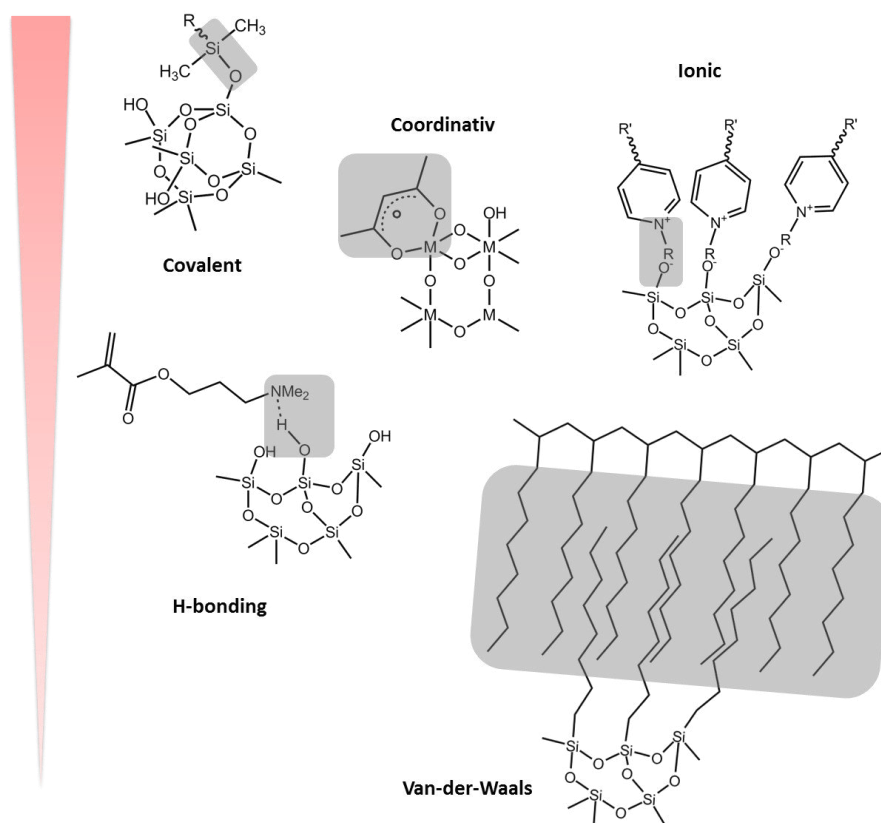


Figure 3 Selected interactions typically applied in hybrid materials and their relative strength.²⁵

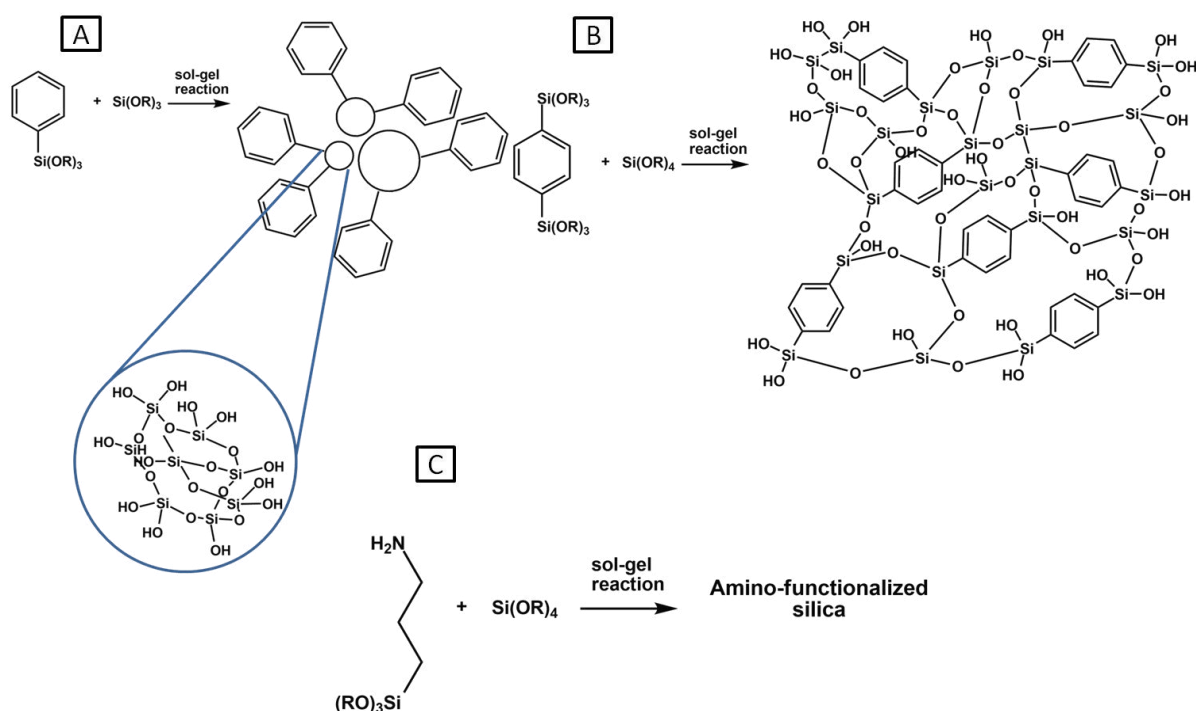


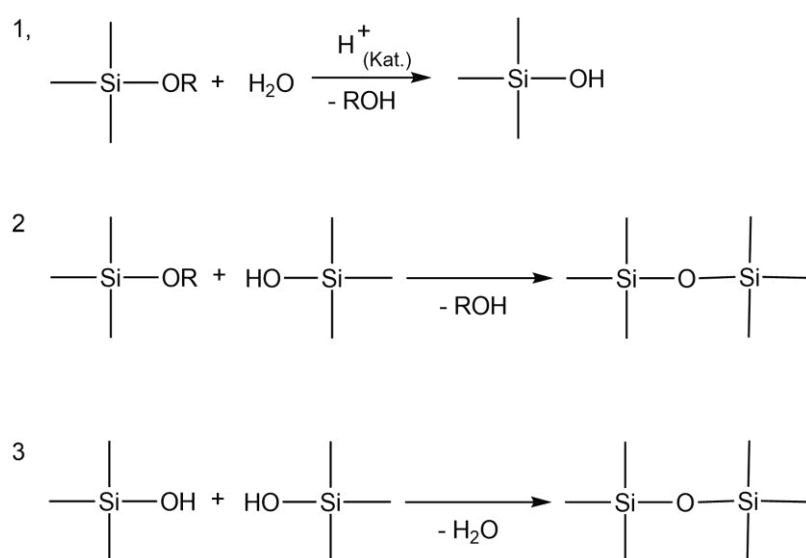
Figure 4 Role of organically functionalized trialkoxysilanes in the silicon-based sol-gel process: A). network modifier, B). network builder, C). network functionalizer.²⁵

In nature, a large number of natural materials, like bones, nacre, pigments etc., consist of inorganic-organic blocks. Their unique and favorable combination of properties within one material inspired scientists to create new chemical pathways of hybrid polymers. In this manner, the sol-gel process was developed which has revolutionized the synthesis of inorganic-organic polymers. A sol-gel process is based on the formation of sol during the mixing of alkoxide precursors, such as tetramethyl-orthosilicate (TMOS) or tetraethyl-orthosilicate (TEOS), with water. The basic sol-gel reaction starts with the hydrolysis reaction of metal alkoxide (RO-Si) followed by a condensation reaction of alcohol and a condensation reaction of water (Scheme 4).²⁶

The properties of the resulting products, for example, the degree of crosslinking, the surface morphology and the porosity, can be affected by the ratio of precursor to solvents, the amount of water and the reaction conditions, such as temperature and pressure as well as the conditions during drying and curing.²⁶

Silicon compounds with a general structure such as $(\text{H}_3\text{CO})_3\text{Si-X}$, are able to condensate with hydroxyl groups which are located on the substrate surface, followed by the cross-linking in the presence of atmospheric moisture. Trialkoxysilanes are adhesion promoters due to the

reaction of hydroxyl groups on different surfaces which can be used to generate a covalent bond interface between the organic coating and metals, glass, silicon or plastic substrates. Sol-gel materials enable the creation of highly adherent, chemically inert coatings on various substrate surfaces that can be prepared from a variety of different commercially available alkoxy precursors. In particular, poly(silsesquioxanes) (PSSQ) are good candidates for the preparation of defined inorganic-organic hybrid coating materials. Generally, PSSQs have a composition of $\text{RSiO}_{3/2}$ with R=aryl, alkyl, hydrogel etc. and allow to form three-dimensional networks due to their three possible access points for further silanol condensation.^{27,28,29}



Scheme 4 Basic reactions of the sol-gel process: 1. hydrolysis of tetra-alkoxysilanes, 2. Condensation reaction of partially hydrolyzed mixtures, 3. Condensation of fully hydrolyzed mixtures.²⁶

Soluble PSSQ materials which are normally used for the preparation of different coating applications are, for example, poly(methylsilsesquioxanes) (PMSSQ) or poly(phenylsilsesquioxanes) (PPSSQ).

The most frequently used PSSQ gels in coating applications are either poly(methylsilsesquioxanes) (PMSSQ), poly(alkylsilsesquioxanes) or poly(phenylsilsesquioxanes) (PPSSQ). These hybrid materials are organic molecules with several silanes can be adjusted for the preparation of various applications, such as in electronics, biomedicine or optics.^{30,31}

5.1 Stimuli-responsive hybrid polymers

The changing of surface wettability can be induced by external stimuli, such as light illumination, solvents, electrical potential, temperature, pH or ion-pair receptors followed by a change in surface behavior.^{1,32,33,34,35,36,37}

Moreover, stimuli-responsive hybrid polymers enable the preparation of superhydrophobic surfaces on the one hand, i. e., very rough surfaces with an advancing water contact angle of very rough surfaces that of at least 150°. On the other hand, so-called superwetting or superhydrophilic surfaces with an apparent contact angle of less than 5° can be obtained.³⁷ For example, a reversible switching from a superhydrophobic to a superhydrophilic surface can also be achieved by electrochemical oxidation-reduction reactions of polyaniline films on a conducting substrate (Figure 5 A). In addition, electroactive self-assembled monolayers on different substrates are able to form a multichannel surface switch by electrical tuning between two redox states which makes such systems interesting for the production of microfluidics and biosensors.^{38,39,40,41,42}

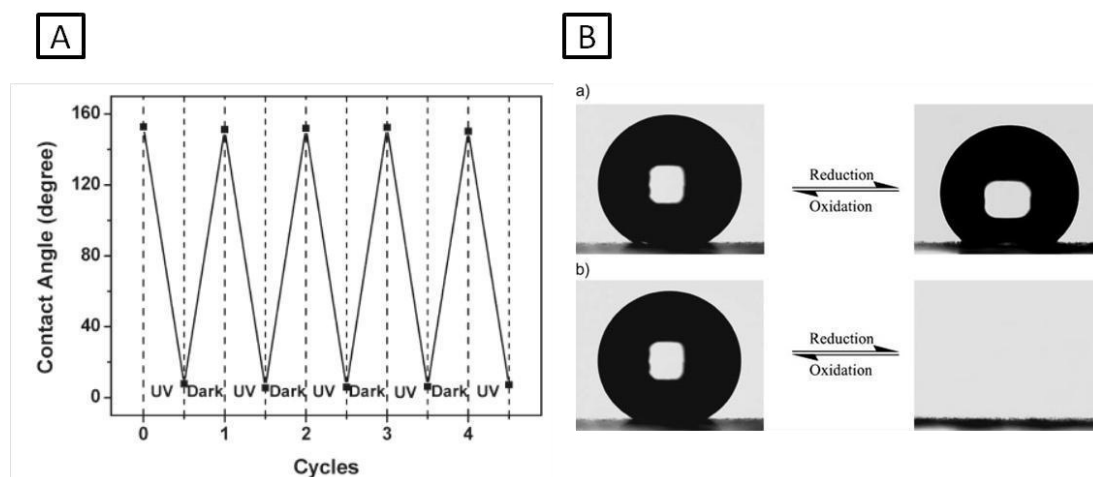


Figure 5 (A) Reversible water contact angle switching of the aligned ZnO nanorod array-coated stainless mesh film under the alternation of UV irradiation and dark storage. (B) Electrical potential-induced wettability conversion between oxidized perfluorooctanesulfonic-doped polyaniline films and reduced polyaniline films.

(a) The switching is conducted in 0.1 M perfluorooctanesulfonic acid solution. (b) The switching is conducted in 0.1 M tetraethylammonium perfluorooctanesulfonate.^{38,43}

Besides organic materials, a large number of inorganic materials are used for stimuli-responsive surfaces. Inorganic oxides, such as ZnO (Figure 5 B), TiO₂ (Figure 6) and SnO₂, are well-known as stable, nontoxic and highly reactive materials which are able to induce large wettability changes.^{3,43,44,45,46,47,48,49}

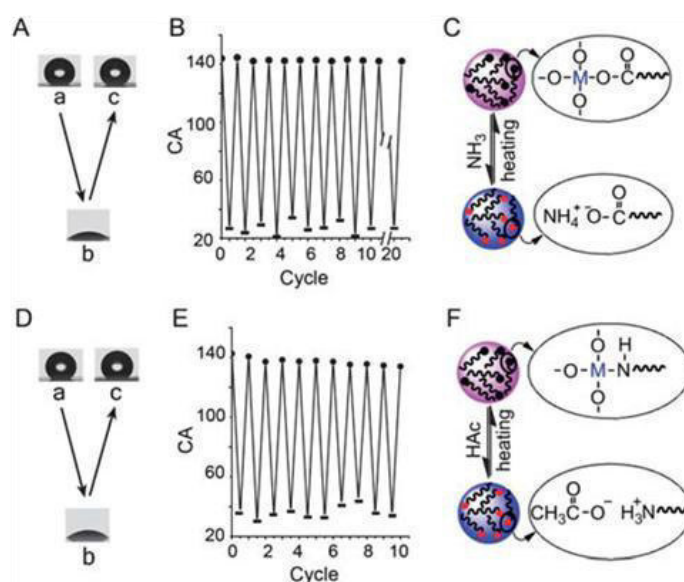


Figure 6 Hydrophobic-hydrophilic switching of titania-carboxyl and titania-amine complex systems.⁴⁹

The group of stimuli-responsive polymers includes biopolymers and synthetic polymers. Stimuli-responsive biopolymers, such as nucleic acids or proteins, occur in nature. In the last decades, thermo-responsive polymers have gained increasing interest for various applications, especially in the field of biomedical applications, such as diagnostics, therapeutics and surgery. The most extensively investigated biocompatible thermo-responsive and water-soluble polymer are poly(*N*-isopropyl acrylamide) (PNIPAm). PNIPAm possesses a lower critical solution temperature (LCST) of 32 °C which is in a physiologically interesting temperature range. This behavior can be explained by reversibly changing between the entropic and the enthalpic contribution to the free energy of thermo-responsive polymers in aqueous solutions.^{49,50} At temperatures below the LCST, the enthalpic effects predominate over the entropic effects, expressed by hydrogen bonds between the polymer chain and water molecules, which leads to the extended solubilized state of the PNIPAm chains. Upon increasing the temperature above 32 °C, the entropic contribution increases, resulting in the breaking of the intermolecular hydrogen-bonds

between the polymer chains and the water molecules. Hence, a collapsed state of the polymer chains can be obtained.

Due to the lower critical solution temperature at 32 °C PNIPAm is able to act a surface-immobilized function which leads to a temperature-responsive wetting behavior (Figure 7). Below the LCST, PNIPAm is soluble in water which results in more hydrophilic surfaces. This change in surface hydrophobicity is accompanied by further property changes, e.g., a collapsed PNIPAm surface above the LCST which promotes protein adsorption and cell adhesion.^{51,52,53,54,55,56,57,58,59,60,61}

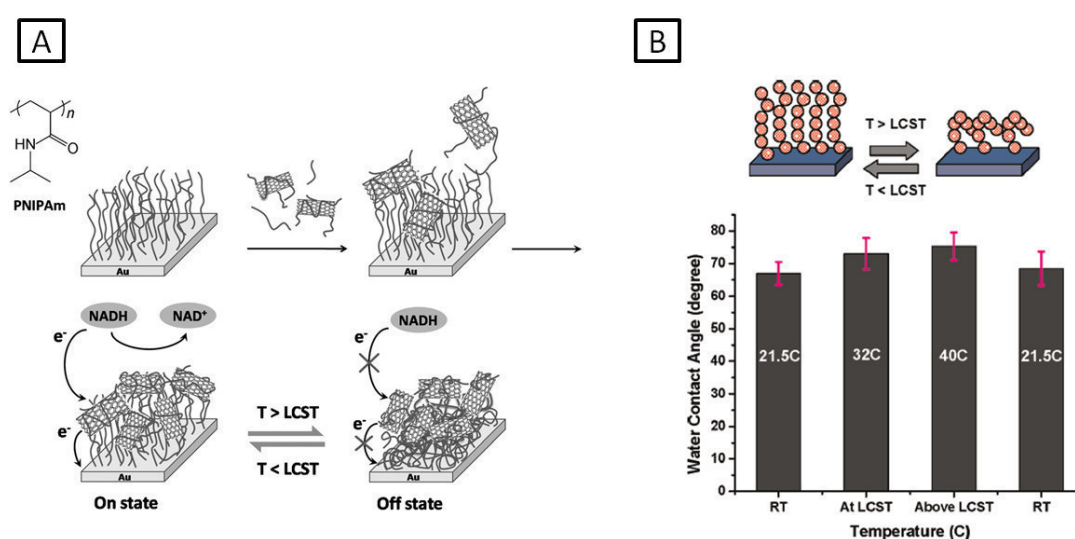
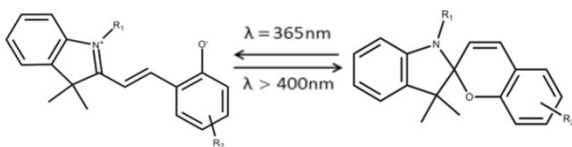
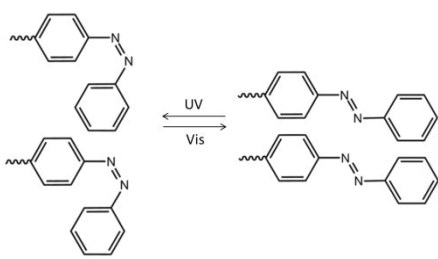
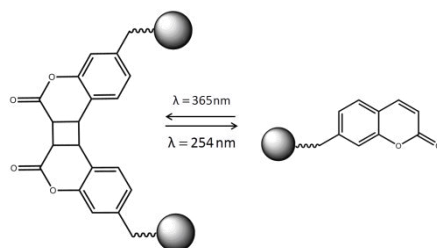


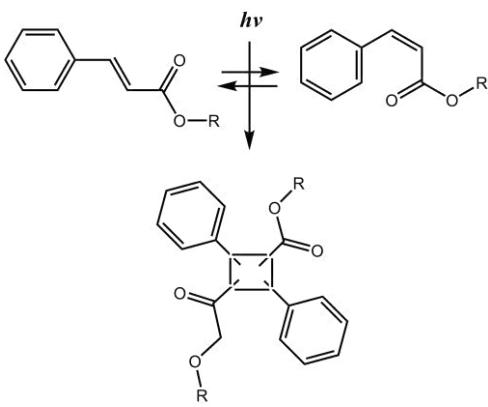
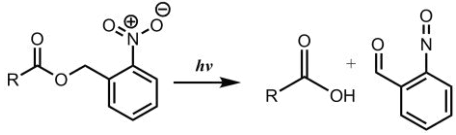
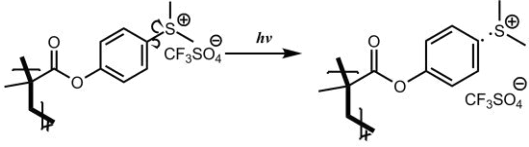
Figure 7 (A) Schematic depiction of the functionalization steps leading to the PNIPAm-grafted multiwalled carbon nanotubes/PNIPAm–Au substrate and the reversible bioelectrocatalysis of 1,4-dihydro-*b*-nicotinamide adenine dinucleotide (NADH) which are controlled by temperature. NAD=nicotinamide adenine dinucleotide. (B) Static water contact angle measurement for the PNIPAm brushes as a function of temperature. The surface changed from hydrophilic to hydrophobic below and above the LCST.^{51,56}

Synthetic light-stimuli responsive polymers are good candidates for a preparation of light-switchable surfaces. As already mentioned above, light- or photo-responsive surface coatings are capable of changing their wetting behavior upon irradiation with light of a defined wavelength. Azobenzene is probably the most well-known candidate used in light-responsive surfaces because it can switch between two isomeric forms, *trans*- and *cis*-azobenzene, upon exposure to UV light resulting in a change of molecular properties such as surface wettability, viscosity, free volume, dipole moment or solubility.^{62,63,64,65,66,67}

Not only a reversible light-responsive behavior but also an irreversible one is known. Such irreversible effects for example, can be obtained in polymers with photocleavable moieties containing photochromic units. The polymers, which contain light-responsive groups, undergo an irreversible transformation upon exposure to UV light resulting in more polar species. One representative of this group is the ortho-nitrobenzyl ester (ONB) that can be used for the preparation of photopatternable polymer thin films.^{67,68,69,70,71,72}

Table 1 Light-switchable chromophores.

Light-switchable chromophores	
Reversible switching	<p>Spiropyran derivative</p> 
	<p>Azobenzene derivatives</p> 
	<p>CMFST nanoparticles</p> 

Reversible/Irreversible switching	<p>Cinnamates derivatives</p>  <p>The scheme illustrates the photochemical behavior of cinnamate derivatives. At the top, a reversible photoisomerization is shown between the <i>trans</i>-cinnamate ester and the <i>cis</i>-cinnamate ester, with the equilibrium controlled by light ($h\nu$). Below this, an irreversible photocycloaddition reaction is depicted, where the <i>cis</i>-isomer reacts with another molecule to form a [2+2] photodimer, a cyclobutane ring fused to two benzene rings, with ester groups attached to the cyclobutane carbons.</p>
Irreversible switching	<p><i>o</i>-nitro-benzyl derivatives</p>  <p>The reaction shows the irreversible photolysis of an <i>o</i>-nitro-benzyl ester. Upon irradiation with light ($h\nu$), the molecule undergoes a Norrish Type II-like cleavage, yielding a carboxylic acid ($R-COOH$) and an <i>o</i>-nitrobenzaldehyde derivative.</p>
	<p>Sulfonium triflate based PAG</p>  <p>The reaction shows the irreversible photolysis of a sulfonium triflate-based photoinitiator (PAG). The molecule consists of a polymer chain attached to a benzene ring, which is linked to a sulfonium group (S^+Me_2) and a triflate counterion ($CF_3SO_3^-$). Upon irradiation with light ($h\nu$), the sulfonium group is cleaved, generating a polymer-bound sulfonium cation (S^+Me_2) and a triflate anion ($CF_3SO_3^-$).</p>

6 Thin film characterization

For analysis of the obtained polymer films, a range of different characterization methods allow both the analysis of the chemical composition the physical properties and morphology. The methods used for investigation of the achieved surface coatings are explained below.

6.1 X-ray photoelectron spectroscopy (XPS)

X-ray photoelectron spectroscopy (XPS) is a surface-sensitive quantitative spectroscopic technique, which allows to examine the chemical compositions and electronic state of the elements on the substrate surface and the physical topography.^{73,74,75}

XPS spectra are obtained by irradiation of the sample with a beam of X-rays under high vacuum or ultra-high vacuum conditions from the top 0 to 10 nm of the material. Thus, the kinetic energy and the number of released electrons are being measured at the same time.

The binding energy of the emitted electron can be determined by the equilibrium of Rutherford:

$$E_{binding} = E_{photon} - E_{kinetic} - \phi \quad (1)$$

where E_{photon} is the energy of the X-ray photons used, $E_{kinetic}$ is the kinetic energy of the emitted electrons and ϕ is the work function of the material.

The energy of the escaped core electrons provides further information about the elemental composition. From the difference in the shifts of the binding energy, additional information can be obtained, for example, on the oxidation state of the element. Additionally, the information about a deep profile of the thin film can be achieved by ion bombardment.⁷⁶

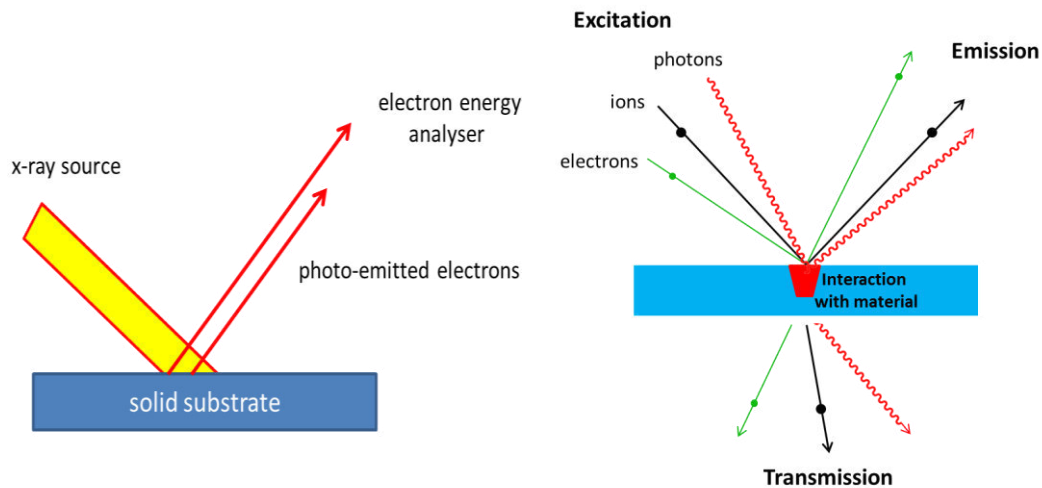


Figure 8 XPS setup and operating principle.

6.2 Atomic Force Microscopy (AFM)

Atomic force microscopy (AFM) is a very important type of scanning probe microscopes (SPM), which allows the investigation of nanoobjects and surfaces at high resolution. This technique has several advantages, for example, it can provide a 3-D surface profile of a sample and it is a non-destructive method, which works without any special treatment such as a high vacuum.

The method is based on the attractive and repulsive forces between a small tip at the end of a cantilever which is scanning across the sample and the substrate surface. In dependence on surface topography, the cantilever undergoes a deflection, which is measured by a laser beam. This is reflected from the top of the cantilever in an array of photodiodes. The sample is placed on a piezoelectric holder, which can be moved in all three space directions (x and y - scanning the sample, z - maintaining a constant force). The scanning process is evaluated in a topographical image of the surface (Figure 9).

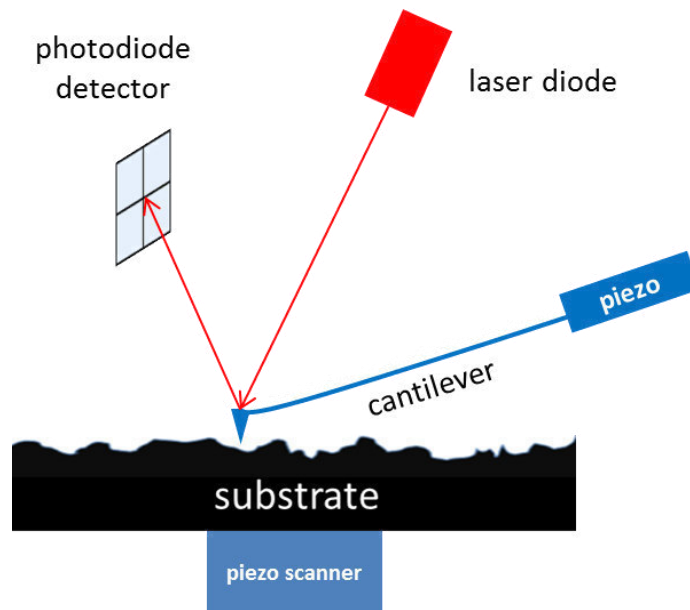


Figure 9 General setup of an atomic force microscope.

The most frequently used operating modes for an AFM are contact mode, non-contact mode and dynamic contact mode. Depending on the nature of the sample and the desired information about the surface tips, different motions can be applied.

In the contact mode, the cantilever deflection is kept constant because the force between the surface and the tip remains constant during the whole scanning time. In the non-contact mode, the tip does not contact the surface of the sample. The cantilever oscillates with the resonance frequency which is influenced by van-der-Waals forces between the tip and the surface. The changes in resonance frequency result in changes in oscillation compared to the external reference oscillation, which allow the scanning software to provide information about the topography of the sample.

The dynamic contact or so-called tapping mode is normally used for soft materials and polymeric samples. In this mode, the cantilever oscillates in a similar way to that of the non-contact mode, resulting in amplitudes of 20 to 200 nm. During scanning, the tip slightly touches the sample surface, with the oscillation amplitude remaining constant by vertical movement of the piezo scanner.⁷⁷

6.3 ATR-FTIR spectroscopy

Attenuated-total-reflection Fourier-transform infrared (ATR-FTIR) spectroscopy is a technique to investigate the chemical composition of liquid or solid samples without further preparation.^{73,78}

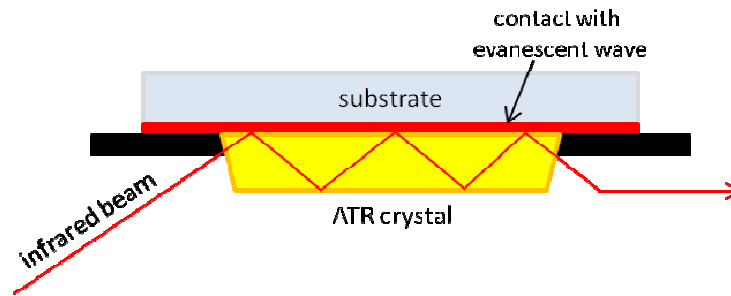


Figure 10 ATR-FTIR setup to measure coating characteristics on the coated substrate.^{73,79}

Infrared spectroscopy is based on the measurement of the absorption of specific frequencies, which are characteristic for the particular structures.

IR wave-like radiation passes through molecules and excites bonds of particular atoms or functional groups to flex and vibrate around their molecular bonds. In the case of a resonance between the oscillation of the molecular bond with the wavelength of the IR-radiation source, absorption can occur. There are many different molecular motions which can lead to molecular oscillation such as stretching and contraction of molecular bonds, or rocking, twisting and wagging of functional groups. Therefore, IR spectroscopy can be used for structural identification in various applications due to the molecular oscillation of the functional group present in a molecule.

The absorption of IR irradiation is related to the concentration of specific bonds and can be described by the Beer-Lambert equation as follows:⁷⁹

$$A = \epsilon c_n l \quad (2)$$

In this equation, c_n is concentration, ϵ is extinction coefficient, l is the path length.

In an ATR technique, the beam penetrates the surface before reflection occurs. This radiation is known as the evanescent wave, the depth of penetration of the evanescent wave can be varied by the choice of crystal. IR radiation is focused on the end of the crystal

and reflects along the length of the crystal. Furthermore, the evanescent wave can be determined by wavelength of radiation, refractive indices and the angle of incidence.⁸⁰

6.4 Contact angle measurements

The contact angle is an angle between three phases: solid, liquid and gas. It describes the wetting behavior of solid surfaces and can be quantified through the Young equation.⁸¹

$$\gamma_L \cdot \cos\theta = \gamma_S - \gamma_{SL} \quad (3)$$

where γ_S , γ_L , γ_{SL} are interfacial tensions of the solid, the liquid, and the vapor phases.

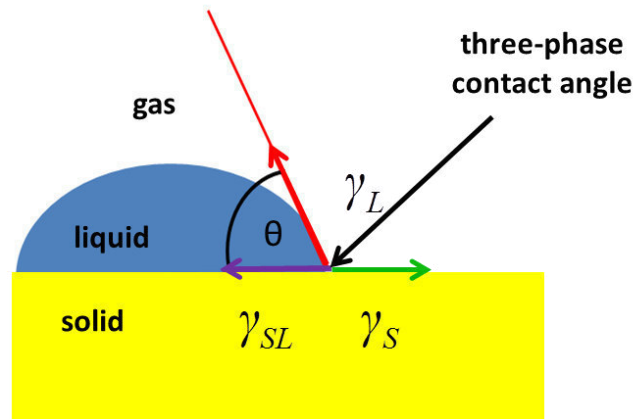


Figure 11 Contact angle of the solid surface and three interface tensions.

A drop of liquid can show different behaviors on solid surfaces, either the liquid spreads completely over the solid or a drop with a material-specific contact angle (CA, θ) is formed. The contact line where the liquid, the solid and the gas phase interact is the three-phase contact line (Figure 11).

In the contact angle measurements, the interfacial tension of the solid surface plays an essential role, therefore it is higher than the interfacial tension of the solid–liquid interface ($\gamma_S > \gamma_{SL}$). In this case, the contact angle is smaller than 90 °, which leads to the partial wetting of the solid surface. The hydrophobic surfaces exhibit an energetically less solid–liquid interface than the bare solid surface ($\gamma_S < \gamma_{SL}$), in such cases, the contact angle is larger than 90 °.

The contact angle and the interface tension are important characteristics of a coatings: Depending on the applications, the contact angles of different liquids can be used for the calculation of the surface energy. In the following, the static contact angle of water on a solid/coated surface under ambient conditions is discussed.^{82,83}

The most commonly used method is the sessile drop method, in which the contact angle of a liquid drop is observed with a microscope. Contact angle of a drop, which appears dark because of the light source placed behind it, can be determined by means of a goniometer or by a video system.

An alternative method is that of the captive bubble, which is based on the measurement of the angle at the edge of a bubble, which is placed under the substrate within the liquid. Another technique is the capillary rise method, which is suitable for liquid contact angle measurements of powders. In this case, the liquid rises inside a thin coated capillary and the contact angle can be calculated from the meniscus height.^{82,83,84}

Real surfaces behave differentl to ideal surfaces and are influenced by different factors, such as surface roughness, chemical heterogeneity and/or changes of the surface structure caused by the wetting line or by adsorbed molecules on the surface. In such cases, the calculation of the contact angle is more difficult, because of hysteresis. Hysteresis is defined as the difference between an advancing (θ_{adv}) and a receding (θ_{rec}) contact angle. The advancing contact angle (θ_{adv}) is the contact angle, which is measured while the volume of the drop increases. The receding contact angle (θ_{rec}) is measured while the volume of the drop decreases, just before the wetting line recedes. Usually the receding contact angle is significantly lower than the advancing contact angle.

In addition to the influence of surface roughness and chemical heterogeneity, the contact angle hysteresis can be influenced by the mean contact angle.

The effect of the surface roughness on those surfaces that are not too rough can be described by the Wenzel equation:⁸⁴

$$\cos\theta_{app} = R_{rough} \cdot \cos\theta \quad (4)$$

In this equation, R_{rough} is surface roughness, which is the ratio between the actual and the projected surface area. θ_{app} is the apparent contact angle, which can be observed with the eye or with an optical microscope. The surface roughness is always larger or equal to one

($R_{rough} \geq 1$), hence the apparent contact angle decreases by the surface roughness for $\theta < 90^\circ$ in hydrophilic surfaces. For hydrophobic surfaces the apparent contact angle ($\theta > 90^\circ$) increases if roughness is present.

The influence of the chemical heterogeneity on the contact angle hysteresis is described by the Cassie and Baxter equation:⁸⁵

$$\cos\theta_{app} = f_1\cos\theta_1 + f_2\cos\theta_2 \quad (5)$$

Therefore, for solid and chemically inhomogeneous surfaces two different kinds of regions exist with contact angles θ_1 and θ_2 , for which occupy the surface ratios f_1 and f_2 apply.⁸⁶

The most prominent example of hydrophobic and rough surfaces is the Lotus effect. In nature, the surface of a leaf can be covered with hydrophobic spikes, which are responsible for the roughness. Furthermore, air is trapped between the spikes making them responsive to chemical heterogeneity. Hence, the lotus effect is suitable for the preparation of super-water-repellent, so-called superhydrophobic surface coatings.⁸⁷

6.5 Surface free energy measurements

Surface free energy measurement (SFE) is one important application of the contact angle measurement. The surface free energy of the solid corresponds to the surface tension of the liquid. The contact angle describes the wetting behavior of the solid surface but it always depends on the liquid that is used for the measurements.

The most frequently used method for SFE calculations is the OWRK method. This method requires the use of at least two liquids, one polar and one dispersive. For this purpose, water and diiodomethane are the most frequently used liquids.

Owens, Wendt, Rabel and Kaelble created one method of SFE measurement by division of the surface free energy into individual components. In this method, SFE is formed by the components of dispersive and polar SFE, where the interfacial energy γ_{SL} is determined by the contribution of water or diiodomethane, and the delaminated surface is calculated by forming the geometric mean. The model leads to the following relationship:

$$\gamma_{sl} = \gamma_s + \gamma_l - 2 \left(\sqrt{\gamma_s^d \cdot \gamma_l^d} + \sqrt{\gamma_s^p \cdot \gamma_l^p} \right) \quad (5)$$

where γ_s^d and γ_s^p are the dispersive and polar parts of the solid, and γ_l^d , γ_l^p are the respective contributions of the liquid.^{73,74}

6.6 Calculation of the equilibrium contact angle from the meniscus height

To calculate the equilibrium contact angle from the meniscus height (x), Equation 6 was used, where the surface tension (γ_{LG}) of water at a certain temperature was calculated using Equation 7 (Eötvös rule).^{88,89} The density of water (δ) at 15 °C is 999.10 kg/m³ and at 60 °C the density is 983.19 kg/m³.

$$\theta_{equi} = \cos^{-1} \left(\frac{g \cdot r \cdot \sigma \cdot x}{2\gamma_{LG}} \right) \quad (6)$$

$$\gamma_{LG} = 0.07275 \frac{N}{m} \cdot (1 - 0.002 \cdot (T/K - 291)) \quad (7)$$

$$\cos \theta_{equi} = (\frac{1}{2} \theta_a + \frac{1}{2} \theta_r) \quad (8)$$

To compare the obtained values with the contact angles obtained by the sessile drop method, similar coatings were produced on flat glass substrates. After determination of the advancing and the receding contact angle (θ_a , θ_r), the equilibrium contact angle was calculated using Equation 8.

7 Aim of work

In my research work, I am investigating different synthetic approaches for highly cross-linked hybrid polymers, which can build stable and adherent coatings on surfaces, independent of the substrate. Furthermore, I am interested in the development of new concepts of surface functionalization based on these hybrid polymers which are suitable for various purposes and applications.

For the preparation of strongly adherent and stable materials which allow the incorporation of different functionalities in the coating material, hybrid polymers based on trifunctional silanes were used.

The hybrid polymers combine the inorganic part consisting of poly(methylsilsequioxane) (PMSSQ) which is capable of adhering to substrate surface and the reactive organic part. Obtained hybrid polymers are applicable directly from the solution by spin- or dip-coating and show unique adhesion properties on different substrates such as silicon, metals or glass due to the large amount of free silanol groups of the inorganic part. The silanol groups are able to form a cross-linked film by secondary condensation, mechanically interlocking and van der Waals adhesion phenomena leading to reactive and stable surface coatings.

Moreover, for the synthesis of inorganic-organic polymer the preformed PMSSQ should contain reactive chain transfer agent (CTA) moieties which allow a controlled radical polymerization reaction (RAFT). The obtained hybrid polymers can be used for many interesting applications, such as antifouling surfaces, temperature- or light-responsive coatings.

In summary, the scope of this work can be divided into two parts: 1. *sir*-KFR and zwitterionic systems, 2. temperature- and light-responsive capillaries.

Different inorganic-organic hybrid polymers could be successfully synthesized and characterized. Moreover, they could be applied to various substrates, resulting in functional and reactive surface coatings.

In the following, the synthetic concept based on the RAFT polymerization technique will be presented. Subsequently, a summary of general coating properties is shown. Afterwards the obtained reactive and functional surface coatings will be demonstrated.

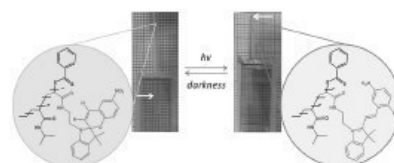
The detailed description of procedures and applied expertises are given in the corresponding publications (Publications I, II, III).

8 Publications

Reactive Coatings in Glass Capillaries: Preparation of Temperature- and Light-Responsive Surfaces and Accurate Determination of Wettability Switching

Natalie Wagner, Daniel Kessler, Patrick Theato*

The inner walls of thin glass capillaries are coated with a reactive precursor coating that can be converted into different temperature- and light-responsive coatings. The switching range of wettability can be determined by measuring the meniscus height of water inside these capillaries at different temperatures and upon UV-light irradiation. In comparison with the sessile drop measurement, very accurate equilibrium contact angles are obtained by this method.



1. Introduction

Water-soluble polymers featuring a temperature-responsive behavior are of great scientific and technological importance. Those polymers undergo a temperature-induced reversible phase transition in aqueous solution. Especially *N*-substituted poly(acrylamides) exhibit such a coil-globule transition at the lower critical solution temperature (LCST).^[1] Below the LCST, the polymers are dissolved as a coil, surrounded by ordered water molecules and stabilized by hydrogen bonding. This hydration shell decreases the entropy of the system. Thus, the free energy is determined by hydrogen bond formation (enthalpy) and an entropy decrease. If the temperature is raised above LCST, the entropy term dominates and the polymer undergoes a coil-globule transition and eventually precipitates out of solution.

N. Wagner, P. Theato
Institute for Technical and Macromolecular Chemistry
University of Hamburg
Bundesstr. 45, D-20146 Hamburg, Germany
E-mail: theato@chemie.uni-hamburg.de
D. Kessler
Institute of Organic Chemistry
Johannes Gutenberg University Mainz
Duesbergweg 10-14, 55099 Mainz, Germany

Besides various applications in solution, those poly(*N*-alkylacrylamides) could be successfully used as surface coatings, featuring a switchable wetting behavior (so called "smart coatings").^[2] Below LCST, the temperature-responsive coating exhibits a hydrophilic behavior, above LCST, the coating switches to a more hydrophobic behavior. Similar to the transition in solution, the transition on the surface is based on intermolecular hydrogen bonding with water below LCST, and intramolecular hydrogen bonds between the polymeric amide bonds themselves above LCST.^[3] This switching ability on surfaces offers the possibility to control important interfacial phenomena, such as wetting,^[4,5] fluid flows,^[6] and adhesion of various proteins.^[7–9] Poly(*N*-isopropylacrylamide) (PNIPAM) is the most prominent example, exhibiting a LCST at $\approx 32^\circ\text{C}$, and several methods were introduced to create responsive coatings based on its LCST phenomenon. *N*-isopropylacrylamide (NIPAM) was grafted from different initiator-derived self-assembled monolayers (SAMs), for example, thiol-based SAMs on gold capable of initiating a free radical polymerization of NIPAM,^[10] or an atom transfer radical polymerization.^[11] Similarly, starting from silicon or glass substrates, alkoxy silane-derived SAMs could be used to graft NIPAM.^[12–14] Other methods rely on grafting end-functionalized PNIPAM onto surfaces with defined functionalities,^[15] on cross-linked

PNIPAM films,^[16,17] or on plasma polymerization of NIPAM.^[18]

The area of single stimulus responsive polymers has been extended to polymers with a responsive behavior to multiple stimuli.^[19–21] Particularly interesting are polymers that are responsive to both light and temperature. In the past years, several reports were published on temperature-responsive polymers, containing light-responsive spiropyran moieties.^[22–24] Spiropyran derivatives are highly interesting candidates for the preparation of light-sensitive polymers because they undergo a chemical photoisomerization induced by irradiation with UV light. Spiropyran isomerizes by a ring-opening reaction upon UV irradiation at typically 365 nm from the spiro-isomer to the colored merocyanine isomer, whereas the reverse isomerization can be triggered by visible light. This photoisomerization also causes changes in the surface free energy, which consequently results in a change in surface wettability.^[25,26]

Recently, we introduced a different approach for the preparation of substrate-independent surface coatings, starting from poly(methylsilsequioxane)–poly(pentafluorophenyl acrylate) (PMSSQ–PPFPA) hybrid polymers. First, a PMSSQ–PPFPA hybrid polymer solution was spin coated onto flat substrates, and after annealing at 130 °C for 1 h, reactive surface coatings were obtained. Thus, stable and adherent coatings could be produced by thermally induced cross-linking of the PMSSQ part on a broad range of substrates, ranging from metals and metal oxides to plastics. The inherent activated esters could then be converted with various amines yielding the respective amides. For example, conversion with isopropylamine yielded a PNIPAM coating, which showed the expected temperature-dependent switching of the surface wettability.^[27]

Independently of the applied method to produce PNIPAM-functionalized surfaces, the common technique to determine the wettability switching relies on contact angle (CA) measurement via the sessile drop method. The disadvantages are that different measurements on one sample may result in different contact angles with a broad variation, and a direct measurement of the equilibrium contact angle (θ_{equi}) is not possible and must be calculated from the advancing and receding contact angles (θ_a , θ_r). Furthermore the placement of lines at a contact angle picture may be subjective. Usually the range of errors of contact angles is $\pm 3^\circ$, whereas for temperature-dependent measurements, errors of $\pm 5^\circ$ are more realistic, due to the temperature difference between substrate and water droplet.^[28]

In the present paper, we describe a convenient method to produce different temperature- and light-responsive coatings with an appropriate method allowing an accurate determination of the wettability switching range. For this, we first describe the synthesis and characterization

of new thermo- and light-responsive copolymers that are derived from alkylamines yielding a thermoresponsive behavior in an aminospiropyran as the corresponding photochromic group. In order to investigate and compare the temperature behavior of new copolymers, we prepared temperature-responsive coatings with different amines, such as isopropylamine, methylethylamine, cyclopropylamine leading to new thermo- and light-responsive surfaces.

2. Results and Discussion

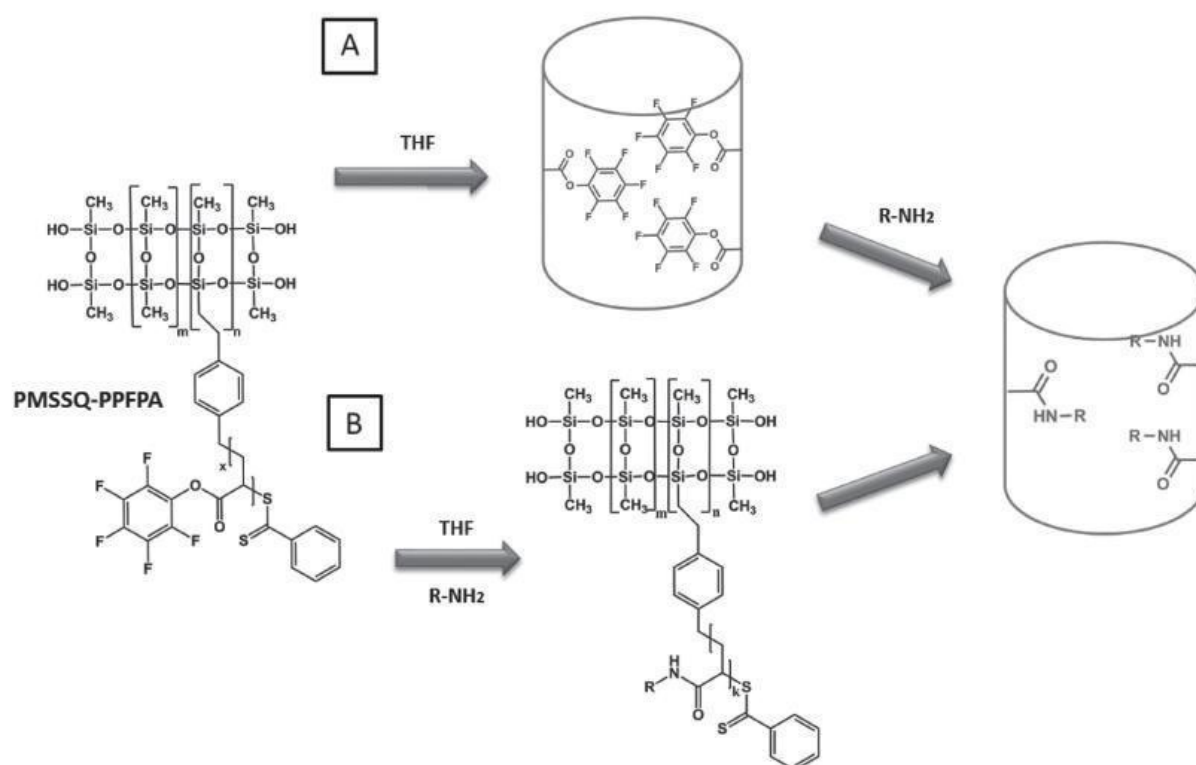
For the preparation of temperature- and light-responsive coatings, two complementary approaches are explored. In the first approach, a reactive hybrid polymer coating is deposited on a surface and subsequently functionalized in a post-modification route yielding the respective responsive surfaces. Alternatively, the reactive hybrid polymer can be modified prior to deposition on a surface.

2.1. Reactive Polymer Coating

For the first approach, thin glass capillaries were coated with PMSSQ–PPFPA to produce glass capillaries with a reactive coating on the inside of the capillary. Afterwards, this reactive surface was converted with different alkylamines, which allowed the preparation of different temperature-responsive coatings in parallel (see Scheme 1A). The switching of contact angles could be determined by the meniscus height of water rising inside the capillary at a certain temperature or after light irradiation.

For this, the hybrid polymer PMSSQ–PPFPA was synthesized according to the literature.^[29] Then, coating of the interior of the capillaries was achieved by dipping the capillary into a solution of 1 wt% PMSSQ–PPFPA in tetrahydrofuran (THF) for 10 min, including five effusion steps. Afterwards the capillary was annealed at 130 °C for 1 h and rinsed with pure THF to remove any nonbonded material or physisorbed polymer. The desired temperature-responsive coating was then prepared via a post-modification step, by dipping the capillary into a 10 wt% solution of the desired amine in THF for 1 h,^[27,33] followed by rinsing five times with THF and five times with water (Scheme 1A).

To determine the conversion of the reactive coating, PMSSQ–PPFPA modified flat silicon substrates (10 wt% PMSSQ–PPFPA solution in THF) were placed in a 10 wt% solution of various amines for 1 h, and the substrates were subsequently analyzed by Fourier transform infrared spectroscopy (ATR-mode: Attenuated Total Reflection Infrared Spectroscopy). Figure 1 shows a complete disappearance of the characteristic band at 1772 and at 1521 cm^{-1} owing to the activated ester groups after the postmodification



■ Scheme 1. Preparation of glass capillaries with temperature-responsive coatings inside.

with different amines (B. isopropylamine, C. methylethylamine, D. cyclopropylamine). Additionally, the characteristic bands for the amide were found at around 1630 cm⁻¹ and at around 1530 cm⁻¹, proving a complete conversion of all active ester groups. Furthermore, a characteristic band for an NH-bond appeared at 3300 cm⁻¹. All spectra showed the characteristic bands of the PMSSQ appearing between 1270 and 900 cm⁻¹, respectively.

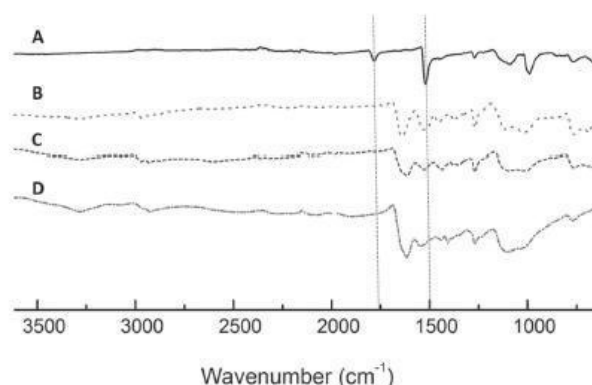


Figure 1. ATR-mode FT-IR spectra of silicon surfaces after modification with PMSSQ-PPFPA (A), functionalized via the polymer analogous reaction with isopropylamine (B), methylethylamine (C), and cyclopropylamine (D).

2.2. Functional Polymer Coating

Alternatively, the post-modification can be conducted before coating the reactive precursor polymer in the capillary (Scheme 1B). In order to compare the methods, PMSSQ-PPFPA was converted with isopropylamine, yielding a temperature-responsive PMSSQ-PNIPAM hybrid polymer (Figure 2).

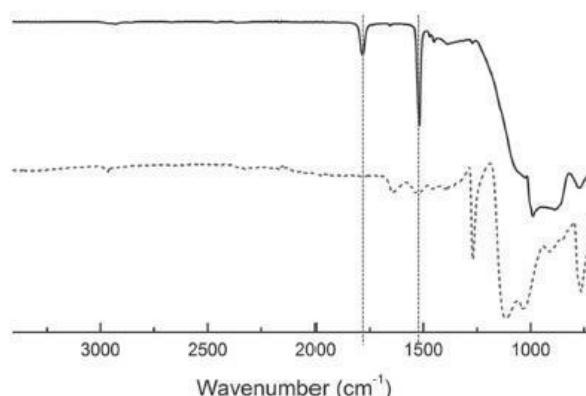


Figure 2. ATR-mode FT-IR spectra of PMSSQ-PPFPA coated silicon surface (solid line, active ester band at 1784 cm⁻¹) and after conversion of PMSSQ-PPFPA with isopropylamine (dashed line, amide bands at 1643 and 1531 cm⁻¹).

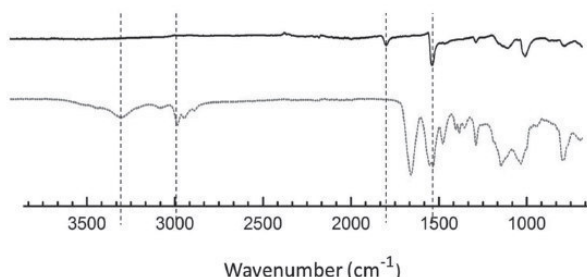


Figure 3. ATR-mode FT-IR spectra of silicon surfaces after modification with PMSSQ-PPFPA (solid line) and after coating by P2 (dashed line).

Next, a light- and temperature-responsive hybrid copolymer P2 was synthesized via a sequential post-polymerization modification of PMSSQ-PPFPA. First, the hybrid polymer PMSSQ-PPFPA was partly converted (46%) with an amino-functionalized spiropyran, followed by reaction with an excess of isopropylamine. A complete conversion of the activated esters had been detected by IR-spectroscopy and the IR spectrum of P2 is shown in Figure 3. Again, the disappearance of the activated ester polymer band at 1783 cm^{-1} and the appearance of the amide bands at 3302 , 1644 , and 1537 cm^{-1} , respectively, were observed. Additionally, ^1H NMR spectroscopy was used to characterize the copolymers (see the Supporting Information), showing the characteristic proton signals for the polyacrylamide backbone (in THF-d_8 : δ/ppm : 3.94, 1.09) and from the spiropyran amine protons (in THF-d_8 : δ/ppm : 8.01, 7.08–6.15).

Subsequently, the light-induced isomerization of the spiropyran amine moieties of the chromophoric copolymers was first investigated in THF solution. Figure 4 shows the UV-vis spectrum of the polymer before and after UV irradiation ($\lambda = 365\text{ nm}$). The rise of the peak at 565 nm is the result of a ring-opening reaction of the spiropyran and the formation of the zwitterionic merocyanine isomer. As expected, the strongest extinction of the

merocyanine at 565 nm was obtained after 15 min of UV irradiation at 365 nm . This photoisomerization is accompanied by a change of color of the hybrid polymer solution that could be observed by eye after UV irradiation for a short time in both THF (tetrahydrofuran) and DMF (N,N-dimethylformamide) (Figure 4B).

Next, dipping the capillary into a THF solution of 1 wt% of either of the functionalized hybrid polymers for 1 h resulted in coated capillaries. After an annealing step at $130\text{ }^\circ\text{C}$ for 3 h and rinsing with THF to remove any non-bonded or physisorbed material, the obtained surfaces were investigated. The switching of the contact angles was determined by the meniscus height of water rising inside the capillary at temperatures below and above LCST. For the temperature- and light-responsive surface, the surface switching was additionally investigated before and after UV irradiation (Scheme 2).

2.3. Wetting Analysis

Typical alkyl-substituted poly(acrylamides) that show a LCST besides PNIPAM are poly(*N*-methyl-*N*-ethylacrylamide) (PNMEAM),^[27] poly(*N*-cyclopropylacrylamide) (PNCAPAM),^[1] and poly(*N,N*-diethylacrylamide) (PNDEAM).^[30] To produce surface coatings containing these functional units, the capillaries coated with a reactive PMSSQ-PPFPA were converted with isopropylamine (IPA), yielding a PNIPAM coating; with methylethylamine (MEA), yielding a PNMEAM coating; with cyclopropylamine (CPA), yielding a PNCAPAM coating; and with diethylamine (DEA), yielding a PNDEAM coating, respectively. For a comparative study, the PMSSQ-PNIPAM hybrid polymer was coated directly inside the capillary. After preparation of these different temperature-responsive surfaces, the meniscus height was determined at $15\text{ }^\circ\text{C}$ (below the LCST of all systems) and at $60\text{ }^\circ\text{C}$ (above the LCST of all systems). For each system, five identical capillaries were prepared. Similar to the capillaries, also five glass plates were functionalized with each coating as comparison samples, used for the

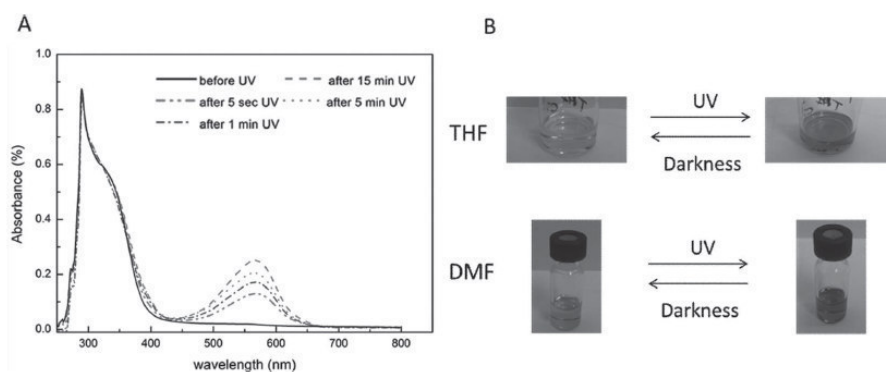
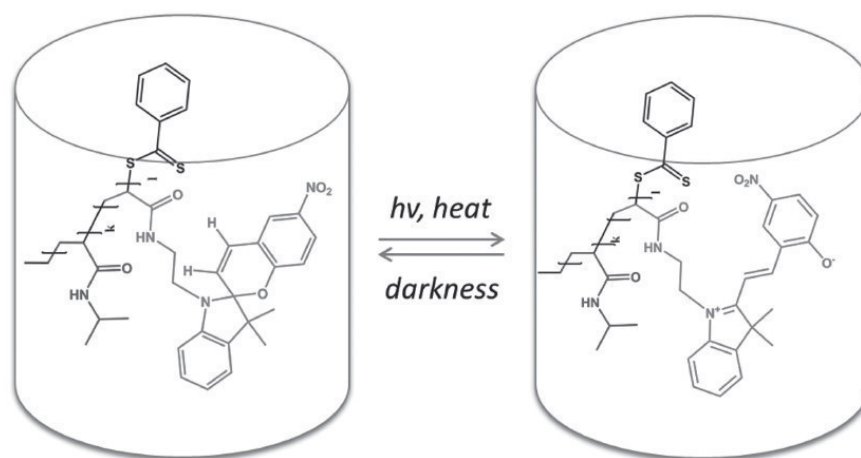


Figure 4. A) UV-vis absorption of the merocyanine in THF after irradiation at $\lambda = 365\text{ nm}$ for different periods of time. B) UV-vis absorption of the merocyanine in THF and DMF solution after irradiation at $\lambda = 365\text{ nm}$.



Scheme 2. Glass capillaries with light- and temperature-responsive coatings inside. Switching of spiropyran moieties under UV-light irradiation.

determination of the contact angles by the sessile drop method.

To calculate the equilibrium contact angle from the meniscus height (x), Equation (1) was used,^[31] therein the surface tension (γ_{LG}) of water at a certain temperature was calculated using Equation (2) (Eötvös rule).^[32] The density of water (δ) at 15 °C is 999.10 kg m⁻³ and at 60 °C the density is 983.19 kg m⁻³. The calculated values for the equilibrium contact angles are summarized in Table 1.

$$\theta_{\text{equi}} = \cos^{-1} \left(\frac{g^* r^* \delta^* x}{2\gamma_{LG}} \right) \quad (1)$$

$$\gamma_{LG} = 0.07275 \text{ N/m} * (1 - 0.002 * (T/K - 291)) \quad (2)$$

$$\cos \theta_{\text{equi}} = (1/2 \cos \theta_a + 1/2 \cos \theta_r) \quad (3)$$

To compare the obtained values with the contact angles obtained by the sessile drop method, similar coatings were produced on flat glass substrates. After determination of the advancing and the receding contact angles (θ_a , θ_r), the equilibrium contact angle was calculated using Equation (3).^[32] The values obtained for θ_a , θ_r , and θ_{equi} are also summarized in Table S1 (Supporting Information).

Figure 5 shows the meniscus heights of all measured capillaries at $T = 15$ °C and $T = 60$ °C. For better contrast, the water was colored with bromocresyl blue, negative menisci are photographed from a slight top view.

The measurement protocol used was as follows: After rinsing the five identical capillaries with water and drying in nitrogen stream, temperature adjustment at either 15 or 60 °C was achieved by keeping the capillaries in water at 15 or 60 °C, respectively, for 30 min. Afterwards, the capillaries were dried again in nitrogen

stream and one end was brought into contact with water of the desired temperature. Usually it took ≈ 5 min to reach a constant meniscus height, which did not change over time (equilibrium meniscus height). The distance between meniscus and water surface was measured.

The maximum difference that occurred during the meniscus height determination of the five identically coated capillaries was ± 1 mm, thus, the error range in the calculated equilibrium contact angle was calculated using Equation (1). The resulting error in θ_{equi} was lower than $\pm 1^\circ$, which is much lower than the error range in the sessile drop method which is $\pm 3^\circ$ to $\pm 5^\circ$.

Figures 6 and 7 show the equilibrium contact angles obtained by the sessile drop method and the capillary rise method at 15 and at 60 °C. Since the error range of the sessile drop method is at least $\pm 3^\circ$, the values obtained were given without decimals, in comparison the values obtained by the capillary rise experiment were much more accurate with an error range of $\pm 1.5^\circ$; therefore, the values are given with one decimal. Compared with the equilibrium contact angle, calculated from θ_a and θ_r observed by the sessile drop method, the corresponding contact angles calculated from the meniscus heights were almost identical in the applicable error ranges.

For example, for the PNIPAM surface prepared by post-modification on the surface (Figure 6 and Table S1, entry #2, Supporting Information) at 15 °C the equilibrium contact angle determined by the sessile drop method was $\theta_{\text{equi}} = 72^\circ$, while with the capillary rise method it was $\theta_{\text{equi}} = 73.7^\circ$. At 60 °C, $\theta_{\text{equi}} = 96^\circ$ was determined by the sessile drop method and $\theta_{\text{equi}} = 93.4^\circ$ was determined by the capillary rise method. Furthermore, the obtained results are in agreement with contact angle measurements on differently prepared PNIPAM surfaces.^[27,33] For comparison, the capillary coated with the hybrid

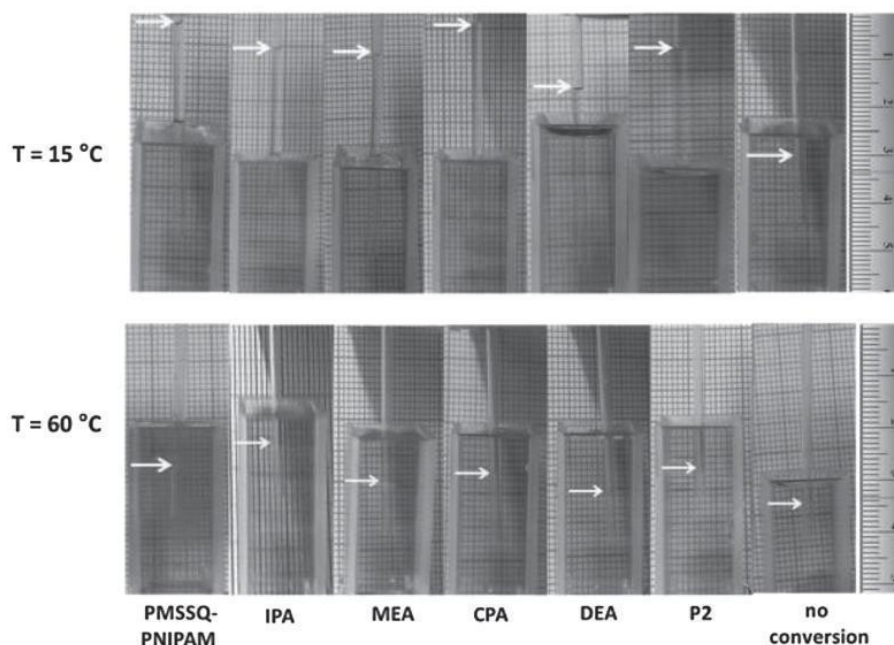


Figure 5. Meniscus heights in glass capillaries coated with PMSSQ–PPFA after conversion with IPA, MEA, CPA, DEA, coating of thermo- and light-responsive copolymer (P2), and PMSSQ–PNIPAM as well as the unconverted surface (no conversion) at $T = 15\text{ °C}$ (below LCST) and at $T = 60\text{ °C}$ (above LCST). For contrast improvement, the water was colored using bromocresyl blue.

polymer PMSSQ–PNIPAM was investigated (Figure 7 and Table S1, entry #1, Supporting Information). At 15 °C , the equilibrium contact angle determined by the sessile

drop method was $\Theta_{\text{equi}} = 72^\circ$, while with the capillary rise method it was $\Theta_{\text{equi}} = 78.8^\circ$. At 60 °C , $\Theta_{\text{equi}} = 97^\circ$ was determined by the sessile drop method and $\Theta_{\text{equi}} = 94.8^\circ$ was determined by the capillary rise method.

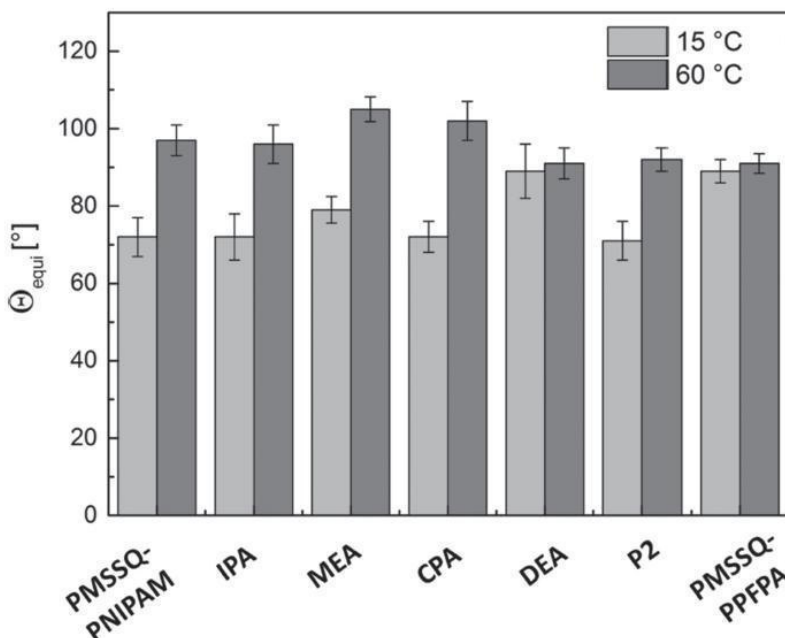


Figure 6. Equilibrium contact angles obtained by the sessile drop method at 15 °C and at 60 °C on silicon surfaces coated with PMSSQ–PPFPA after conversion with IPA, MEA, CPA, DEA, coating of thermo- and light-responsive copolymer (P2), and PMSSQ–PNIPAM as well as the unconverted surface (PMSSQ–PPFPA).

The close agreement of these values indicates that the two coating methods are complementary to each other. On account of the good agreement between the sessile drop results and the capillary rise results on all prepared temperature-responsive coatings, we concluded that the capillary rise method is a convenient alternative measurement for the sessile drop method.

The change of wettability obtained by applying either 15 °C (below LCST) or 60 °C (above LCST) was: $\Delta\Theta_{\text{equi}} = 19.7^\circ$ for PNIPAM (conversion with IPA), $\Delta\Theta_{\text{equi}} = 21.0^\circ$ for PNMEAM (conversion with MEA), $\Delta\Theta_{\text{equi}} = 21.4^\circ$ for PNCPAM (conversion with CPA), and $\Delta\Theta_{\text{equi}} = 13.0^\circ$ for PNDEAM (conversion with DEA). In comparison, the contact angle (or the meniscus height) of the applied reactive coating (PMSSQ–PPFPA, no conversion) showed no temperature dependence of the contact angle at all (Figures 6 and 7, and Table S1, entry #6, Supporting Information).

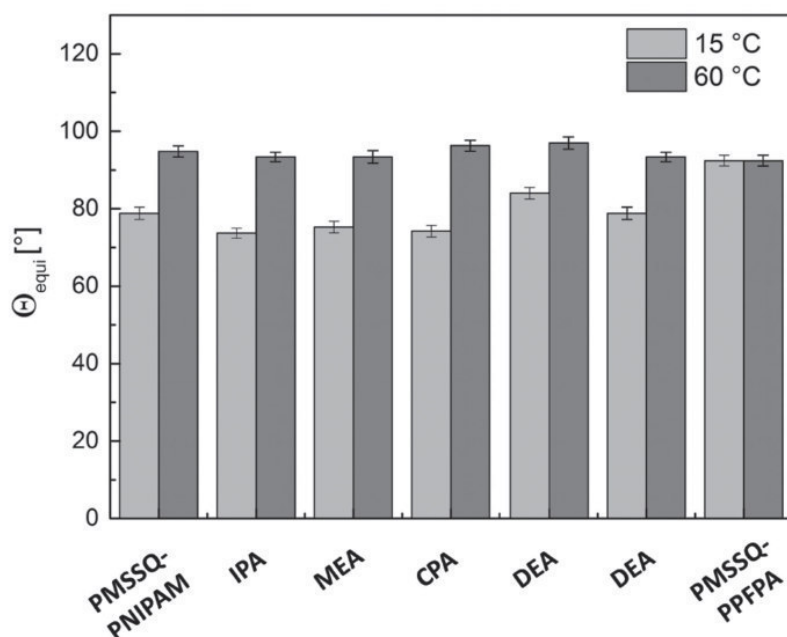


Figure 7. Equilibrium contact angles obtained by the capillary rise method at 15 °C and at 60 °C on silicon surfaces coated with PMSSQ-PPFPA after conversion with IPA, MEA, CPA, DEA, coating of thermo- and light-responsive copolymer (P2), and PMSSQ-PNIPAM as well as the unconverted surface (PMSSQ-PPFPA).

Next, the equilibrium contact angle of the P2 functionalized surface before UV irradiation was determined by the sessile drop method as $\Theta_{\text{equi}} = 71^\circ$ at 15 °C and $\Theta_{\text{equi}} = 92^\circ$ at 60 °C. With the capillary rise method, values of $\Theta_{\text{equi}} = 78.8^\circ$ at 15 °C and $\Theta_{\text{equi}} = 93.4^\circ$ at 60 °C were determined. After UV irradiation at 365 nm for 5 min, the CA values decreased by about 16°; before UV irradiation $\Theta_{\text{equi}} = 93.4^\circ$ was measured, whereas after UV irradiation, a value of

$\Theta_{\text{equi}} = 77.2$ was measured (Figure 8). This reduction of the contact angle occurred because of the structural changes on the surface as a consequence of the formation of a zwitterionic merocyanine structure upon UV irradiation. It is noteworthy that the photoisomerization is fully reversible. Similar to the previous studies, both in the solution as well as on the substrate surface, the transformation to the merocyanin isomer proceeded within 5 min under UV-light irradiation. The reverse isomerization into the spiropyran isomer could be induced after 12 h in the dark resulting in a switching to the hydrophobic state.^[22–24] After UV-light irradiation to yield the merocyanin isomer, the surface was allowed to reisomerize back into the spiropyran isomer overnight, resulting in $\Theta_{\text{equi}} = 79^\circ$ and $\Theta_{\text{equi}} = 93^\circ$, respectively, which are in very good agreement with the CA values measured before irradiation. This reversibility proves the light-switchable properties of the obtained

surface coatings at 60 °C. However, measurements of both contact angle and meniscus height at 15 °C showed no change upon UV-light irradiation (Figure S3, Supporting Information), indicating that the additional change of polarity induced by the spiropyran photoisomerization only contributes in the hydrophobic state of the PNIPAM, i.e., above LCST, while the contribution in the hydrophilic state below LCST is negligible.

3. Conclusions

In summary, we have presented the synthesis of hybrid polymers based on the efficient modification chemistry of PMSSQ-PPFPA, yielding various substrate surfaces that exhibit a thermo- or light-responsive behavior. Furthermore, the reversible isomerization of spiropyran moieties in the copolymers, which was induced by irradiation with UV light, had an influence on the water wettability behavior. First, different temperature-responsive coatings could be prepared by surface-modification reactions inside the capillary and the accessible temperature-controlled switching range of contact angles was directly measured using water of different temperatures. The values obtained are comparable to the results obtained by the sessile drop method, but the error range is much smaller, which allows a more accurate determination of the equilibrium contact angles. This convenient method of reactive coatings inside

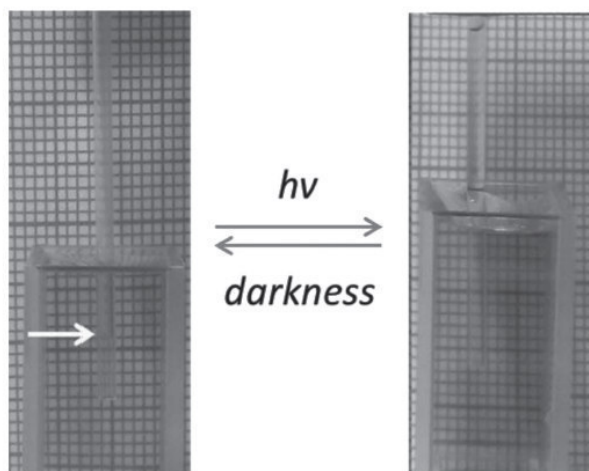


Figure 8. Meniscus heights in glass capillaries coated with P2 before and after UV-light irradiation at 60 °C.

glass capillaries may find further application in searching for other poly(acrylamide)-based stimuli-responsive coatings, which may not be limited to temperature or light as a stimulus. Moreover, we compared two synthetic pathways, post-modified and prior-modified, with each other. In summary, for the preparation of temperature-responsive surfaces with different amines based on the chemistry of the hybrid polymer PMSSQ–PPFPA, both of these ways led to similar results. In contrast, the light- and temperature-responsive surfaces could only be obtained by prior deposition of the new hybrid polymer on the surface.

4. Experimental Section

4.1. Materials

As capillaries with a precisely defined inner diameter we used disposable micropipettes with ring marks (Hirschmann Laborgeräte, Germany, 5/10 μL ringcaps; accuracy $R \leq 0.25\%$, precision $P \leq 0.5\%$, inner radius $r_c = 2 \times 10^{-4}$ m). All chemicals were commercially available and used as received, unless otherwise stated.

4.2. Instrumentation

All ^1H spectra were recorded on Bruker 300 MHz FT-NMR spectrometers in deuterated solvents, and chemical shifts (δ) were given in ppm with solvent peak as internal standard. The number average of the molecular weight (M_n) and the molecular weight distribution (M_w/M_n) of the polymers were calculated on the basis of a polystyrene calibration.

The PMSSQ–PStCHO coatings were prepared by spin coating a solution in THF (10 wt%) using a Laurell WS-650-MZ-23 PP at 3000 rpm for 15 s. The conversions of the reaction on the surface and the film properties after the reaction were investigated by a Nicolet iS10 FT-IR spectrometer.

The CA measurements were conducted using a DataPhysics OCA 20 with a dosing volume of 2 μL at a dosing rate of 1 $\mu\text{L s}^{-1}$. The measurements of advancing and receding contact angles were performed by addition and removal volume method.

4.3. Preparation of Functional Surfaces

4.3.1. Surface Coating and Modification

The 10 wt% polymer solution in THF was spin coated onto clean substrates (15 s at 3000 rpm). Afterwards, the substrates were annealed at 130 $^\circ\text{C}$ for 2 h to crosslink the inorganic block and subsequently washed with THF to remove any remaining material. For post-polymerization reaction, the substrates were placed in 1 wt% amine solution in THF and subsequently dried under ambient conditions.

4.4. Synthesis of PMSSQ Macro-CTA

A preparation of inorganic macro-RAFT (Reversible Addition–Fragmentation Chain Transfer polymerization) CTA (chain transfer agent) was conducted by slightly modifying a previously reported method,^[34] and the typical procedure was as follows: A

dry THF solution (15 mL) containing dithio benzoic acid 4-ethyl-trimethoxy-silyl ester (0.98 g, 2.5 mmol) was placed in a round bottomed flask. The reaction mixture was cooled to 0 $^\circ\text{C}$ and methyltrimethoxysilane (3.47 g, 25 mmol), 500 mmol of water, and 10 mmol of HCl were added and stirred for 3 h at 0 $^\circ\text{C}$. Afterwards, the reaction mixture was dissolved in diethyl ether and washed with water. After drying the organic phase over MgSO_4 , the ether was removed and the product was dried under high vacuum. Yield 3.32 g (1.46 mmol, 58.28%). $^1\text{H-NMR}$ (CDCl_3) δ : 7.99 (br, 1H); 7.36 (br, 8H); 5.80 (br, 8H); 4.55 (br, 2H); 3.48 (br, 2H); 2.71 (br, 2H); 0.99 (br, 2H); 0.17 (br, 69.1H). $M_n = 2279$ g mol^{-1} , $M_w/M_n = 1.6$.

4.5. Synthesis of PMSSQ–PPFPA

A dioxane solution (4 mL) of PMSSQ macro-RAFT agent (0.5 g, 260.6 μmol), Azobisisobutyronitrile (AIBN) (20 mg, 121.7 μmol), and pentafluorophenyl acrylate ester (1.0 g, 4.2 mmol) was placed in a Schlenk flask and degassed by freeze–thaw cycles. The degassed reaction mixture was stirred at 80 $^\circ\text{C}$ for 4 h and afterwards precipitated into methanol to afford a pale colored powder. Yield 0.95 g (0.024 mmol) $^1\text{H-NMR}$ (300 MHz, CDCl_3) δ : 0.40–6.85 (br); 3.05 (br, 1H); 2.81 (br); 2.32–2.10 (br, 2H); 1.50–1.20 (br); 0.15 (br, 1H). $M_n = 39268$ g mol^{-1} , PDI = 1.9.

4.6. Synthesis of P2

4 mg (0.009 mmol) of spiropyran amine was added to the PMSSQ–PPFPA hybrid polymer (300 mg, 0.008 mmol) solution in 4 mL THF. Then 0.01 mL trimethylamine was added and the reaction mixture was stirred for 2 h at room temperature. Afterwards, 1.7 mL of isopropyl amine was added. After an additional 18 h, the product was precipitated three times from hexane and dried under vacuum at room temperature. Yield: 0.29 g (98%). $^1\text{H-NMR}$ (300 MHz, THF-d_6) δ /ppm: 7.40–6.85 (br); 3.05 (br, 1H); 2.81 (br); 2.32–2.10 (br, 2H); 1.50–1.20 (br); 0.15 (br, 1H). $M_n = 129.300$ g mol^{-1} , PDI = 3.

4.7. Surface Coating

Capillaries were coated by dipping the capillary into a solution of 10 wt% of the respective polymer in THF for 1 h. After an annealing step at 130 $^\circ\text{C}$ for three hours and rinsing with pure THF to remove any nonbonded or physisorbed material, five identical capillaries were prepared and analyzed for each sample. Surface conversion of the film of PMSSQ–PPFPA modified flat silicon substrates were placed in a 10 wt% solution of the respective amines for 1 h and thoroughly rinsed afterwards.

4.8. UV Irradiation

The obtained surfaces were irradiated by UV light at 365 nm (UV Hand Lamp Filter VL-6L, 6W-365 nm tube) for 5 min to induce a photoinduced transformation between two isomers, the neutral almost colorless spiropyran and the colored merocyanine.^[24]

Supporting Information

Supporting Information is available from the Wiley Online Library or from the author.

This article was amended on December 21, 2015. Figure 2 was replaced.

Received: August 24, 2015; Revised: October 3, 2015;
Published online: December 2, 2015; DOI: 10.1002/macp.201500324

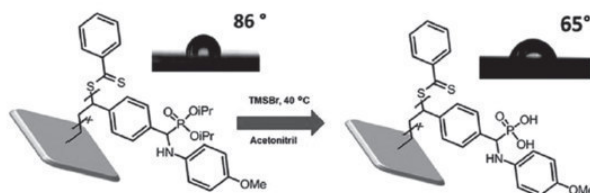
Keywords: capillary rise; contact angle; organic–inorganic hybrids; switching of wettability; temperature-responsive coatings

- [1] Y. Maeda, T. Nakamura, I. Ikeda, *Macromolecules* **2001**, *34*, 1391.
- [2] S. L. Gras, T. Mahmud, G. Rosengarten, A. Mitchell, K. Kalantar-zadeh, *Chem. Phys. Chem.* **2007**, *8*, 2036.
- [3] T. S. Sun, G. Wang, L. Feng, B. Liu, Y. Ma, L. Jiang, D. Zhu, *Angew. Chem.* **2004**, *43*, 357.
- [4] Y. Xia, Y. Qin, D. Yin, *Curr. Opin. Colloid Interface Sci.* **2001**, *6*, 54.
- [5] P. Lenz, *Adv. Mater.* **1999**, *11*, 1531.
- [6] D. E. Kataoka, S. M. Troian, *Nature* **1999**, *402*, 794.
- [7] M. E. Callow, J. A. Callow, L. K. Ista, S. E. Coleman, A. C. Nolasco, G. P. Lopez, *Appl. Environ. Microbiol.* **2000**, *66*, 3249.
- [8] D. Cunliffe, C. de la Heras Alarcon, V. Peters, J. R. Smith, C. Alexander, *Langmuir* **2003**, *19*, 2888.
- [9] L. K. Ista, S. Mendez, V. H. Perez-Luna, G. P. Lopez, *Langmuir* **2001**, *17*, 2552.
- [10] D. M. Jones, J. R. Smith, W. T. S. Huck, C. Alexander, *Adv. Mater.* **2002**, *14*, 1130.
- [11] L. Liang, X. Feng, J. Liu, P. C. Rieke, G. E. Fryxell, *Macromolecules* **1998**, *31*, 7845.
- [12] H. Kanazawa, K. Yamamoto, Y. Matsushima, *Anal. Chem.* **1996**, *68*, 100.
- [13] L. Liang, P. C. Rieke, G. E. Fryxell, J. Liu, M. H. Engehard, K. L. Alford, *J. Phys. Chem. B* **2000**, *104*, 11667.
- [14] T. Yakushiji, K. Sakai, *Langmuir* **1998**, *14*, 4657.
- [15] M. D. Kurkuri, M. R. Nussio, A. Deslandes, N. H. Voelcker, *Langmuir* **2008**, *24*, 4238.
- [16] L. Liang, P. C. Rieke, J. Liu, G. E. Fryxell, J. S. Young, M. H. Engelhard, K. L. Alford, *Langmuir* **2000**, *16*, 8016.
- [17] X. Cheng, H. E. Canavan, M. J. Stein, J. R. Hull, S. J. Kweskin, M. S. Wagner, G. A. Somorjai, D. G. Castner, B. D. Ratner, *Langmuir* **2005**, *21*, 7833.
- [18] D. Kessler, P. J. Roth, P. Theato, *Langmuir* **2009**, *25*, 10068.
- [19] D. Li, Q. He, Y. Yang, H. Möhwald, J. Li, *Macromolecules* **2008**, *41*, 7254.
- [20] J. P. Magnusson, A. K. G. Pasparakis, A. Saeed, W. Wang, C. Alexander, *J. Am. Chem. Soc. Rev.* **2008**, *30*, 10852.
- [21] G. Wang, X. Tong, Y. Zhao, *Macromolecules* **2004**, *37*, 8911.
- [22] D. Kessler, F. D. Jochum, J. Choi, K. Char, P. Theato, *ACS Appl. Mater. Interfaces* **2011**, *3*, 124.
- [23] D. Wang, P. J. Jiao, J. Wang, Q. Zhang, L. Feng, Z. Yang, *J. Appl. Polym. Sci.* **2012**, *125*, 870.
- [24] N. Wagner, P. Theato, *Polymer* **2014**, *55*, 3436.
- [25] M. Kettunen, R. J. Silvennoinen, N. Houbenov, J. Ruokolainen, J. Sainio, N. Pore, M. Kemell, M. Ankerfors, T. Lindström, *Adv. Funct. Mater.* **2011**, *3*, 510.
- [26] J. Choi, P. Schattling, F. D. Jochum, J. Pyun, K. Char, P. Theato, *J. Polym. Sci., Part A: Polym. Chem.* **2012**, *50*, 4010.
- [27] D. Kessler, P. Theato, *Macromol. Symp.* **2007**, *424*, 249.
- [28] N. A. Plate, T. L. Lebedeva, L. I. Valuev, *Polym. J.* **1999**, *31*, 21.
- [29] I. Idziak, D. Avoce, D. Lessard, D. Gravel, X. X. Zhu, *Macromolecules* **1999**, *32*, 1260.
- [30] I. Idziak, D. Gravel, X. X. Zhu, *Tetrahedron Lett.* **1999**, *40*, 9167.
- [31] G. Li, H.-J. Butt, K. Graf, *Langmuir* **2006**, *22*, 11395.
- [32] *Contact Angle, Wettability and Adhesion* (Ed: K. L. Mittal), VSP, Leiden, The Netherlands **2006**.
- [33] D. Kessler, P. Theato, *Langmuir* **2009**, *25*, 14200.
- [34] D. Kessler, N. Metz, P. Theato, *Macromol. Symp.* **2007**, *254*, 34.

Installation of Zwitterionic α -Amino Phosphonic Acid Moieties on Surfaces via a Kabachnik-Fields Post-Polymerization Modification

Natalie Wagner, Lilli Schneider, Martin Michelswirth, Karsten Küpper, Patrick Theato*

An organic–inorganic hybrid polymer, composed of poly(methylsilsesquioxane) (PMSSQ) and poly(4-vinyl benzaldehyde) (PStCHO), is prepared by reversible addition–fragmentation chain transfer (RAFT) polymerization of 4-vinyl benzaldehyde (StCHO) using a macro-chain transfer agent (CTA) based on PMSSQ. The obtained PMSSQ–PStCHO is spin-coated on substrates such as silicon wafers or copper plates to afford aldehyde-functionalized surfaces. Successful Kabachnik-Fields post-polymerization modification (KF-PMR) of the aldehyde-functionalized surfaces is conducted with amines and dialkyl phosphonates, and characterized by surface analysis techniques including IR, energy-dispersive X-ray (EDX), and X-ray photoelectron spectroscopy (XPS) measurements, documenting the installation of α -amino phosphonates onto surfaces with practically quantitative conversion of aldehydes. In addition, the generated α -amino phosphonates are successfully deprotected to afford the corresponding α -amino phosphonic acids on surfaces, which make this route a reliable tool-enabling surface functionalization with α -amino phosphonic acids.



1. Introduction

As a direct consequence of the growing demand of substrates featuring specifically designed functionalities, chemists have been seeking synthetic protocols that allow a robust and reliable installation of desired molecules on

surfaces. To expand the scope of functional materials featuring designed surface characteristics, a number of highly reactive and selective reactions, so-called “click reactions”, have been employed. This includes Cu(I)-catalyzed and metal-free 1,3-dipolar cycloaddition (CuCAAC) reaction of organo-azides and alkynes,^[1,2] thiol-ene, thiol-maleimide,^[3] nucleophile-isocyanate,^[4] and activated ester-amine reactions, which all realize a facile functionalization of substrate surfaces.^[5–8] In spite of the fact that these click reactions have been employed in surface modification chemistry, the intrinsic drawbacks of these conventional “click reactions” are: 1) only one functionality per one reaction can be achieved and 2) no functionality owing to linkages that are generated via reactions. In order to target material surfaces featuring more sophisticated functionalities, chemists need to propose a synthetic strategy realizing installation two or more functional molecules per single reactive site accompanied with a generation of an attracting linkage.

N. Wagner, Prof. P. Theato
Institute for Technical and Macromolecular Chemistry
University of Hamburg, Bundesstr. 45
D-20146 Hamburg, Germany
E-mail: theato@chemie.uni-hamburg.de
L. Schneider, Dr. K. Küpper
Department of Physics, University of Osnabrück
Barbarastr. 7, D-49076 Osnabrück, Germany
M. Michelswirth
Center for Free-Electron Laser Science, Attosecond Research
and Science Group, University of Hamburg, Luruper Chaussee
149, 22761 Hamburg, Germany

When considering a new stream in polymer functionalization techniques, multi-component reactions (MCRs)^[9] have been appreciated recently as a new synthetic toolbox in the field of polymer chemistry.^[10]

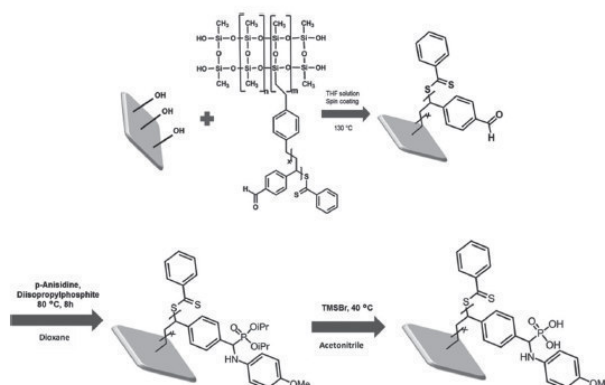
Boosted by pioneering work of utilizing MCRs in polymer chemistry by the groups of Meier and Li, MCRs have been rapidly recognized as an attracting synthetic toolbox.^[11] Until now, numerous MCRs have been utilized in polymer synthesis, which include the Passerini reaction, the Ugi reaction, the Biginelli reaction, the Cu(I)-catalyzed three-component reaction, and the Kabachnik–Fields reaction (KFR).^[12–20] We tuned our attention to the KFR, because the KFR between aldehydes, amines, and dialkyl phosphonates is known to proceed very efficiently without any catalytic species and generates α -amino phosphonate moieties, which are structural analogues to α -amino acids.^[21–25] Although the integration of zwitterionic amino acids onto substrate surfaces is rather limited due to limited synthetic protocols, incorporation of zwitterionic amino acids on substrate surfaces was revealed to provide anti bio-fouling effects.^[26–33] In this context, the utilization of KFR for a surface modification is expected to be highly rewarding, because KFR would enable not only an efficient click-type modification of surfaces but also the concurrent construction of α -amino phosphonic acids on substrates.^[9,20,34,35] In a previous study, we have reported that the Kabachnik–Fields post-polymerization modification reaction (KF-PMR) proceeded efficiently on poly(4-vinyl benzaldehyde) (PStCHO) with amines and dialkyl phosphonates in the absence of a catalyst, implying that KFR can be employed for surface modification reactions.^[36,37] In addition, the group of Theato has succeeded in immobilizing organic polymers via curing of organic–inorganic hybrid polymer composed of poly(methylsilsequioxane) (PMSSQ) and organic polymer segments such as PMMA and PSt, encouraging us to conduct KFR on surfaces by using the organic–inorganic hybrid polymer immobilization approach.^[38–42]

Here, we now report on the installation of α -amino phosphonic acids onto surfaces via surface KFR (sur-KFR) on aldehyde-decorated surfaces that are prepared by coating of PMSSQ featuring PStCHO hybrid polymers and subsequent deprotection of phosphonates generated on surfaces by *sur*-KFR, as highlighted in Scheme 1.

2. Results and Discussion

2.1. Hybrid Polymer Synthesis

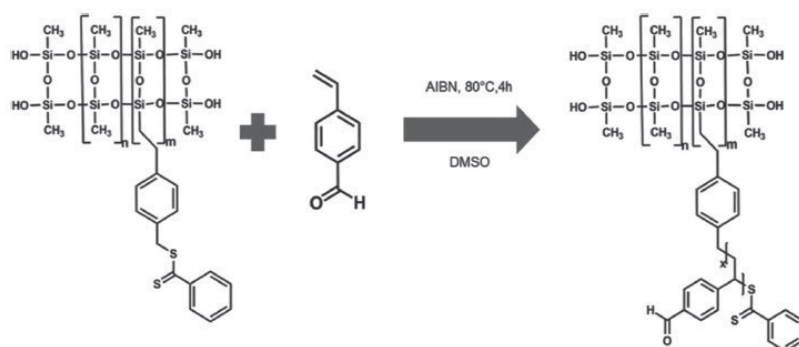
In order to install polymeric α -amino phosphonic acids onto substrates surfaces, surface KF-PMR and subsequent deprotection of α -amino phosphonates have to be conducted on aldehyde-functionalized substrates surfaces.



Scheme 1. Scheme of a Kabachnik–Fields post-polymerization modification reaction on surfaces.

For this, aldehyde-functionalized surfaces were prepared by coating of organic–inorganic hybrid polymers featuring aldehyde moieties onto substrates, following our recently reported method.^[38,40,43–47] In this context, poly(methylsilsequioxane)-poly(4-vinylbenzaldehyde) (PMSSQ–PStCHO) was prepared via reversible addition–fragmentation chain transfer (RAFT) polymerization. As shown previously, macro-RAFT agents derived from PMSSQ–chain transfer agent (PMSSQ–CTA) are readily accessible and can be used as RAFT agents to control the polymerization of vinyl monomers such as MMA and styrene, yielding in organic–inorganic hybrid polymers featuring PMSSQ as an inorganic component.^[40] Consequently, PMSSQ–PStCHO hybrid polymers were synthesized under RAFT conditions in DMSO using PMSSQ–CTA as the macro-CTA, StCHO as the vinyl monomer and AIBN as a radical source at 80 °C within 4 h (Scheme 2). The initial reaction was set as $[PMSSQ-CTA]_0/[AIBN]_0/[St-CHO]_0 = 1/2.8/158$ and the obtained polymers were purified by precipitation in methanol (Table 1).

The monomer conversion of the RAFT polymerization using PMSSQ–CTA as a chain transfer agent reached 96.0% as determined by ¹H NMR spectroscopy of the reaction medium. In the ¹H NMR spectrum of the purified obtained polymer (Figure 1), peaks ranging from 0.07 to 5.29 ppm owing to PMSSQ backbone and those ranging from 6.74 to 9.92 ppm owing to PStCHO were observed, confirming that the obtained polymer was consistent with the target PMSSQ–PStCHO hybrid polymer. Successful integration of PStCHO was further confirmed by IR spectroscopy. The ATR-mode IR spectrum of the obtained hybrid polymers showed an intense peak at 1699 cm^{−1} owing to aldehyde moieties. Next, a SEC analysis of the obtained polymer showed a monomodal trace with reasonable molecular weights (M_n around 21 400 g mol^{−1}) and a moderate dispersity ($\bar{D} = 1.6$). In order to determine the ratio of organic and inorganic components, the obtained PMSSQ–PStCHO



Scheme 2. Synthetic pathway towards reactive PMSSQ-PStCHO hybrid polymers. (Note: The structure of poly(methylsilsesquioxane) does not represent the actual real structure. The hybrid polymers certainly contain cage- and ladder-type fractions, among others, but for a simpler representation a ladder-type structure is shown throughout.)

hybrids polymers were analyzed by thermogravimetric analysis (TGA). In a TGA profile of all obtained hybrid polymer (examples shown in Figure 2), a clear weight decrease was observed between 100 °C and 160 °C owing to a secondary condensation of free silanol groups (Si-OH) of the inorganic PMSSQ fraction. Another large weight decrease was observed around 400 °C owing to a decomposition of the organic PStCHO polymer chains. Based on the above-mentioned weight decrease, weight ratios of organic to inorganic components were determined and are listed in Table 1. The experimentally found ratios of all hybrid polymers are in reasonable agreement with the initial weight feed ratio of monomer to macro-RAFT agent. There is, however, a tendency for a slightly enriched incorporation of PMSSQ for hybrid polymers with smaller targeted inorganic fractions.

2.2. Coating of Aldehyde Containing Hybrid Polymers on Surfaces

In order to provide surfaces featuring aldehyde moieties, we focused on coating PMSSQ-PStCHO hybrid polymers onto substrates. For this, thin polymer films on silicon substrates were prepared by spin-coating of a PMSSQ-PStCHO solution (10 wt% in THF) at 3000 rpm for 15 s and subsequent curing at 130 °C for 2 h. Because aldehyde moieties are known to be unstable, the obtained substrate was characterized by IR measurements. In Figure 3, a distinct peak at 1691 cm⁻¹ owing to aldehyde groups was observed. In addition, a uniform and thin-layer formation was confirmed by

atomic force microscopy (AFM) measurements of the cured films on the substrate (Figure S4, Supporting Information), showing a successful installation of aldehydes without any structural and chemical defects.

The chemical composition on the surface was revealed to be dependent on the ratio of organic to inorganic components of the hybrid copolymers, as shown in previous studies.^[45] Therefore, PMSSQ-PStCHO hybrid polymers with different organic-to-inorganic ratios were prepared via RAFT polymerization by varying the initial ratio of macro-RAFT agent to monomer, as summarized in Table 1. The contact angles (CAs, θ) of all coated thin films were then measured and are also summarized in Table 1. Due to the distinct chemical nature of PMSSQ and PStCHO, the CAs provide a first insight into the chemical composition of the surfaces. Figure 4 shows

Table 1. Synthetic, compositional, and contact angle values of PMSSQ-PStCHO hybrid copolymers.

Polymer	4-Vinyl benzaldehyde [g]	$M_w, \text{PMSSQ-StCHO}$ [g mol ⁻¹]	Monomer conversion [%]	Expected wt ratio [Inorganic]/[Organic]	wt ratio by TGA [Inorganic]/[Organic]	$D_{\text{PMSSQ-StCHO}}$	θ_{static} [°]	θ_a/θ_r [°]
PMSSQ	/	2300	/	100/0	100/0	1.6	91	115/50
P7	0.1	21 100	75.3	90/10	91/9	2.1	89	110/78
P6	0.3	30 400	80.2	70/30	59/51	2.5	87	100/77
P5	0.4	18 000	71.1	60/40	55/55	1.9	85	101/52
P4	0.6	23 800	88.1	40/60	46/54	1.9	86	103/53
P3	0.7	21 900	98.6	30/70	37/63	1.8	82	107/71
P2	0.8	24 000	n.d.	20/80	34/66	1.9	81	102/63
P1	0.9	21 500	96.0	10/90	29/71	1.6	75	94/51
PStCHO ^{a)}	0.1	42 000	/	0/100	0/100	2.4	61	86/40

^{a)}Data taken from literature.^[9] n.d. = Not determined

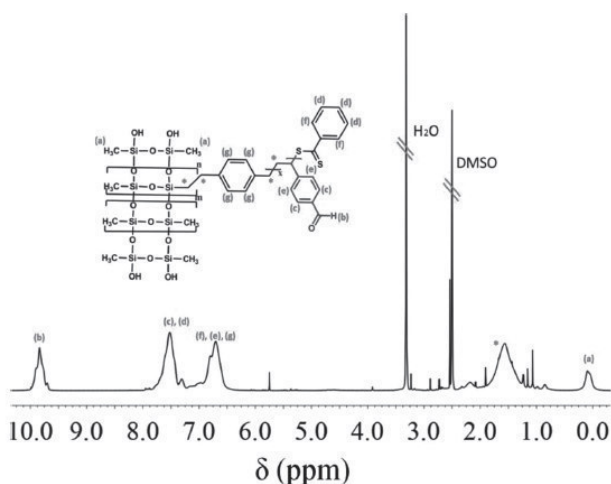


Figure 1. ^1H NMR spectra of purified PMSSQ-PStCHO.

the relationship between organic-to-inorganic ratios of the PMSSQ-PStCHO hybrid polymers and the CA values of the respective thin films. Figure 4 clearly shows that the CA values of surfaces coated with PMSSQ-PStCHO remained constant, with CA values around 90° , until the PStCHO component reached around 50 wt%. With increasing amounts of PStCHO (>50 wt%) in the hybrid polymers, the CA values started to decrease significantly and approached 61° , which represents the CA for pure PStCHO films. This CA value variation caused by varying organic-to-inorganic ratio of PMSSQ-PStCHO hybrid polymers is not only in good agreement with our previous reports^[45] but is also proving that aldehyde moieties can be made accessible on the coating surface when the PStCHO content of the hybrid polymers was more than 50 wt%.

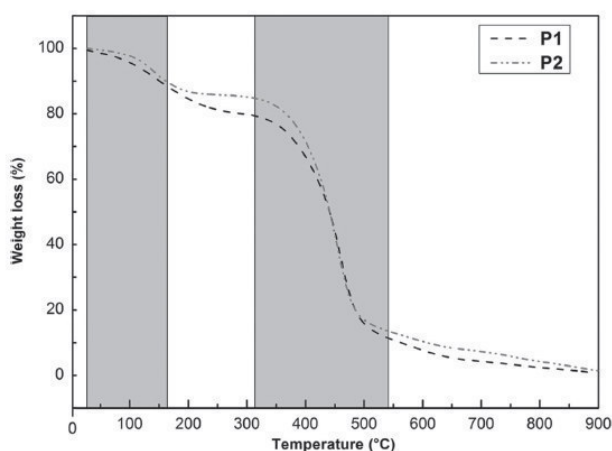


Figure 2. Exemplary thermogravimetric analysis of PMSSQ-PStCHO P1 with 10% CTA and P2 with 20% CTA.

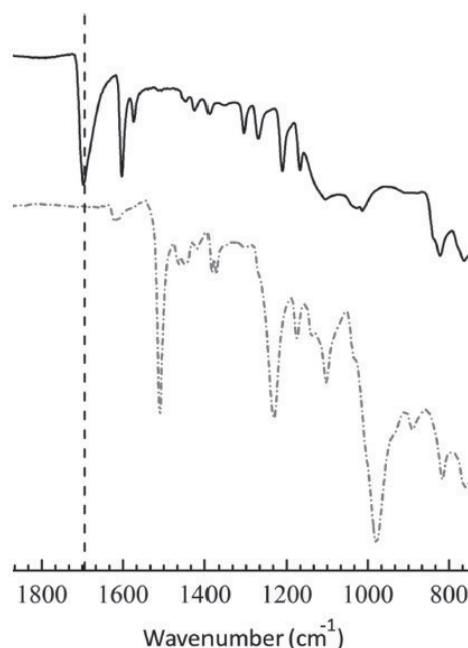


Figure 3. FT-IR spectra of P1 cured silicon surfaces before (upper, solid line) and after (lower, dash-dotted line) sur-KFR for run R2.

2.3. Kabachnik-Fields Post-Polymerization Modification on the Surface

Based on the above-established protocol that allows facile installation of aldehydes on surfaces, we next focused on surface Kabachnik-Fields reaction (sur-KFR) to construct polymeric α -amino phosphonates on substrate surfaces. A sur-KFR was conducted on a silicon substrate functionalized with PMSSQ-PStCHO (Si-CHO) **P1** whose organic component was 71 wt% in order to guarantee that PStCHO chains are exposed to the surface (Figure 4, Table 2).

A sur-KFR of Si-CHO was carried out with *p*-anisidine and diisopropyl phosphonate (R2) in 1,4-dioxane at 80°C for 4 h. The IR spectra of the silicon surfaces before sur-KFR (Figure 3) showed an intensive band at 1692 cm^{-1} owing to the C=O stretching of aldehydes, which clearly disappeared after sur-KFR. Additionally, a new band at 1510 cm^{-1} owing to phosphonates developed, proving a practically quantitative conversion of aldehydes. Additional insights into sur-KFR were obtained by energy-dispersive X-ray (EDX) and X-ray photoelectron spectroscopy (XPS) measurements. In order to provide a high-resolution EDX spectrum, Cu- and Al-substrates were modified instead of silicon substrates with **P1** and the subsequent sur-KFR conducted as runs R1 and R5. In the EDX spectra before and after sur-KFR (Figure S6 and S7, Supporting Information), distinct peaks owing to phosphorous and nitrogen appeared after sur-KFR, showing that not only amines but also dialkyl phosphonates were installed. The

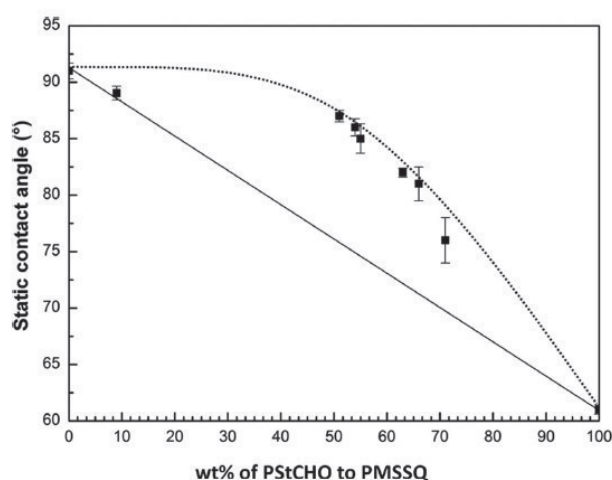


Figure 4. Relationship between the organic–inorganic ratio of PMSSQ–PStCHO and the contact angle values of PMSSQ–PStCHO thin films, after being spin-coated from 10 wt% solution in THF and subsequent curing at 130 °C for 2 h.

PMSSQ–PStCHO coating on Cu- and Al-substrates was also possible (despite their high surface energies) and KFR was revealed to proceed as expected, making this coating/

functionalization approach substrate independent. It is known that the covalent bonds between silicon substrates and PMSSQ arise, which are documented by strong adhesions measured by ISO tape tests.^[35–37]

Further, XPS measurements were performed to confirm the successful sur-KFR of P1-modified substrates and examples are shown in Figure 5 for runs R13 (B) and R17 (C). A detailed analysis of the signature of R13 and R17 was performed by fitting the P_{2p} signatures (see curve D in Figure 5). A $P_{2p_{3/2,1/2}}$ doublet shift of 0.87 eV is ensured in the fit model; a branching ratio (by area) of about 1.37 is verified by the performed analysis of both spectra. An additional species being chemical shifted about -1.18 ± 0.41 eV is obtained from the spectrum of the R17-modified substrate (D, dashed curve). This gives an evidence to a O–(P=O) group formation due to the sur-KFR. The species is assigned referring to spectra of $H(NO_3)$ etched phosphide solid-state surfaces.^[44] The amount of the O–(P=O) formation associated spectroscopic species with respect to the overall P_{2p} signature obtained from the R17-functionalized surface was found to be 0.254. This turned out to be nearly equal to the one being observed in the corresponding spectrum of the 13 functionalized surface (see Figure 5),

where a value of area amount of 0.262 is retrieved analyzing this P_{2p} spectrum by fit. An additional “phosphate-like” environment is observed in the case of sur-KFR with R13 (B). The associated spectroscopic fraction turned out to be chemical shifted about $(-3.00 \pm 0.26$ eV). This corresponds to an appearance of a $(+1.44 \pm 0.15$ eV) shifted additional feature in the O_{1s} spectra of this sample. A successful reaction of both sur-KFR on P1-modified substrates is strongly verified by the N_{1s} measurements. The analyzed N_{1s} spectra are shown in Figure 5E. The appearance of the N_{1s} feature for both surface reactions corresponding samples (B and C) gives a clear evidence of the successful sur-KFR in both cases. Noteworthy, no N_{1s} signature was found for the non-functionalized PMSSQ–PStCHO surfaces. A successful modification of the surface is further proven by the observation of a F_{1s} signature (Binding energy: 689.0 eV)^[45] according to the sur-KFR R17 (Figure 5F). Thus, the formation of different α -amino phosphonates in all cases of the P1-functionalized surfaces with amines and dialkyl phosphonates is verified resuming our XPS observations (The fit results of all spectra are given as Supporting Information).

Table 2. Components used in sur-KFR starting from PMSSQ–PStCHO (P1).

Run	Amine	Dialkyl phosphonate
R1	4'-aminoacetanilide	Dimethyl phosphonate
R2	<i>p</i> -anisidine	Diisopropyl phosphonate
R3	4-(trifluoromethoxy) aniline	Diisopropyl phosphonate
R4	<i>p</i> -toluidine	Diisopropyl phosphonate
R5	4-bromoaniline	Diisopropyl phosphonate
R6	4'-aminoacetanilide	Diisopropyl phosphonate
R7	<i>p</i> -anisidine	Bis(2,2,2-trifluoroethyl) phosphonate
R8	4-(trifluoromethoxy) aniline	Bis(2,2,2-trifluoroethyl) phosphonate
R9	<i>p</i> -toluidine	Bis(2,2,2-trifluoroethyl) phosphonate
R10	4-bromoaniline	Bis(2,2,2-trifluoroethyl) phosphonate
R11	4'-aminoacetanilide	Bis(2,2,2-trifluoroethyl) phosphonate
R12	<i>p</i> -anisidine	Dibenzyl phosphonate
R13	4-(trifluoromethoxy) aniline	Dibenzyl phosphonate
R14	<i>p</i> -toluidine	Dibenzyl phosphonate
R15	4-bromoaniline	Dibenzyl phosphonate
R16	4'-aminoacetanilide	Dibenzyl phosphonate
R17	<i>p</i> -anisidine	Dibutyl phosphonate
R18	4-(trifluoromethoxy) aniline	Dibutyl phosphonate
R19	<i>p</i> -toluidine	Dibutyl phosphonate
R20	4-bromoaniline	Dibutyl phosphonate
R21	4'-aminoacetanilide	Dibutyl phosphonate
R22	4-bromoaniline	Dimethyl phosphonate

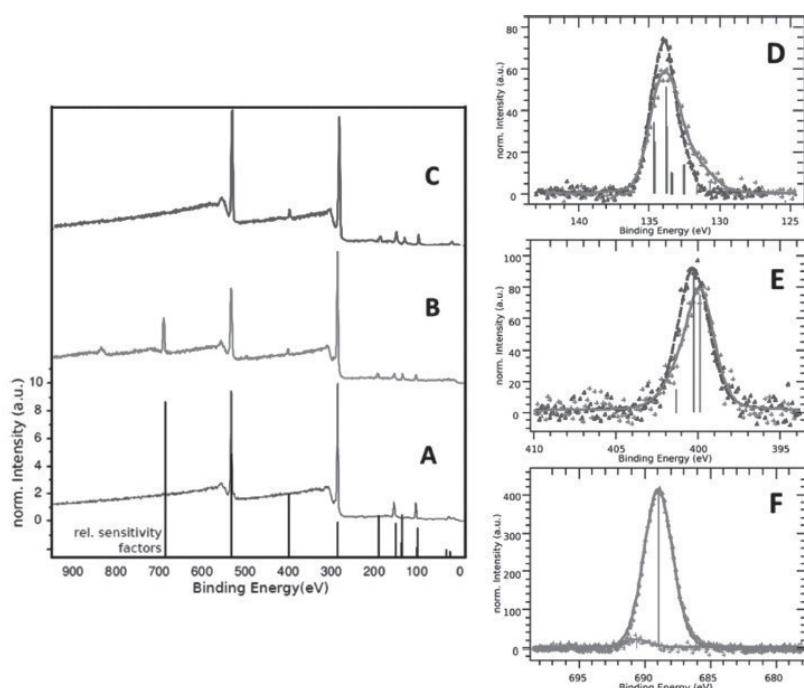


Figure 5. A) XPS analytics of P1-modified surfaces; B) after sur-KFR with R17; C) after sur-KFR with R13; D) $P_{2p3/2,1/2}$ spectra of (B) (solid curve) and of (C) (dashed curve); E) N_{1s} spectra of (B) (solid curve) and of (C) (dashed curve); F) F_{1s} spectra of (B) (dark gray curve) and nonfunctionalized PMSSQ-StCHO (light gray curve).^[54]

In order to show the direct advantages of sur-KFR, a library of different surfaces has been synthesized by employing various combinations of amines and dialkyl phosphonates and CA measurements of functionalized surfaces were conducted (Table 2). Based on the above-established sur-KFR, amines and dialkyl phosphonates featuring diverse functionalities were successfully integrated with high efficiency on substrate surfaces. As shown in Figure 6, advancing CA values varied between 91° and 102° , respectively, depending on the employed combination of amines and dialkyl phosphonates. This shows that despite the successful installation of polymeric α -amino phosphonates with diverse functionalities via sur-KFR, the obtained CAs did not vary dramatically due to the small chemical differences between the employed amines and dialkyl phosphonates.

2.4. Deprotection of α -amino Phosphonates in Solution

It is the aim of this work to establish of surface functionalization that allows facile and universal installation of zwitterionic α -amino phosphonic acids. Although deprotection of α -amino phosphonates is well established in organic chemistry, deprotection processes for polymeric α -amino phosphonates have not been studied in detail. Consequently, we first focused on establishing the deprotection process of polymeric α -amino phosphonates in

solution and then adopting it to the deprotection on surfaces. In order to achieve this, PStCHO was reacted with diisopropyl phosphonate and *p*-toluidine in 1,4-dioxane at 80°C under Ar atmosphere to afford polymeric α -amino phosphonates (P(St-AP-^{*i*}Pr)) according to an established KF-PMR protocol. Deprotection of α -amino phosphonates is known to be carried out by using either 1) HBr in aqueous medium or 2) TMSBr in polar organic solvents. Taking the limited solubility of P(St-AP-^{*i*}Pr) in water into account, the latter protocol was the only reasonable choice to be explored. Thus, deprotection of P(St-AP-^{*i*}Pr) was conducted in CH_3CN at 40°C in the presence of a large excess amount of TMSBr. As expected, the solubility of the deprotected polymer was dramatically different from that of P(St-AP-^{*i*}Pr). For example, THF was a good solvent for P(St-AP-^{*i*}Pr) but a poor solvent for the deprotected polymer, suggesting a clear increase in polarity of the deprotected polymer. As shown in Figure 7, the deprotection of the phosphonate moiety was confirmed by ^1H NMR spectroscopy.

To be precise, intensive peaks at 0.75 ppm and at 1.2 ppm owing to isopropyl groups disappeared completely. The peak at 5.4 ppm occurring after deprotection is due to acetic hydroxyl groups. Thus, the obtained polymer after deprotection can be clearly assigned to the targeted zwitterionic polymeric α -amino phosphonic acid (P(St-AP-OH)).

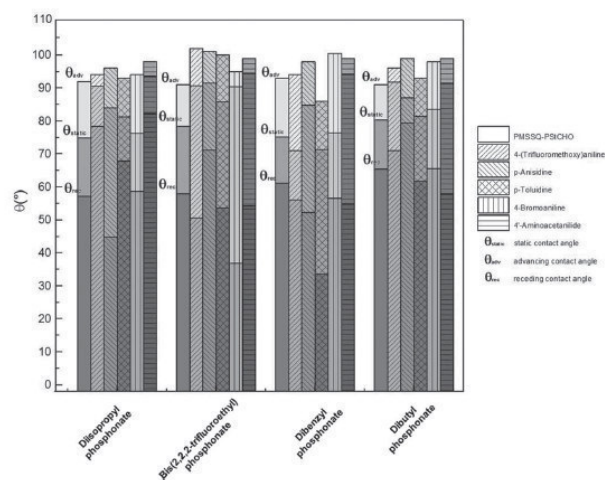


Figure 6. Water static contact angle (CA) and advancing/receding CA of P1 cured silicon surfaces before (not filled line) and after sur-KFR with various amines and dialkyl phosphonates.

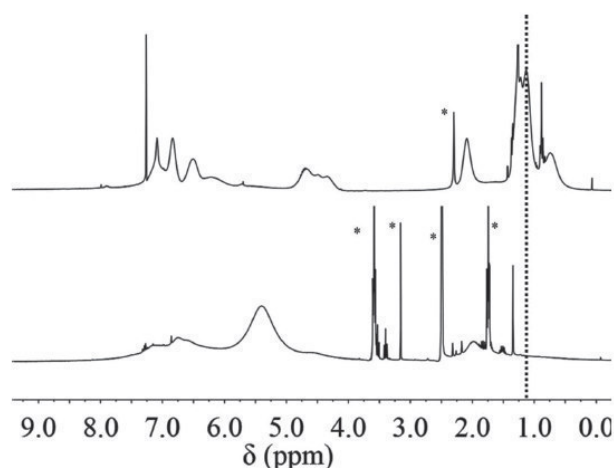


Figure 7. ^1H NMR spectra of P(St-AP-IPr) before (upper in CDCl_3) and after (lower in DMSO-d_6) deprotection reaction on P(St-AP-IPr) with TMSBr. The symbol (*) refers to peaks owing to residual solvents.

Furthermore, IR measurements of the polymers before and after the deprotection process provided further information on the successful deprotection reactions (Figure 8). The IR spectra of the polymers before and after the deprotection revealed that a strong band at 1380 cm^{-1} clearly disappeared. To give direct evidence that the phosphonate moiety was converted into phosphonic acids, ^{31}P NMR measurements before and after the deprotection reaction were conducted and revealed that an obvious peak at 20.8 ppm owing to phosphonates disappeared and a clear peak at 18.8 ppm owing to phosphonic acid developed (Figure 9). These experiments clearly supported

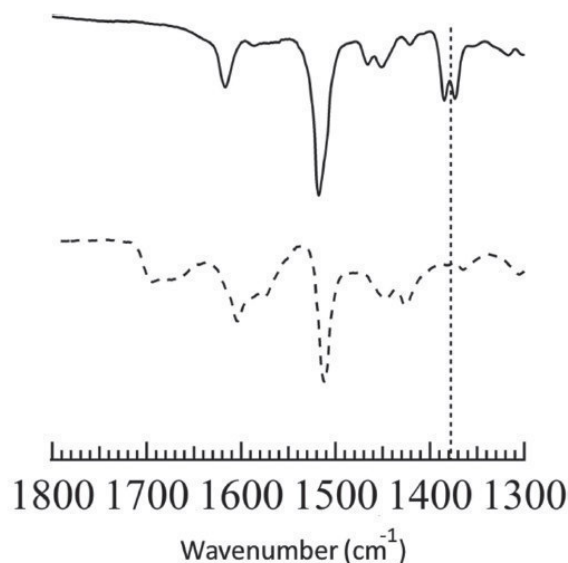


Figure 8. ATR-mode IR spectra of P(St-AP-IPr) before (solid line) and after (dashed line) deprotection reaction on P(St-AP-IPr) with TMSBr.

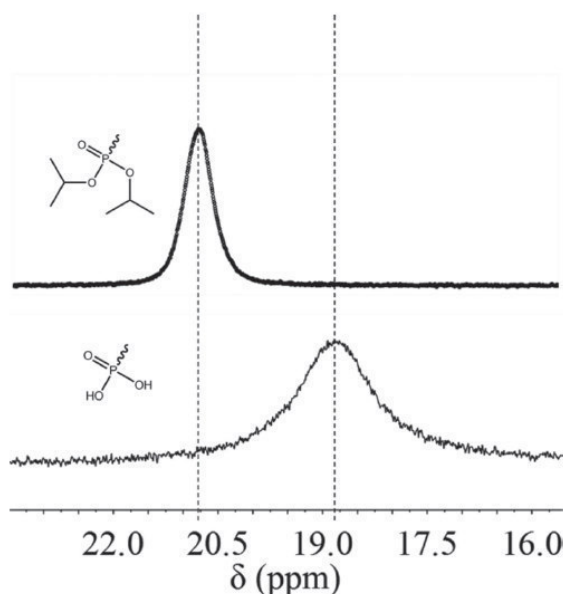


Figure 9. ^{31}P NMR spectra of P(St-AP-IPr) before (upper in CDCl_3) and after (lower in DMSO-d_6) deprotection reaction on P(St-AP-IPr) with TMSBr in the presence of triphenylphosphine as an internal reference.

a successful synthesis of polymeric α -amino phosphonic acids. The successful deprotection processes on polymers was compared to the KFR and subsequent deprotection with low-molecular-weight model compounds, which were monitored by using ^1H and ^{31}P NMR and IR spectroscopy measurements (see Supporting Information).

2.5. Synthesis of α -amino Phosphonic Acids on the Surface

In order to take advantage of sur-KFR, we finally targeted the synthesis of α -amino phosphonic acid moieties on the surfaces. Based on the above-mentioned deprotection reaction of polymeric α -amino phosphonates, deprotection of polymeric α -amino phosphonates immobilized on a silicon substrate was conducted. The deprotection reaction of substrates functionalized with polymeric α -amino phosphonates was conducted in acetonitrile in the presence of large excess amount of TMSBr at 40°C for 1 h (Table 2, R15). This deprotection of phosphonate moieties was confirmed by FT-IR measurements. The IR spectra of the silicon surfaces before and after sur-KFR (Figure 10) show that the peak at 1370 cm^{-1} owing to the alkyl ester groups of the phosphonates clearly disappeared after the deprotection, confirming a practically quantitative deprotection of phosphonate moieties.

As a direct consequence of the structural changes from α -amino phosphonates to α -amino phosphonic acids, the CA values decreased by 21° after deprotection (R5 in Figure 11). This decrease in CA angle is caused by

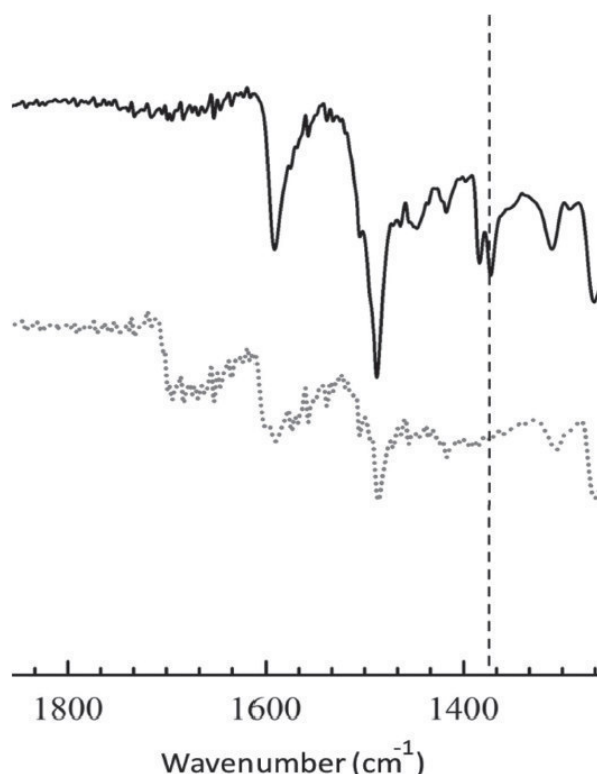


Figure 10. ATR-mode FT-IR spectra of silicon surfaces functionalized via sur-KFR with R5 before (solid line) and after (dashed line) the deprotection reaction with TMSBr.

the structural changes from a non-polar phosphonate ester to a polar zwitterionic α -amino phosphonic acid. Figure 12 summarizes the decrease of the water CAs after deprotection for numerous surfaces. Reduction of CAs up to 42° could be obtained for sur-KFR with 4-bromoaniline and dibenzyl phosphonate (Table 2, R15).

3. Conclusion

We successfully established a reliable and universal synthetic protocol that allows installation of α -amino phosphonic acid moieties on surfaces by taking advantage of the high reactivity and selectivity of the KFR. The successful KFR of aldehyde-functionalized surfaces with amines and dialkyl phosphonates was proven by precise analysis of the obtained surfaces, which included IR, EDX,

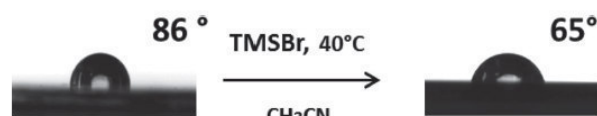


Figure 11. Water contact angle of silicon surfaces functionalized sur-KFR with R5 before (left) and after (right) the deprotection reaction with TMSBr.

and XPS measurements, confirming a practically quantitative conversion of aldehydes without any detectable structural defects. Afterwards, we have demonstrated a deprotection strategy for creating surfaces functionalized with zwitterionic species, thereby opening the possibilities for new anti-fouling surfaces.

4. Experimental Section

4.1. Materials

4-Vinyl benzaldehyde and PStCHO were synthesized according to previous reports.^[48] 2,2'-Azobisisobutyronitrile (AIBN) was recrystallized from diethylether. All other chemicals were commercially available and used without further purification unless otherwise stated.

4.2. Instrumentation

All ^1H and ^{13}C NMR spectra were recorded on Bruker 300 and 400 MHz FT-NMR spectrometers in deuterated solvents and chemical shifts (δ) were given in ppm with solvent peak as internal standard. ^{31}P NMR spectra were recorded on a Bruker 162 MHz FT-NMR spectrometer in deuterated solvents with triphenylphosphine as an internal reference (−6 ppm). Size-exclusion chromatography (SEC) was performed at room temperature in DMF containing 0.01 mol L^{−1} LiBr at a flow rate of 1.0 mL min^{−1}. The number-average molecular weight (M_n) and molecular weight distribution (M_w/M_n) of the polymers were calculated on the basis of a polystyrene calibration. Mass spectroscopy was measured by using Agilent 6224 ESI-TOF.

The PMSSQ–PStCHO coatings were prepared by spin-coating using of Laurell WS-650-MZ-23 PP at 3000 rpm for 15 s. The conversions of the reaction on the surface and film properties after reaction were investigated by Nocolet iS10 FT-IR spectrometer, JPK Nanowizard II AFM and EDX Zeiss MA 10. XPS measurements were recorded PHI 5600ci multitechnique spectrometer with monochromatic Al K α ($h\nu = 1486.6$ eV) radiation of 0.3 eV FWHM bandwidth. The spectra were analyzed performing a scaled Levenberg Marquardt fits, where Gaussian/Lorentzian combined profiles were used.^[49–51] The CA measurements were conducted using a DataPhysics OCA 20. In general, 46 samples have been measured, six data points on each sample. Subsequently, the average values of resulting measured data were calculated.

4.3. Kabachnik-Fields Post-polymerization Modification Reactions on Poly(4-vinyl benzaldehyde) with *p*-Toluidine and Diisopropyl Phosphonate in Solution to Produce Poly(St-AP-ⁱPr)

Under Ar atmosphere at 80 °C, diisopropyl phosphonate (3.8 mL, 22.6 mmol) was added to a dry dioxane solution (2.5 mL) of PStCHO (500 mg, [CHO]₀ = 3.8 mmol) and *p*-toluidine (1.22 g, 11.4 mmol). After the reaction mixture was stirred for 8 h at 80 °C, the reaction mixture was passed through silica gel. The filtrate was concentrated under vacuum. The obtained crude product was dissolved with small amount of THF and poured

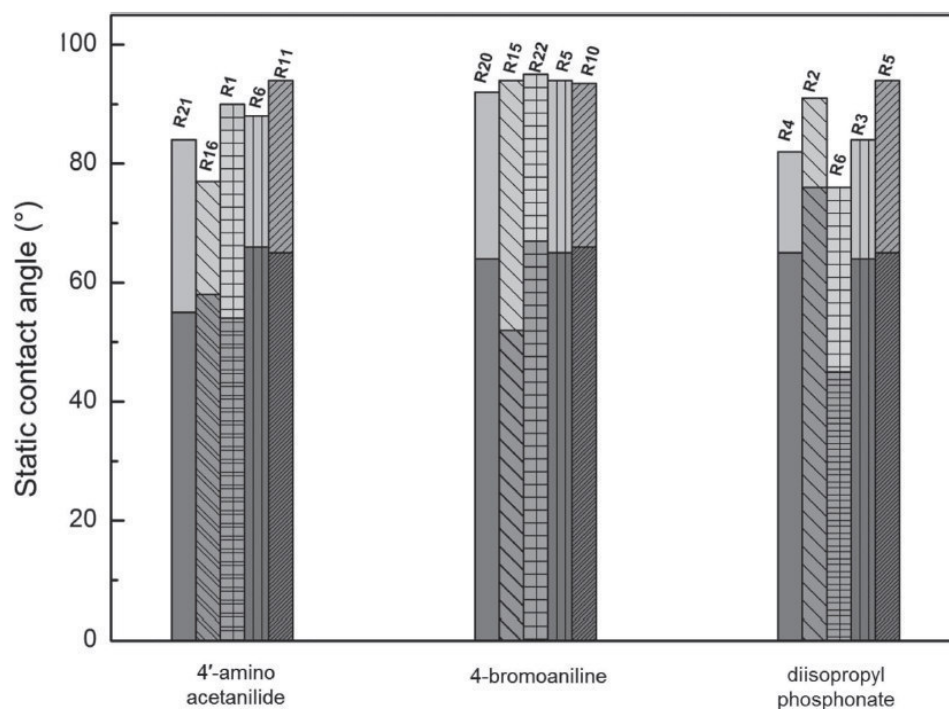


Figure 12. Water contact angle of P1 cured silicon surfaces after sur-KFR with various amines and dialkyl phosphonates (total columns) and after deprotection (lower part of columns).

into a large portion of hexane. The precipitate was dissolved in THF and passed through silica gel. The filtrate was concentrated under vacuum. The obtained crude product was dissolved with small amount of CH_2Cl_2 and poured into a large portion of hexane to produce P(St-AP- Pr) as a pale yellow powder. Yield: 1.35 g (91.5%). ^1H NMR (CDCl_3) δ : 6.97–7.23 (m, 4H); 6.84–6.93 (m, 4H), 5.18–6.65 (m, 4H); 3.95–5.10 (br, 4H); 2.08–2.22 (br, 3H); 0.75–1.40 (m, 12H). ^{31}P NMR (162 MHz, CDCl_3) δ : 20.8 ppm.

4.4. Deprotection Reactions on Polymeric α -Amino Phosphonates in Solution

Trimethylsilyl bromide (1.03 mL, 7.8 mmol) was added to a dry CH_3CN solution (1.5 mL) of P(St-AP- Pr) (300 mg, 0.78 mmol). After the reaction mixture was stirred for 16 h at 40 °C, 2 mL of methanol was added to the reaction mixture under open condition. After stirring for additional 1 h, the reaction mixture was diluted with MeOH. The MeOH solution was then poured into a large portion of THF. This cycle was repeated three times to give P(St-AP-OH) as a pale yellow solid. Yield: 205 mg (86.8%). ^1H NMR (300 MHz, CD_3OD) δ : 7.09–7.74 (m, 9H), 5.38 (br, H), 3.95–4.71 (br, 4H), 1.91 (br, 3H). ^{31}P NMR (162 MHz, CD_3CN) δ : 18.8.

4.5. Synthesis of PMSSQ macro-CTA

A preparation of inorganic macro-RAFT CTA was conducted by slightly modifying a previously reported method^[35] and the typical procedure was as follows: A dry THF solution (15 mL) containing dithio benzoic acid 4-ethyltrimethoxy-silylester (0.98 g, 2.5 mmol) was placed in a round bottomed flask. The reaction

mixture was cooled to 0 °C and methyltrimethoxysilane (MTMS, 3.47 g, 25 mmol) and 500 mmol water and 10 mmol HCl were added and stirred for 3 h at 0 °C. Afterwards, the reaction mixture was dissolved in diethyl ether, washed with water. After drying organic phase over MgSO_4 , ether was removed and the product was dried in high vacuum. Yield 3.32 g (1.46 mmol, 58.28%). ^1H NMR (CDCl_3) δ : 7.99 (br, 1H); 7.36 (br, 8H); 5.80 (br, 8H); 4.55 (br, 2H); 3.48 (br, 2H); 2.71 (br, 2H); 0.99 (br, 2H); 0.17 (br, 69.1H). $M_n = 2279 \text{ g mol}^{-1}$, PDI = 1.6.

4.6. Synthesis of PMSSQ-PStCHO

A DMSO solution (4 mL) of PMSSQ macro RAFT agent (0.5 g, 219.4 μmol), AIBN (10 mg, 60.89 μmol), and 4-vinylbenzaldehyde (1.0 g, 7.56 μmol) was placed in a Schlenk flask and degassed by freeze–thaw cycles. The degassed reaction mixture was stirred at 80 °C for 4 h and afterwards precipitated into methanol to afford a pale colored powder. Yield 0.91 g (0.042 mmol, 82%). ^1H NMR (300 MHz, $\text{DMSO}-d_6$) δ : 9.92 (br); 8.13–7.93 (br, 2H); 7.39–7.82 (br, 2H); 7.30–6.90 (br); 6.37–6.80 (br); 5.18–5.42 (br, 1H); 0.7–1.85 (br); 0.10 (br, H). $M_n = 21\,400 \text{ g mol}^{-1}$, PDI = 1.63.

4.7. Preparation of Functional Surfaces

4.7.1. Surface Coating and Modification

The 10 wt% polymer solution in THF was spin-coated onto clean substrates (30 s at 3000 rpm). Afterwards, the substrates were annealed at 130 °C for 2 h to cross-link the inorganic block and subsequently washed with THF to remove any remaining material.

4.7.2. Typical Procedures for Post-Modification on Surfaces

The aldehyde-modified substrate was placed in a Schlenk tube and purged with Argon atmosphere. Dry dioxane (1.5 mL) was charged into the reaction flask and heated to 80 °C under Ar atmosphere. Then, diisopropyl phosphonate (2.2 mL, 13.3 mmol) and *p*-anisidine (0.82 g, 6.6 mmol) were added and the reaction mixture was stirred for 6 h at 80 °C. Subsequently, the fictionalized substrate was washed with THF and dried in vacuum at 40 °C.

FT-IR (ATR mode): 2931 cm⁻¹ (C—H valence band), 1618 cm⁻¹ (C=N stretching vibration), 1510 cm⁻¹ (P=O vibration), 1452 cm⁻¹ (CH₃ deformation vibration), 1368 cm⁻¹ (C—H deformation vibration), 1233 cm⁻¹ (C=H deformation relation), 1101 cm⁻¹ (P=O stretching vibration), 985 cm⁻¹ (O—Si—O stretching vibration), 821 cm⁻¹ (C=H deformation vibration).

4.7.3. Deprotection of Polymeric α -amino Phosphonates on the Surface

By KF-PMR functionalized substrate was placed in a Schlenk tube. 1.65 mL (9.29 mmol) trimethylsilyl bromide was added to a 2.4 mL dry acetonitrile solution under Ar atmosphere at room temperature. The reaction mixture was stirred for 2 h at 40 °C. Then, 3.25 mL methanol was added under open conditions and it was stirred for 1 h. Subsequently, substrate was washed with methanol and THF and died in vacuum at 40 °C. FT-IR (ATR mode): 3357 cm⁻¹ (broad O—H and N—H stretching vibration), 2924 cm⁻¹ (C—H stretching vibration), 1691 cm⁻¹ (P—OH deformation vibration), 1510 cm⁻¹ (P=O stretching vibration).

4.8. Characterization of Functional Surfaces

4.8.1. XPS Measurements

X-ray photoelectron spectroscopy (PHI 5600ci multitechnique spectrometer with monochromatic Al K α ($h\nu = 1486.6$ eV) radiation of 0.3 eV FWHM bandwidth) was used for determining the composition of the films before and after the KF-PMR. The resolution of the analyzer was 1.5% of the pass energy, which is about 0.4 eV. All spectra were obtained using a 400 μ m diameter analysis area. An emission angle of about $15 \pm 5^\circ$ was given adjusting the sample to ensure a surface-sensitive detection measurement. The pressure in the main chamber was kept within the range of 10^{-8} mbar. The sample was kept at room temperature (see Supporting Information). The spectra were recorded in a surface-sensitive detection. This ensures a depth of information of about 0.8 nm referring to a mean free path about 2.9 nm (for C_{1s} emission).^[52] The axis of binding energy is aligned with respect to the C_{1s} aliphatic feature, which is set to 285 eV.^[53] The recorded data (P_{2p} , N_{1s} , O_{1s} , F_{1s}) are scaled referring to the C_{1s} raw area (range: 274.3 eV (BE)–295.7 eV (BE)), respectively. The baselines are obtained by a Shirley background subtraction.^[54] The spectra were analyzed performing a scaled Levenberg Marquardt fits, where Gaussian/Lorentian combined profiles were used.^[52,55,56]

Acknowledgements: The authors thank Dr. H. Heller, Institute for Physical Chemistry, University of Hamburg, for assistance

with the EDX measurements and data analysis. Dr. R. Kakuchi, Institute of Science and Engineering, Kanazawa University, is greatly acknowledged for investigations of KF-PMR of low-molecular species and his support during the preparation of the manuscript.

Received: December 9, 2014; Revised: January 9, 2015;
Published online: February 6, 2015; DOI: 10.1002/macp.201400591

Keywords: hybrid polymer; surface functionalization; post-polymerization modification; Kabachnik-Fields; α -amino phosphonates

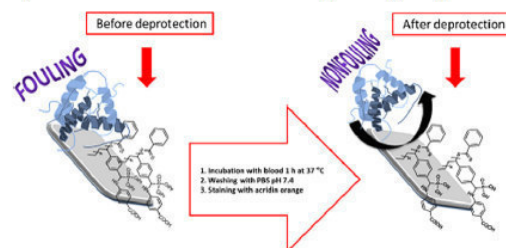
- [1] J.-F. Lutz, *Angew. Chem. Int. Ed.* **2007**, *46*, 1018.
- [2] P. L. Golas, K. Matyjaszewski, *Chem. Soc. Rev.* **2010**, *39*, 1338.
- [3] C. E. Hoyle, A. B. Lowe, C. N. Bowman, *Chem. Soc. Rev.* **2009**, *39*, 1355.
- [4] F. Biedermann, E. A. Appel, J. del Barrio, T. Gruending, C. Barner-Kowollik, O. A. Scherman, *Macromolecules* **2011**, *44*, 4828.
- [5] R. K. Iha, K. L. Wooley, A. M. Nyström, D. J. Burke, M. J. Kade, C. J. Hawker, *Chem. Rev.* **2009**, *109*, 5620.
- [6] C. Barner-Kowollik, F. E. Du Prez, P. Espeel, C. J. Hawker, T. Junkers, H. Schlaad, W. V. Camp, *Angew. Chem. Int. Ed.* **2011**, *50*, 60.
- [7] R. Hoogenboom, *Angew. Chem., Int. Ed.* **2010**, *49*, 3415.
- [8] P. Theato, *J. Polym. Sci., Part A: Polym. Chem.* **2008**, *46*, 6677.
- [9] R. Kakuchi, *Angew. Chem. Int. Ed.* **2014**, *53*, 46.
- [10] *Multicomponent reactions* (Eds: J. Zhu, H. Bienayme), Wiley-VCH, Weinheim, Germany, **2005**.
- [11] Q. Li, H. Zhou, D. A. Wicks, C. E. Hoyle, D. H. Magers, H. R. McAlexander, *Macromolecules* **2009**, *42*, 824.
- [12] I. Ugi, D. U. Fetzer, U. Eholzer, H. Knupfer, K. Offermann, *Angew. Chem. Int. Ed.* **1965**, *4*.
- [13] B. Yang, Y. Zhao, C. Fu, C. Zhu, Y. Zhang, S. Wang, Y. Wei, L. Tao, *Polym. Chem.* **2014**, *5*, 2704.
- [14] Y. Zhao, B. Yang, C. Zhu, Y. Zhang, S. Wang, C. Fu, Y. Wei, L. Tao, *Polym. Chem.* **2014**, *5*, 2695.
- [15] C. Zhu, B. Yang, Y. Zhao, C. Fu, L. Tao, Y. Wei, *Polym. Chem.* **2013**, *4*, 5395.
- [16] P. Biginelli, *Gazz. Chim. Ital.* **1893**, *23*, 360.
- [17] C. V. Robotham, C. B. B. Cuevas, K. Abboud, D. L. Wright, *Mol. Diversity* **2003**, *6*, 237.
- [18] A. Rahmati, T. Kenarkoobi, M. Ahmadi-Varzaneh, *Mol. Diversity* **2013**, *17*, 619.
- [19] D. B. Ramachary, S. Jain, *Org. Biomol. Chem.* **2011**, *9*, 1277.
- [20] N. Isambert, M. del Mar Sanchez Duque, J. C. Plaquevent, Y. Genisson, J. Rodriguez, T. Constantieux, *Chem. Soc. Rev.* **2011**, *40*, 1347.
- [21] Y. Zhang, Y. Zhao, B. Yang, C. Zhu, Y. Wei, L. Tao, *Polym. Chem.* **2014**, *5*, 1857.
- [22] G. Keglevich, E. Bálint, *Molecules* **2012**, *17*, 12821.
- [23] A. B. Lowe, C. L. McCormick, *Chem. Rev.* **2002**, *102*, 4177.
- [24] R. Wang, A. B. Lowe, *J. Polym. Sci., A: Polym. Chem.* **2007**, *45*, 2468.
- [25] Y. Iwasaki, N. Nakabayashi, K. Ishihara, *Anal. Bioanal. Chem.* **2005**, *381*, 534.
- [26] L. Xu, P. Ma, B. Yuan, Q. Chen, S. Lin, X. Chen, Z. Hua, J. Shen, *RSC Adv.* **2014**, *4*, 15030.
- [27] P. Liu, Q. Chen, L. Li, S. Lin, J. Shen, *J. Mater. Chem. B* **2014**, *2*, 7222.

- [28] A. L. Gui, E. Luais, J. R. Peterson, J. J. Gooding, *ACS Appl. Mater. Interfaces* **2013**, *5*, 4827.
- [29] S. Chen, L. Li, C. Zhao, J. Zheng, *Polymer* **2010**, *51*, 5283.
- [30] R. Yang, J. Xu, G. Ozaydin-Ince, S. Y. Wong, K. K. Gleason, *Chem. Mater.* **2011**, *23*, 1263.
- [31] X. Shen, Y. Zhao, L. Chen, *Biofouling* **2013**, *29*, 991.
- [32] W. Zhao, Q. Ye, H. Hu, X. Wang, F. Zhou, *J. Mater. Chem. B* **2014**, *2*, 5352.
- [33] R. Yang, K. K. Gleason, *Langmuir* **2012**, *28*, 12266.
- [34] K. Shiraishi, T. Ohnishi, K. Sugiyama, K. Okada, O. Matsuo, *Chem. Lett.* **1997**, *26*, 863.
- [35] K. Shiraishi, M. Kohta, K. Sugiyama, *Chem. Lett.* **2004**, *33*, 646.
- [36] R. Kakuchi, P. Theato, *Polym. Chem.* **2014**, *5*, 2320.
- [37] R. Kakuchi, P. Theato, *ACS Macro Lett.* **2014**, *3*, 329.
- [38] D. Kessler, F. D. Jochum, J. Choi, K. Char, P. Theato, *ACS Appl. Mater. Interfaces* **2011**, *3*, 124.
- [39] D. Kessler, N. Metz, P. Theato, *Macromol. Symp.* **2007**, *254*, 34.
- [40] D. Kessler, P. J. Roth, P. Theato, *Langmuir* **2009**, *25*, 10068.
- [41] D. Kessler, P. Théato, *Macromol. Symp.* **2007**, *249–250*, 424.
- [42] T. P. Russell, *Science* **2002**, *297*, 964.
- [43] D. Kessler, M. C. Lechmann, S. Noh, R. Berger, C. Lee, J. S. Gutmann, P. Theato, *Macromol. Rapid Commun.* **2009**, *30*, 1238.
- [44] K. T. Wiss, D. Kessler, T. J. Wendorff, P. Theato, *Macromol. Chem. Phys.* **2009**, *210*, 1201.
- [45] D. Kessler, C. Teutsch, P. Theato, *Macromol. Chem. Phys.* **2008**, *209*, 1437.
- [46] D. Kessler, H. Löwe, P. Theato, *Macromol. Chem. Phys.* **2009**, *210*, 807.
- [47] D. Kessler, P. Théato, *Macromolecules* **2008**, *41*, 5237.
- [48] G. Sun, C. Cheng, K. L. Wooley, *Macromolecules* **2007**, *40*, 793.
- [49] W. H. Press, S. A. Teukolsky, W. T. Vetterling, P. B. Flannery, *Numerical Recipes: The Art of Scientific Computing*, 3rd ed., Cambridge University Press, Cambridge, UK, **2007**, p. 656.
- [50] R. Hesse, P. Streubel, R. Szargan, *Surf. Interface Anal.* **2007**, *39*, 381.
- [51] S. Evans, *Surf. Interface Anal.* **1991**, *17*, 85.
- [52] G. Beamson, D. Briggs, *The Scienta ESCA300 Database*, Wiley & Sons, New York **1992**.
- [53] P. A. Bertrand, *J. Vac. Sci. Technol.* **1981**, *18*, 28.
- [54] J. Scofield, *J. Electron. Spectrosc. Relat. Phenom.* **1976**, *8*, 129–137.
- [55] Y. X. Ni, B. Feng, J. Wang, X. Lu, S. Qu, J. Wenig, *J. Mater. Sci.* **2009**, *44*, 4031.
- [56] P. R. Davies, N. G. Newton, *Appl. Surf. Sci.* **2001**, *181*, 296.

Investigation of Antifouling Properties of Surfaces Featuring Zwitterionic α -Aminophosphonic Acid Moieties

Natalie Wagner, Phyllis Zimmermann, Peter Heisig, Franziska Klitsche, Wolfgang Maison, Patrick Theato*

Zwitterionic thin films containing α -amino phosphonic acid moieties were successfully introduced on silicon surfaces and their antifouling properties were investigated. Initially, the substrates were modified with a hybrid polymer, composed of poly(methylsilsesquioxane) (PMSSQ) and poly(4-vinyl benzaldehyde) (PStCHO). Next, a Kabachnik–Fields post-polymerization modification (*sur*-KF-PMR) of the functionalized aldehyde surfaces was conducted with different amines and dialkyl phosphonates. After subsequent deprotection reaction of dialkyl phosphonates, the obtained zwitterionic surfaces were characterized by various techniques and we found excellent antifouling properties of the resulting films.



1. Introduction

Polymer science has diversified dramatically over the last decades. Applications range from simple elastic and daily-use polymers, such as polyethylene, polypropylene, and PMMA (poly (methyl methacrylate)), to polymers with more specific and advanced features targeting interdisciplinary areas, in particular directed toward biological and medical applications.^[1–5] In this context, the installation of naturally occurring molecules such as amino acids, peptides, or sugars onto polymer structures is a rational

synthetic strategy to produce biocompatible and/or bio-active polymers that take advantage of the bio-related functionality directly originating from the installed naturally occurring units. Amino acid containing polymers are a very established class of materials. In contrast, the introduction of the corresponding α -amino phosphonic acid on polymer chains is still in its infancy, mainly due to missing synthetic protocols. In particular, it is of great interest to maintain the zwitterionic nature of α -amino phosphonic acids when conjugated to polymers, because it could be shown that surfaces featuring zwitterionic structures can be used as a protection against protein absorption, i.e., prevent biofouling.^[6–9]

The zwitterionic nature has been revealed to play a unique and indispensable role in polymer chemistry and its solution physics. Zwitterionic polymers possess two very distinguishing properties: (1) antifouling properties and (2) stealth properties in media such as blood.^[10–12] The reduction of the protein adsorption on surfaces has been a very big challenge within the last three decades because of its essential role in various medical, biochemical, marine, industrial applications, and in water purification systems. Many different polymers have been used as non-fouling

P. Theato, N. Wagner

Institute for Technical and Macromolecular Chemistry, University of Hamburg, Bundesstr. 45, D-20146 Hamburg, Germany
E-mail: theato@chemie.uni-hamburg.de

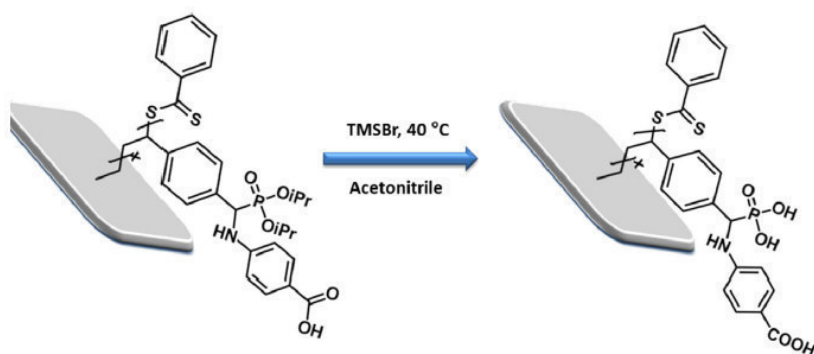
Fax: +49 (0) 40 42838 6008

P. Zimmermann, P. Heisig

Institute of Biochemistry, Pharmaceutical Biology and Microbiology, University of Hamburg, Bundesstr. 45, D-20146 Hamburg, Germany

F. Klitsche, W. Maison

Institute of Pharmacy, University of Hamburg, Bundesstr. 45, D-20146 Hamburg, Germany



■ Scheme 1. Deprotection reaction of *sur*-KFR-modified substrate surfaces.

materials with the most prominent example being poly(ethylene glycol) (PEG). But also zwitterionic polymers, such as poly(sulfobetaine methacrylate) (PSBMA), have been found to provide non-fouling properties. Polymers incorporating zwitterionic moieties, for example, phosphorylcholine and carboxybetaine are excellent candidates for the creation of antifouling surfaces due to their anionic and cationic terminal groups, which form a strong hydration layer as an effect of the solvation of the charged groups.^[13–21,22]

In the present study, we report on the generation of zwitterionic moieties on the poly(methylsilsequioxane)-poly(4-vinyl-benzaldehyde) (PMSSQ-PStCHO)-modified silicon surfaces based on surface Kabachnik–Fields reaction (*sur*-KFR) to install polymeric α -aminophosphonates and the subsequent deprotection of phosphonate groups (Scheme 1).^[23–27]

2. Results and Discussion

2.1. Synthesis of α -Aminophosphonic Acids on the Surface

Herein, we are investigating the synthesis of α -aminophosphonic acids on the surface. For this, we conducted a surface Kabachnik–Fields reaction (*sur*-KFR) to install polymeric α -aminophosphonates starting from a poly(methylsilsequioxane)-poly(4-vinyl-benzaldehyde) (PMSSQ-PStCHO) coating. Next, the deprotection of polymeric α -aminophosphonates immobilized on a silicon substrate was conducted.^[28]

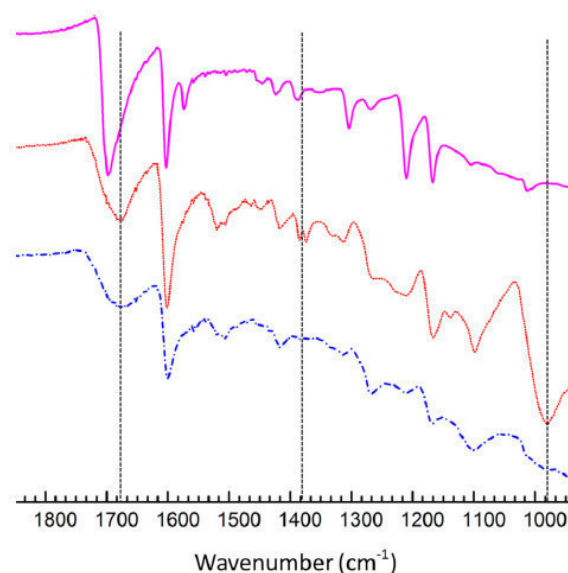
The deprotection reaction of substrates functionalized with diisopropyl phosphonate/4-aminobenzoic acid by *sur*-KFR was carried out in acetonitrile in the presence of a large excess of TMSBr at 40 °C for 1 h. Successful deprotection of the phosphonate moieties was confirmed by FT-IR measurements. The IR spectra of the silicon surfaces before and after *sur*-KFR (Figure 1) clearly showed that the peak at 1370 cm^{-1} owing to the alkyl ester groups of the

phosphonates, which disappeared after the deprotection, confirming a practically quantitative deprotection of phosphonate moieties.

Additionally, the water contact angle (CA) was measured on the obtained surfaces. Because of the structural changes on the film surface after *sur*-KFR with 4-aminobenzoic acid/diisopropyl phosphonate and after deprotection reactions with TMSBr, the CA values decreased by 8° and by 22°, respectively (Figure 2). This reduction of the contact angle proves the formation of a more polar surface, which can be explained by

the formation of zwitterionic α -aminophosphonic acid moieties on the silicon substrate surface.

It can be expected that variations of the amine used in the KFR will have an influence on the contact angles of the surface. Figure 3 illustrates the decrease of the water contact angles of PMSSQ-PStCHO-modified silicon substrates, after *sur*-KFR with three different aromatic amines and after the subsequent deprotection reaction. This decrease in the CA angle is a direct consequence of the structural changes from a non-polar phosphonate to a polar zwitterionic α -aminophosphonic acid. For all cases, a reduction of contact angles after deprotection could be observed. In the case for the *sur*-KFR with *p*-aminobenzoic



■ Figure 1. ATR-mode FT-IR spectra of silicon surfaces after modification with PMSSQ-PStCHO (pink), functionalized via *sur*-KFR with diisopropyl phosphonate/4-aminobenzoic acid (red-dashed line) and after the deprotection reaction with TMSBr (blue-dashed line).

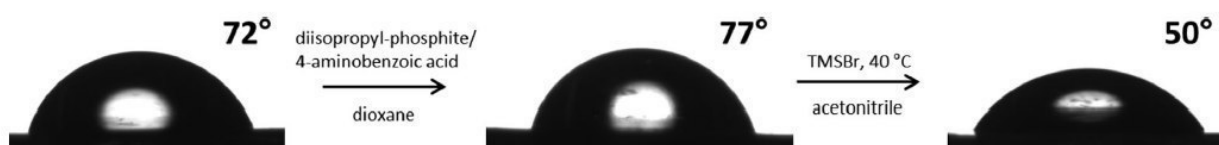


Figure 2. Water contact angle of PMSSQ-PStCHO-modified silicon surfaces before and after functionalization via *sur*-KFR with diisopropyl phosphonate/4-aminobenzoic acid and after the deprotection reaction with TMSBr.

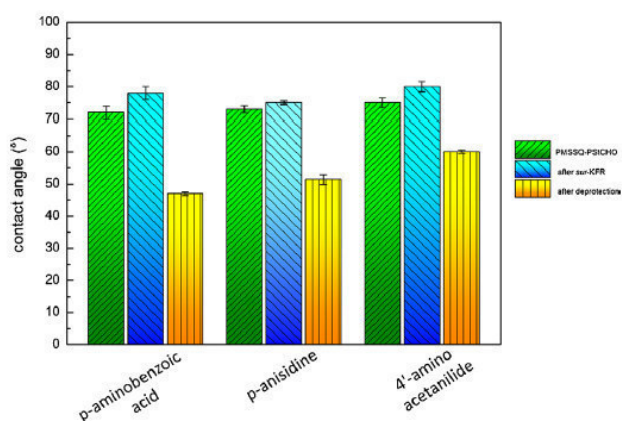


Figure 3. Water static contact angle of PMSSQ-PStCHO-cured silicon surfaces before and after *sur*-KFR with various amines and diisopropyl phosphonates.

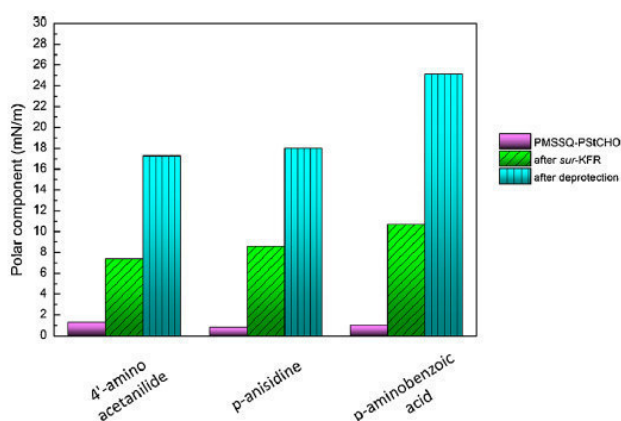


Figure 4. Polar component of PMSSQ-PStCHO-cured silicon surfaces, after *sur*-KFR and after deprotection reaction with various amines and diisopropyl phosphonates.

acid and diisopropyl phosphonate the largest decrease in CA of 31° was observed. Further, the obtained CA depends on the hydrophobicity of the employed amine, which it can be seen when comparing surfaces with *p*-aminobenzoic acid and 4'-aminoacetanilide. Surfaces functionalized with *p*-aminobenzoic acid resulted in a final contact angle of 50° after deprotection, while surface prepared from 4'-aminoacetanilide showed a contact angle of 60° after deprotection.

Based on the results of the CA measurements, the surface energy (SE) and the polar components of α -aminophosphonic acid-containing surfaces were calculated using SCA 20 SE calculation software with the method of OWRK (Owens, Wendt, Rabel, and Kaelble) (Data Physics OCA 20, Hamburg). In this method, SE is formed by the components of dispersive and polar SE, whereas the interfacial energy γ_{sl} is determined by the contribution of water or diiodomethane and the delaminated surface is calculated by forming the geometric mean. The model leads to the following relationship:

$$\gamma_{sl} = \gamma_s + \gamma_l - 2 \left(\sqrt{\gamma_s^d \cdot \gamma_l^d} + \sqrt{\gamma_s^p \cdot \gamma_l^p} \right)$$

where γ_s^d and γ_s^p are the dispersive and polar parts of the solid, and γ_l^d , γ_l^p are the respective contributions of the liquid.^[29,30]

In Figure 4, the trends of surface energy are shown. It can be concluded that the polar component of surfaces increased moderately after *sur*-KFR and increased remarkably after deprotection, proving the installation of zwitterionic α -aminophosphonic acid moieties. The highest polar component could be determined after deprotection reaction of a silicon wafer that was modified with diisopropyl phosphonates and *p*-aminobenzoic acid during *sur*-KFR.

2.2. Blood Adsorption Assays on the Zwitterionic Moieties-Bearing Surfaces

Next, first antifouling properties were investigated by a qualitative protein adsorption assay using human blood stabilized with EDTA.^[31] For this purpose, *sur*-KFR functionalized and deprotected silicon substrates were incubated with blood for 1 h at 37 °C. Subsequently, the obtained surfaces were washed with PBS buffer solution (pH 7.4) and stained by dipping them into an aqueous solution of acridine orange for 10 min at room temperature. After washing with water and PBS buffer, the obtained substrates were analyzed by fluorescence microscopy. Figure 5 shows the resulting fluorescence images, which exhibited a high level of adsorption of biomaterial on the *sur*-KFR-functionalized surface (A), while after deprotection the zwitterionic α -aminophosphonic

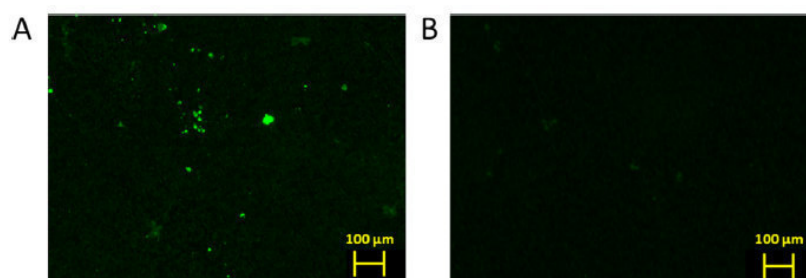


Figure 5. Fluorescence images after incubation with human blood (1 h) and acridine orange staining. Silicon surfaces after *sur*-KFR functionalization with 4'-aminoacetanilide/bis(2,2,2-trifluoroethyl) phosphonate (A) and after deprotection reaction with TMSBr (B).

acid moieties bearing surfaces were almost free of adsorbed biomaterial.

2.3. Comparative Bacterial Adhesion Test With Skin Colonizing Bacteria

Additionally, bacterial adsorption assays on the zwitterionic surfaces were conducted by incubation with *Staphylococcus*

epidermidis (skin colonizing bacteria). The *sur*-KFR-functionalized surfaces and deprotected substrates were incubated with bacteria, subsequently washed, and plated onto a petri dish containing agar. After additional incubation overnight, the images of the obtained surfaces were captured in white light using the Desaga CabUVis viewing system combined with a digital camera and Providoc Software.

Figure 6 shows the antifouling effect of the obtained polymer films after *sur*-KFR (F) with *p*-anisidine/diisopropyl phosphonate and after subsequent deprotec-

tion reaction with TMSBr (E). The surfaces containing α -aminophosphonic acid zwitterionic moieties exhibited a clear antifouling effect with almost no bacterial colonization on the coated silicon substrates.

In contrast to the zwitterionic coatings (Figure S3C, D, and E), the uncoated silicon substrate surface and PMSSQ–PStCHO-modified substrate (Figure S3 A and B) showed growth of bacterial cells.

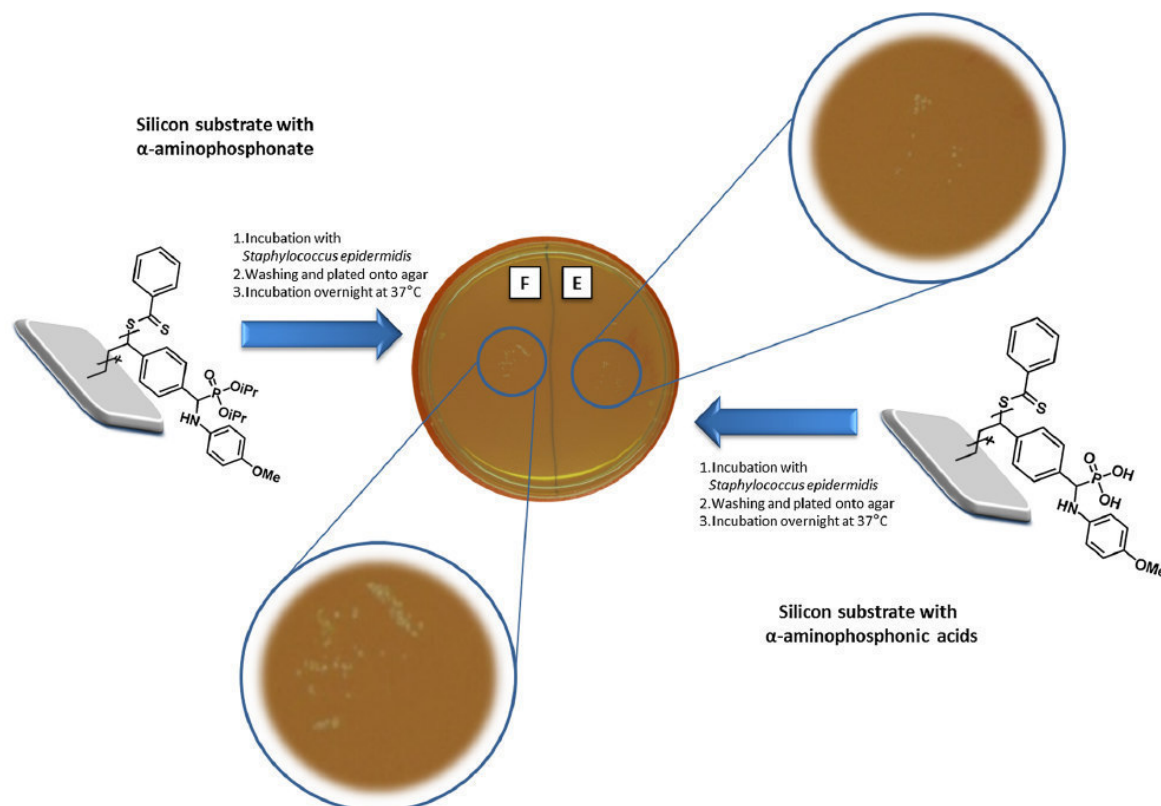


Figure 6. Antifouling assay on silicone substrates. Incubation of surfaces after *sur*-KFR treatment with *p*-anisidine/diisopropyl phosphonate (F) and after deprotection reaction with TMSBr (E) with *S. epidermidis*.

3. Conclusion

We have demonstrated an effective two-step approach to integrate zwitterionic α -aminophosphonic acids onto substrate surfaces, which were shown to provide antifouling effects. After successful *sur*-KFR treatment of aldehyde-functionalized surfaces with amines and dialkyl phosphonates, deprotection reactions were conducted in order to create zwitterionic-functionalized polymer surfaces on substrates. The obtained zwitterionic-functionalized polymer substrates exhibited a low protein adsorption in PBS buffer and showed reduced adhesion properties against *S. epidermidis* cells.

4. Experimental Section

4.1. Materials

4-Vinyl benzaldehyde (StCHO) and poly(4-vinyl benzaldehyde) (PStCHO) were synthesized according to previous reports.^[32] PMSSQ Macro-CTA and PMSSQ-PStCHO were synthesized as described in ref.^[28]

4.2. Instrumentation

All ^1H and ^{13}C NMR spectra were recorded on Bruker 300 and 400 MHz FT-NMR spectrometers in deuterated solvents, and chemical shifts (δ) were given in ppm with solvent peak as internal standard. The number-average of the molecular weight (\overline{M}_n) and molecular weight distribution ($\overline{M}_w/\overline{M}_n$) of the polymers were calculated on the basis of a polystyrene calibration. Mass spectroscopy was measured by using Agilent 6224 ESI-TOF.

The PMSSQ-PStCHO coatings were prepared by spin-coating a solution in THF (10 wt%) using a Laurell WS-650-MZ-23 PP at 3000 rpm for 15 s. The conversions of the reaction on the surface and the film properties after the reaction were investigated by a Nicolet iS10 FT-IR spectrometer.

The CA measurements were conducted using a DataPhysics OCA 20. The fluorescence images were taken using a fluorescence microscope Leica CTR6000. The surface energy was characterized by water contact angle measurement using a DataPhysics OCA 20 device.

4.2.1. Synthesis of PMSSQ Macro-CTA

A preparation of inorganic macro-RAFT CTA was conducted by slightly modifying a previously reported method^[33] and the typical procedure was as follows: a dry THF solution (15 mL) containing dithio benzoic acid 4-ethyltrimethoxy-silylester (0.98 g, 2.5 mmol) was placed in a round-bottomed flask. The reaction mixture was cooled to 0 °C and methyltrimethoxysilane (MTMS, 3.47 g, 25 mmol) and 500 mmol water and 10 mmol HCl were added and stirred for 3 h at 0 °C. Afterward, the reaction mixture was dissolved in diethyl ether, washed with water. After drying organic phase over MgSO_4 , the ether was removed and the product was dried in high vacuum. Yield 3.32 g (1.46 mmol, 58%). ^1H -NMR (CDCl_3) δ : 7.99 (br, 1H); 7.36

(br, 8H); 5.80 (br, 8H); 4.55 (br, 2H); 3.48 (br, 2H); 2.71 (br, 2H); 0.99 (br, 2H); 0.17 (br, 69.1H). ^{13}C -NMR (300 MHz, CDCl_3) δ : 132.86; 129.84; 128.80; 127.34; 68.43; 26.06. $\overline{M}_n = 2\,279\text{ g} \cdot \text{mol}^{-1}$, PDI = 1.6.

4.2.2. Synthesis of PMSSQ-PStCHO

A DMSO solution (4 mL) of PMSSQ macro RAFT agent (0.5 g, 219.4 μmol), AIBN (10 mg, 60.89 μmol), and 4-vinylbenzaldehyde (1.0 g, 7.56 μmol) was placed in a Schlenk flask and degassed by freeze-thaw cycles. The degassed reaction mixture was stirred at 80 °C for 4 h and afterward precipitated into methanol to afford a pale-colored powder. Yield 0.91 g (0.042 mmol, 82%). ^1H -NMR (300 MHz, $\text{DMSO}-d_6$) δ : 9.92 (br); 8.13–7.93 (br, 2H); 7.39–7.82 (br, 2H); 7.30–6.90 (br); 6.37–6.80 (br); 5.18–5.42 (br, 1H); 0.7–1.85 (br); 0.10 (br, H). ^{13}C -NMR (300 MHz, $\text{DMSO}-d_6$) δ : 236.66; 192.80; 134.69; 129.89; 128.07; 99.79. $\overline{M}_n = 21\,400\text{ g} \cdot \text{mol}^{-1}$, PDI = 1.63.

4.3. Preparation of Functional Surfaces

4.3.1. Surface Coating and Modification

The 10 wt% polymer solution in THF was spin-coated onto clean substrates (15 s at 3000 rpm). Afterward, the substrates were annealed at 130 °C for 2 h to crosslink the inorganic block and subsequently washed with THF to remove any remaining material.

4.4. Typical Procedures for Post-Modification on Surfaces

The aldehyde-modified substrate was placed in a Schlenk tube and purged with Argon atmosphere. Dry dioxane (1.5 mL) was charged into the reaction flask and heated to 80 °C under Ar atmosphere. Then, diisopropyl phosphonate (2.2 mL, 13.3 mmol) and 4-amino-benzoic acid (0.90 g, 6.6 mmol) were added and the reaction mixture was stirred for 6 h at 80 °C. Subsequently, the functionalized substrate was washed with THF and dried in vacuum at 40 °C.

FT-IR (ATR mode): 2931 $\cdot \text{cm}^{-1}$ (C–H valence band), 1684 $\cdot \text{cm}^{-1}$ (C=O stretching vibration), 1605 $\cdot \text{cm}^{-1}$ (C=N stretching vibration), 1517 $\cdot \text{cm}^{-1}$ (P=O vibration), 1452 $\cdot \text{cm}^{-1}$ (CH_3 deformation vibration), 1379 $\cdot \text{cm}^{-1}$ (C–H deformation vibration), 1164 $\cdot \text{cm}^{-1}$ (C–H deformation relation), 1096 $\cdot \text{cm}^{-1}$ (P=O stretching vibration), 976 $\cdot \text{cm}^{-1}$ (O–Si–O stretching vibration).

4.5. Deprotection of Polymeric α -Aminophosphonates on the Surface

The substrate, which had previously been functionalized by Kabachnik–Fields post-polymerization modification reaction, was placed in a Schlenk tube. 1.65 mL (9.29 mmol) of trimethylsilyl bromide was added to a 2.4 mL dry acetonitrile solution under Ar atmosphere at room temperature. The reaction mixture was stirred for 2 h at 40 °C. Then 3.25 mL methanol was added under open conditions, and the mixture was then stirred for 1 h. Subsequently, the substrate was washed with methanol and THF and dried in vacuum at 40 °C. FT-IR (ATR mode): 3357 $\cdot \text{cm}^{-1}$ (broad O–H and N–H stretching vibration), 2924 $\cdot \text{cm}^{-1}$ (C–H stretching vibration), 1679 $\cdot \text{cm}^{-1}$ (P–OH deformation vibration), 1510 $\cdot \text{cm}^{-1}$ (P=O stretching vibration).

4.6. Fouling Assay With Human Blood

The surfaces bearing zwitterionic moieties were washed with PBS solution and dried before treatment with human blood, which was stabilized with EDTA.^[31] After incubation for 1 h at 37 °C, the surfaces were rinsed with water and then washed three times with 2 mL PBS buffer. Subsequently, the surfaces were stained in 2 mL of 0.1% acridine orange solution in water for 10 min at room temperature and washed with 3 mL PBS solution.

4.7. Comparative Bacterial Adhesion Test

Bacterial cell adhesion assays on zwitterionic moieties were conducted as follows. Cells of *S. epidermidis* DSM20044 were grown at 37 °C with shaking at 130 rpm in LB medium (10 g · L⁻¹ tryptone, 5 g · L⁻¹ yeast-extract, and 10 g · L⁻¹ NaCl adjusted to pH 7.0). The cells were harvested during the early exponential growth phase (optical density at 550 nm [OD₅₅₀] 0.38) by centrifugation (5 min, 5 000g). The pellet was suspended in sterile PBS to obtain a cell density of 9.9×10^6 cfu · mL⁻¹.

The surfaces of pure-uncoated silicone substrate and a PMSSQ–PStCHO-modified silicon substrate were functionalized by means of *sur*-KFR surfaces with *p*-anisidine/diisopropyl phosphonate and subsequent deprotection reaction before treating with 70% ethanol, for 5 min, drying at 60 °C, and placing them into 9.6 cm² sterile Petri dishes. Dried surfaces were covered with 3 mL of the bacterial suspension and subsequently incubated for 1 h at 37 °C. Further, the cells were removed and substrates were washed three times with 50 mL sterile PBS buffer each and subsequently transferred upside down onto contact plates (LB medium containing agar 15 g · L⁻¹). After a contact time of 30 s, samples were removed and agar plates were incubated overnight at 37 °C for detecting bacterial growth.

Three substrates, which had previously been functionalized by *sur*-KFR with diisopropyl phosphonate and different amines (4-aminobenzoic acid, 4-bromoaniline, and *p*-anisidine) were deprotected and tested as described above.

Acknowledgements: The authors gratefully acknowledge S. Petersen and C. Khenkhar for their support during the preparation of the manuscript.

Received: May 21, 2015; Revised: July 22, 2015; Published online: September 2, 2015; DOI: 10.1002/mabi.201500196

Keywords: antifouling properties; zwitterionic thin film

- [1] E. Ralston, G. Swain, *Bioinspir. Biomim.* **2009**, *4*, 015007.
- [2] B. Carpentier, O. Cerf, *J. Appl. Bacteriol.* **1993**, *75*, 499.

- [3] A. N. Zelikin, *ACS Nano* **2010**, *4*, 2494.
- [4] R. Mout, D. F. Moyano, S. Rana, V. M. Rotello, *Chem. Soc. Rev.* **2012**, *41*, 2539.
- [5] W. J. Costerton, L. Montanaro, N. Balaban, C. R. Arciola, *Int. J. Artif. Organs* **2009**, *32*, 699.
- [6] J. W. Costerton, P. S. Stewart, E. P. Greenberg, *Science* **1999**, *284*, 1318.
- [7] A. G. Gristina, *Science* **1987**, *237*, 1588.
- [8] L. Hall-Stoodley, J. W. Costerton, P. Stoodley, *Nature Rev. Microbiol.* **2004**, *2*, 95.
- [9] J. D. Bryers, *Biotechnol. Bioeng.* **2008**, *100*, 1.
- [10] K. Sugiyama, H. Aoki, *Polym. J.* **1994**, *26*, 561.
- [11] R. Kakuchi, *Angew. Chem. Int. Ed.* **2014**, *53*, 46.
- [12] P. Theato, *J. Polym. Sci. Part A: Polym. Chem.* **2008**, *46*, 6677.
- [13] H. S. Sundaram, X. Han, A. K. Nowinski, J. R. Ella-Menye, C. Wimbish, P. Marek, K. Senecal, S. Jiang, *ACS Appl. Mater. Interfaces* **2014**, *6*, 6664.
- [14] W. Y. Tsai, P. L. Taberna, P. Simon, *J. Am. Chem. Soc.* **2014**, *136*, 8722.
- [15] R. Yang, K. K. Gleason, *Langmuir* **2012**, *28*, 12266.
- [16] W. Zhao, Q. Ye, H. Hu, X. Wang, F. Zhou, *J. Mater. Chem. B* **2014**, *2*, 5352.
- [17] R. Yang, J. Xu, G. Ozaydin-Ince, S. Y. Wong, K. K. Gleason, *Chem. Mater.* **2011**, *23*, 1263.
- [18] S. Chen, L. Li, C. Zhao, J. Zheng, *Polymer* **2010**, *51*, 5283.
- [19] A. L. Gui, E. Luais, J. R. Peterson, J. J. Gooding, *ACS Appl. Mater. Interfaces* **2013**, *5*, 4827.
- [20] P. Liu, Q. Chen, L. Li, S. Lin, J. Shen, *J. Mater. Chem. B* **2014**, *2*, 7222.
- [21] L. Xu, P. Ma, B. Yuan, Q. Chen, S. Lin, X. Chen, Z. Hua, J. Shen, *R. Soc. Chem. Adv.* **2014**, *4*, 15030.
- [22] H. Yin, T. Akasaki, T. Lin Sun, T. Nakajima, T. Kurokawa, T. Nonoyama, T. Taira, Y. Saruwatari, J. Ping Gong, *J. Mater. Chem. B* **2013**, *1*, 3685.
- [23] R. Kakuchi, P. Theato, *Polym. Chem.* **2014**, *5*, 2320.
- [24] R. Kakuchi, P. Theato, *ACS Macro Letters* **2014**, *3*, 329.
- [25] D. Kessler, F. D. Jochum, J. Choi, K. Char, P. Theato, *ACS Appl. Mater. Interfaces* **2011**, *3*, 124.
- [26] D. Kessler, P. Theato, *Macromolecules* **2008**, *41*, 5237.
- [27] D. Kessler, C. Teutsch, P. Theato, *Macromol. Chem. Phys.* **2008**, *209*, 1437.
- [28] N. Wagner, L. Schneider, M. Michelswirth, K. Küpper, P. Theato, *Macromol. Chem. Phys.* **2015**, *7*, 783.
- [29] D. K. Owens, R. C. Wendt, *J. Appl. Polym. Sci.* **1969**, *13*, 1741.
- [30] Y. Q. Zhu, C. X. Yu, Y. Li, Q. Q. Zhu, L. Zhou, C. Cao, T. T. Yu, F. P. Du, *Pest Manag. Sci.* **2014**, *70*, 462.
- [31] F. Khalil, E. Franzmann, J. Ramcke, O. Dakischew, K. S. Lips, A. Reinhardt, P. Heisig, W. Maison, *Colloids Surf. B* **2014**, *117*, 185.
- [32] G. Sun, C. Cheng, K. L. Wooley, *Macromolecules* **2007**, *40*, 793.
- [33] D. Kessler, N. Metz, P. Theato, *Macromolecular Symp.* **2007**, *254*, 34.

9 Results und discussion

9.1 *Synthesis of Inorganic-Organic Hybrid Polymers*

Hybrid organic-inorganic materials can be used to generate coatings on a variety of substrates, for example, silicon, glass or metal. Furthermore, a large number of functional groups can be installed onto the presynthesized polymers via the so-called post-polymerization modification or polymer analogous reactions.

The active esters are very classical functional groups that were discovered by Ringsdorf and Ferruti in 1972. This is one of the most useful groups for post-polymerization modifications because of very mild reaction conditions between amines and active esters and an excellent conversion of the corresponding amides (almost 100%). A library of different monomers which have frequently been used for the synthesis of functional polymer materials has been investigated, for example, pentafluorophenyl acrylate (PFPA), *N*-hydroxy succinimide acrylate (NHSA), pentafluorophenyl 4-vinylbenzoate (PFP4VB) and 4-acryloxyphenyl-dimethylsulfonium triflate (DMSPA).⁹⁰

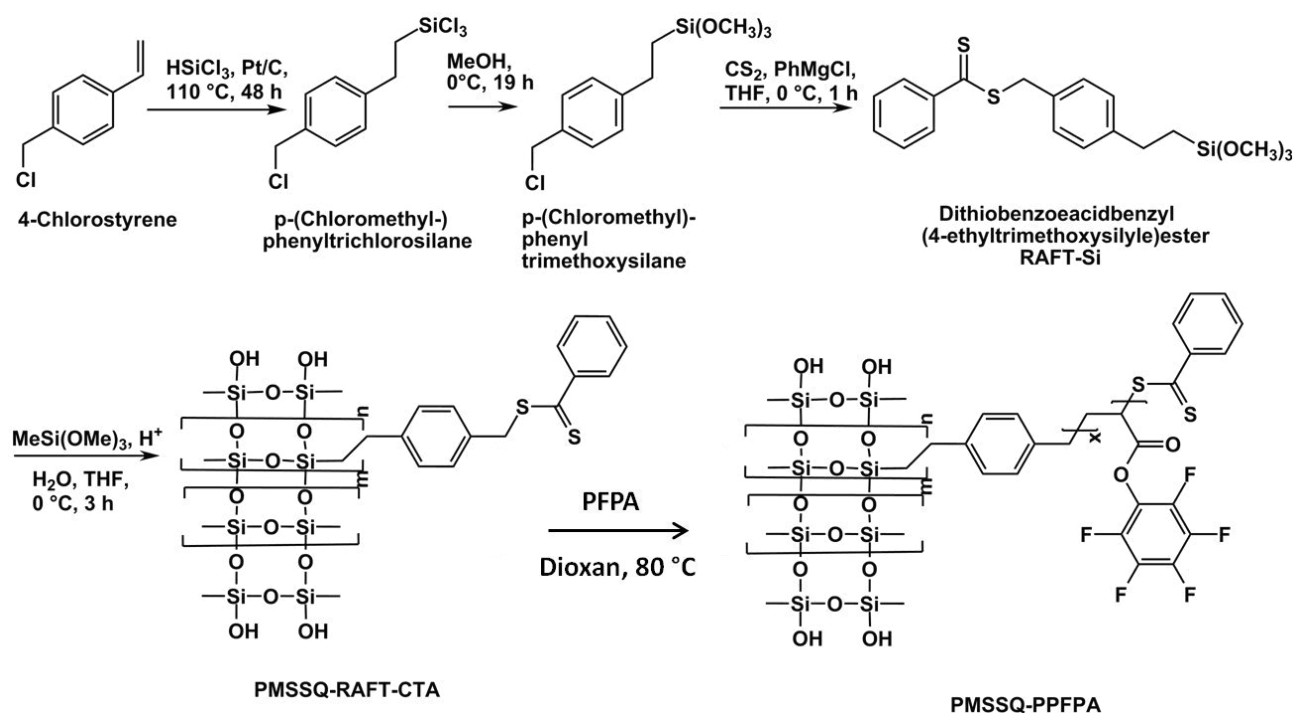
To produce hybrid polymers based on the chemistry of poly(silsesquioxanes), two different synthesis paths we compared with each other: A). a post-modified one and B). a prior-modified one. In summary, both of these ways are suitable for the preparation of temperature-responsive surfaces with different amines based on the chemistry of the hybrid polymer PMSSQ-PPFPA. The zwitterionic α -amino phosphonic acid moieties on surfaces based on the chemistry of poly(methylsilsesquioxane)-poly(4-vinyl benzaldehyde) (PMSSQ-PStCHO) could be obtained after successful Kabachnik-Fields post-polymerization modification (KF-PMR) of the aldehyde-functionalized surfaces. In contrast, the light- and temperature-responsive surfaces could only be obtained by prior deposition of the new hybrid polymer on the surface.^{91,92,93}

First, co-condensation of organically modified trifunctionalized silane and PMSSQ was performed, leading to macro chain transfer agents (mCTA) which are able to initiate a RAFT polymerization. Subsequently, inorganic-organic hybrid polymers could be obtained by grafting of different monomers (Scheme 5).^{94,95}

9.1.2 Hybrid Polymer Synthesis Using RAFT

In the context of my Dr. rer. nat. thesis, was investigated the synthesis of polymers based on poly(methylsilsequioxane) (PMSSQ). I am particularly interested in organic-inorganic hybrid-polymers that are especially suited for surface coatings due to their reactive character. The reactive coating, based on an activated ester such as pentafluorophenyl ester, can be converted into the desired functional polymer by a simple polymer-analogous reaction.⁹⁶

The hybrid polymers were synthesized as shown in Scheme 5. Initially, dithiobenzoic acid benzyl-(4-ethyltrimethoxysilyl) ester was co-condensed with methyltrimethoxysilane (MTMS) to yield the macro initiator PMSSQ-CTA. This species provides a high functionality of unreacted silanol groups and initiating moieties for the reversible addition fragmentation chain transfer polymerization. Subsequently, RAFT polymerization reaction of pentafluorophenylacrylate (PFPA) was performed.⁹⁶



Scheme 5 Synthesis of PMSSQ-PPFPA. 1. Co-condensation of the macro-CTA. 2. Grafting-from polymerization via RAFT polymerization yielding in an inorganic-organic hybrid polymer.^{92,93}

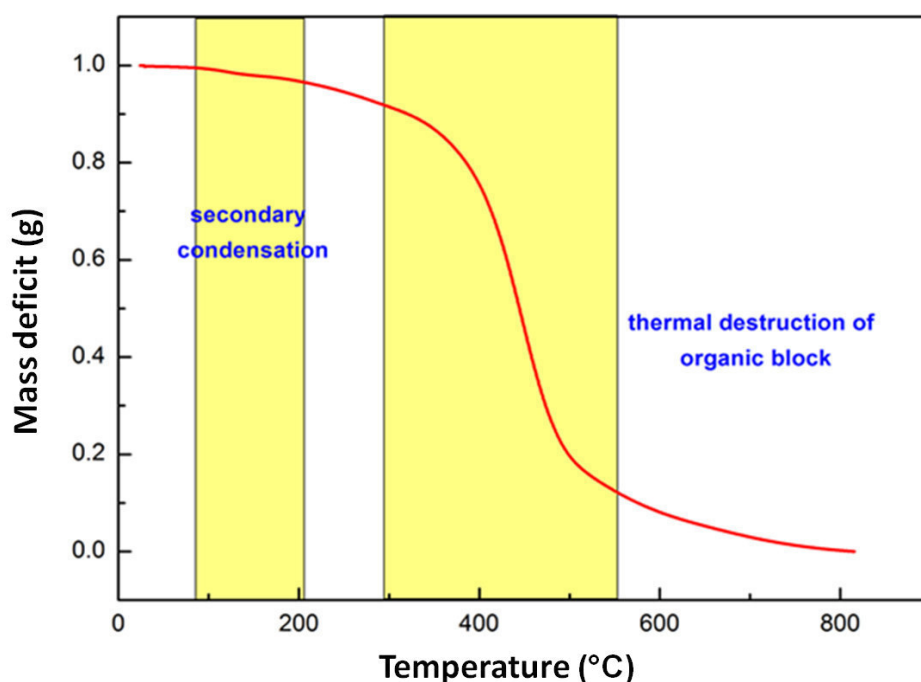
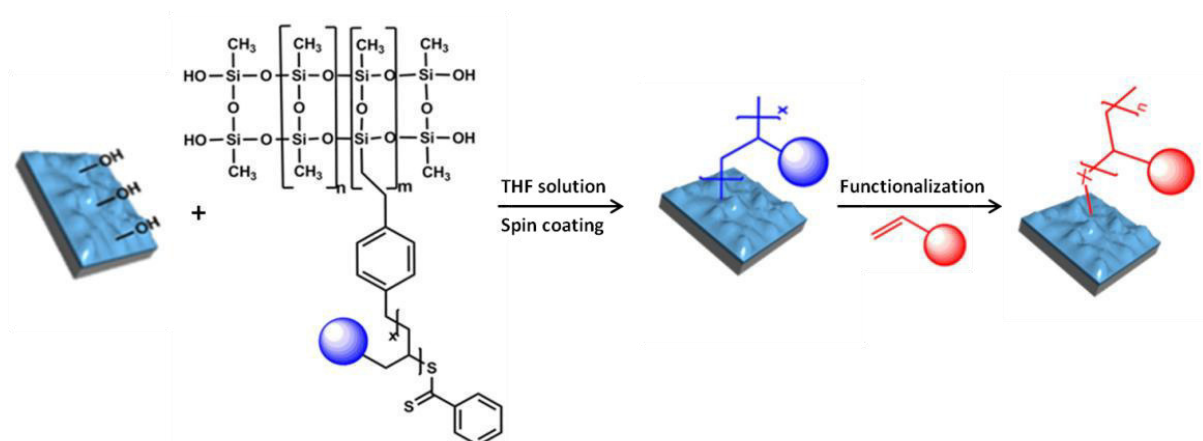


Figure 12 Thermo gravimetric analysis of synthesized hybrid-polymers.

Obtained hybrid-polymers had molecular weight ranging from approx. 12000 g/mol to approx. 7000 g/mol and are soluble in THF. Furthermore, they were investigated by thermo-gravimetric analysis (TGA). A very thermal decomposition behavior of hybrid-polymers could be shown. First, a secondary condensation occurred between 120 °C and 160 °C. Then, at 400 °C, the decomposition of the pentafluorophenyl ester block was observed.

The block ratio between the organic and the inorganic blocks of two different hybrid-polymers was detected from the mass deficits. Figure 13 shows the resultant hybrid polymer consisting of 80 wt% PFPA and 20 wt% PMSSQ which was in good agreement with the starting materials. As already shown in previous studies, the reactive surfaces could be prepared from the polymer solution by using spin-coating on glass and silicon substrates (Scheme 6).



Scheme 6 Surface analogous reaction to create different surface coatings, starting from reactive precursor coating.

9.2 General Coating Properties

As mentioned above, two different synthetic approaches for the preparation of new inorganic organic hybrid polymers were used. A variety of different functional and reactive polymers were synthesized and characterized by different techniques such as AFM or FT-IR. When using the first technique (A), hybrid polymers were prepared by RAFT polymerization from a library of different monomers using a macro-CTA agent based on PMSSQ. Second technique (B) was used for the preparation of light- and temperature-responsive surface coatings. First, a light- and temperature-responsive hybrid copolymer was synthesized via a sequential post-polymerization modification of PMSSQ-PPFPA. Subsequently, the hybrid polymer PMSSQ-PPFPA was converted with an amino-functionalized spiropyran and isopropylamine.

The obtained hybrid polymers show versatile and interesting properties, which are summarized below.^{97,98,99}

- All obtained hybrid polymers are soluble in all common organic solvents which allows both dip-coating and spin-coating, irrespective of the substrate used.
- All coating materials could be annealed at 130 °C for 2-4 hours, independently from the organic part.
- All film coatings are stable and insoluble in any common organic solvent.
- Independently from organic functionality, stable and adherent films could be prepared from all synthesized hybrid polymers.

- For the preparation of stable and adherent surface coatings, 10-20 % of the inorganic part are sufficient (Figure 13).
- AFM measurements show very smooth surface coatings without any structural and chemical defects (Figure 14).
- All coated surfaces exhibit a unique wetting behavior which is only determined by the ratio of the inorganic to the organic part.

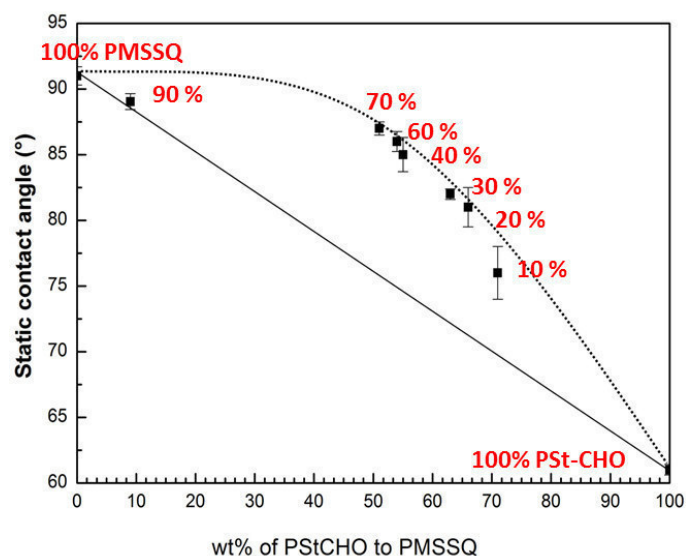


Figure 13 Influence of the variation of the organic to the inorganic weight ratio on the observed contact angle after spin coating on a silicon substrate (spin-coated from 10 wt% solution in THF). (*Installation of Zwitterionic α -Amino Phosphoric Acid Moieties on Surfaces via a Kabachnik-Fields Post-Polymerization Modification*, N. Wagner, L. Schneider, M. Michelswirth, K. Küpper, P. Theato, *Macromolecular Chemistry and Physics* 216, 783-793 (2015)).

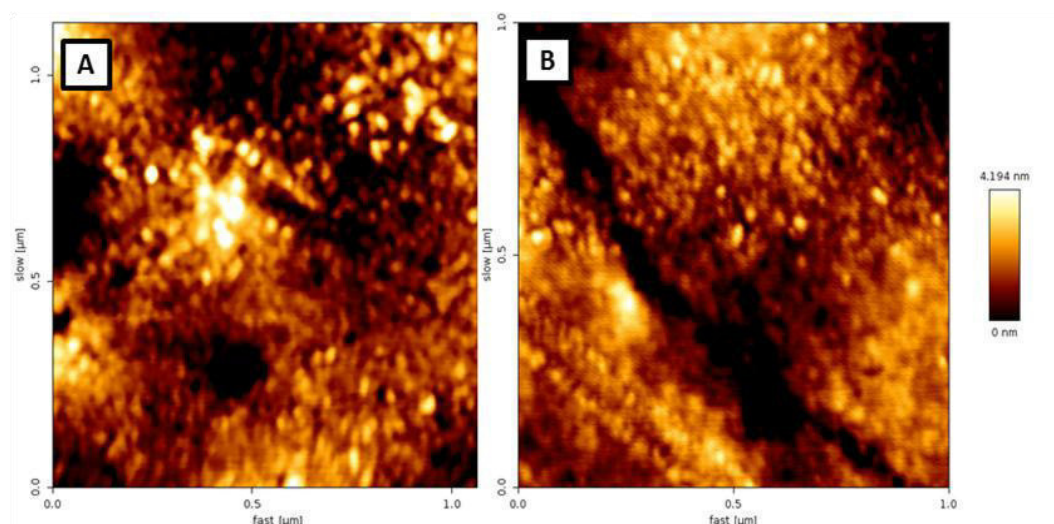


Figure 14 AFM height image of Si-surfaces after spin-coating with PMSSQ-PStCHO (A) and after post-polymerization modification by the Kabachnik-Fields reaction (B). (*Installation of Zwitterionic α -Amino Phosphoric Acid Moieties on Surfaces via a Kabachnik-Fields Post-Polymerization Modification*, **N. Wagner, L. Schneider, M. Michelswirth, K. Küpper, P. Theato, *Macromolecular Chemistry and Physics* 216, 783-793 (2015).**).

In order to create functional surface coatings with specific desired properties, such as antifouling or light - and temperature-responsive characteristics, inorganic-organic hybrid polymers have to be synthesized by RAFT polymerization reaction. Afterwards, the desired functionalities can be introduced into the PMSSQ network by post-polymerization reaction, for example through *sur*-KFR. In contrast, the light- and temperature-responsive surfaces could only be obtained by prior deposition of the new hybrid polymer on the surface.

In the following, several examples of functional surface coatings are presented.

9.2.1 Temperature- and Light-Responsive Capillaries

A new convenient method to produce different temperature- and light-responsive coatings with an appropriate method allowing an accurate determination of the wettability switching range will be described in detail in the publication III. First, a new thermo- and light-responsive copolymer was synthesized via a sequential post-polymerization modification of PMSSQ-PPFPA. Then the hybrid polymer PMSSQ-PPFPA was partly converted with an amino-functionalized spiropyran, followed by reaction with an excess of isopropylamine. Subsequently, the light- and temperature-responsive surfaces were obtained by prior deposition of the new hybrid polymer on the silicon surface or inside of glass capillaries. For

this purpose, 10% hybrid polymer solution in THF was spin-coated onto clean silicon substrate surfaces. The glass capillaries were coated by dipping them into a polymer solution.

The obtained functional surface coatings were investigated. The switching of the contact angles was determined by the meniscus height of water rising inside the capillary at temperatures below and above LCST. For the temperature- and light-responsive surface, the surface switching was additionally investigated before and after UV irradiation.

The meniscus height of the prepared glass capillaries was determined at 15 °C (below LCST) and at 60 °C (above LCST). To compare the obtained values with the contact angles which were obtained by the sessile drop method, similar coatings were produced on flat silicon substrates. Additionally, the measurements of advancing and receding contact angles were performed by the method of addition and removal of volume. Then the equilibrium contact angle from the meniscus height was calculated and compared with the values obtained from the measured contact angles.

Moreover, temperature-responsive surfaces on silicon substrates with different amines (cyclopropylamine (CPA), diethylamine (DEA), isopropylamine (IPA), methylethylamine (MEA) based on the chemistry of the hybrid polymer PMSSQ-PPFPA were prepared and contact angle measurements were conducted by the sessile drop method. As with the functional surface coatings, the glass capillaries were functionalized with amines by postmodification reaction. The meniscus height of the prepared glass capillaries was determined at 15 °C and at 60 °C.^{99,100,101,102}

The obtained values of advancing, receding and equilibrium contact angles are summarized in Table S1, Publication III. Figure 16 shows the equilibrium contact angles obtained by the sessile drop method (A) and the capillary rise method (B) at 15 °C and at 60 °C.

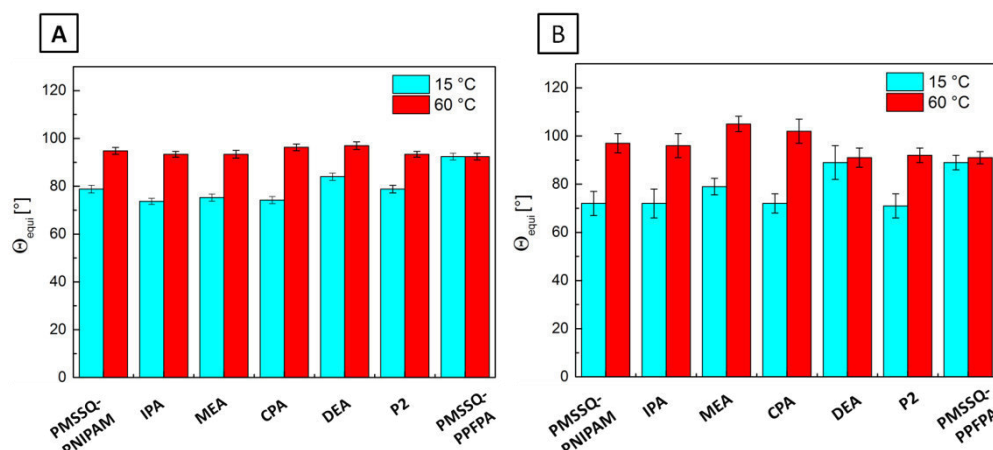


Figure 15 Equilibrium contact angles obtained by the sessile drop method (A) and equilibrium contact angles obtained by the capillary rise method at 15 °C and at 60 °C on silicon surfaces coated with PMSSQ–PPFPA after conversion with IPA, MEA, CPA, DEA, coating of thermo- and light-responsive copolymer (P2), and PMSSQ–PNIPAM as well as the unconverted surface (PMSSQ–PPFPA). (*Reactive Coatings in Glass Capillaries: Preparation of Temperature- and Light-Responsive Surfaces and Accurate Determination of Wettability Switching*, N. Wagner, D. Kessler, P. Theato, *Macromolecular Chemistry and Physics*, **217**, 92-100. (2016)).

To sum it up, the synthesis of hybrid polymers based on the efficient modification chemistry of PMSSQ–PPFPA leads to the substrate surfaces which exhibit a thermo- or light-responsive behavior.

Moreover, it was observed that the reversible isomerization of spiropyran moieties in the copolymers that is induced by irradiation with UV light influences the water wettability behavior. Different temperature-responsive coatings can be prepared by surface-modification reactions inside the capillary and the temperature-controlled switching range of the contact angles was measured at different temperatures. The values obtained are comparable to those obtained by the sessile drop method, but the error range is much smaller. This convenient method of reactive coatings inside glass capillaries allows a more accurate determination of the equilibrium contact angles.

Further, two synthetic pathways, post-modified and prior-modified, were compared with each other. In conclusion, it can be said that both of these ways are suitable for the preparation of temperature-responsive surfaces with different amines based on the chemistry of PMSSQ–PPFPA. Contrary, the functional surfaces using the new light- and temperature-responsive hybrid polymer could only be obtained by prior deposition of the hybrid polymer on the surface. For detailed information see publication III.¹⁰⁰

9.2.2 Zwitterionic α -Aminophosphonic Acid Moieties on Surfaces

Multicomponent reactions (MCRs) were discovered by Strecker in 1850 and gained increasingly in importance ever since. This type of reaction class is very versatile and provides many advantages for organic and polymer chemistry. Particularly interesting are MCRs for post-polymerization modification reactions of the chain ends or the side chains having different amounts of functional groups simultaneously. Therefore, MCRs have become a favorite type of reaction leading to different patterns of polymers, such as star-shaped or branched polymers.^{103,104,105}

Various MCRs include many reactions, for example, the Biginelli reaction, the Gewald reaction, the Passerini reaction, the Mannich reaction, the Hantzsch reaction, the Ugi reaction and the Kabachnik-Fields reaction.¹⁰⁶

In recent years, a series of multicomponent reactions has emerged as an innovative synthetic platform in the field of organic chemistry. This has not only boosted drug discovery, but also the construction of new skeletons. Although multicomponent reactions have triggered new chemistry and new applications, only little attention has been paid to polymer chemistry. A mainstream of polymer chemistry has been to shift from simple polymer systems to widespread application fields, such as drug delivery, electronic devices, solar cells, etc. This requires that polymer chemists must develop a robust and reliable synthetic platform to install functional groups into polymer structures. In this context, the use of multicomponent reactions to functionalize polymers is rationally expected to be a fruitful synthetic strategy, not only for polymer chemists but also for material scientists.

For the many multicomponent reactions reported so far, I turned my attention to the combination of inorganic-organic hybrid polymers with multicomponent reactions, such as the Kabachnik-Fields reaction (KFR) because they allow the incorporation of modified amines, amino acids and other functionalities. As shown in previous studies, the incorporation of amino acids into polymers is a promising strategy to obtain functional polymers, and amino acid conjugation is still an important issue in polymer chemistry. Hence, a novel functionalization strategy for artificial polymers is proposed, using multicomponent reactions in order to produce novel types of amine/phosphonic acid fused polymers.

Publication I reports on the installation of α -aminophosphonic acids onto surfaces of different substrates, for example Al or Cu, via surface KFR (*sur*-KFR) on aldehyde-bearing

exhibiting surfaces based on the chemistry of the hybrid polymer PMSSQ-PStCHO. First of all, new aldehyde-functionalized surfaces were prepared by applying coating of organic-inorganic hybrid polymers bearing aldehyde moieties onto substrates. In this context, poly(methylsilsesquioxane)-poly(4-vinylbenz-aldehyde) (PMSSQ-PStCHO) was prepared via RAFT polymerization. As mentioned previously, macro-RAFT agents derived from PMSSQ (PMSSQ-CTA) can be used as RAFT agents to control the polymerization of vinyl monomers, such as 4-vinyl-benzaldehyd yielding new organic-inorganic hybrid polymers

In order to provide surfaces featuring aldehyde moieties, PMSSQ-PStCHO hybrid polymers were introduced onto substrates. For this, thin polymer films on silicon substrates were prepared by spin-coating of a PMSSQ-PStCHO solution. Contact angles measurements of the obtained surfaces have shown that aldehyde moieties can be made accessible on the coating surface when the PStCHO content of the hybrid polymers was is more than 50 wt%.

In order to show the direct advantages of *sur*-KFR, a library of different surfaces has been synthesized by employing various combinations of amines and dialkyl phosphonates, and contact angle measurements of functionalized surfaces were performed. Depending on the employed combination of amines and dialkyl phosphonates, the values of the advancing contact angle changed proving the successful installation of polymeric α -amino phosphonates with diverse functionalities via *sur*-KFR. However, the obtained contact angles did not vary dramatically due to the small chemical differences between the employed amines and the dialkyl phosphonates (Figure 6, Paper I).^{107,108}

In addition, the PMSSQ-PStCHO coatings were prepared on Cu- and Al-substrates and KFR was conducted making this coating/functionalization approach substrate-independent (see Supporting Information, Publication I).

Subsequently, zwitterionic α -amino phosphonic acids should be installed on the substrate surface by deprotection reaction of α -aminophosphonates. For this purpose, the deprotection processes for polymeric α -amino phosphonates were studied in detail. First, the deprotection process was performed in solution and then adopted to the deprotection on surfaces. In order to achieve this, diisopropyl phosphonate and *p*-toluidine were used for the Kabachnik-Fields postmodification reaction (KF-PMR). After deprotection obtained polymer can be clearly assigned to the targeted zwitterionic polymeric α -amino phosphonic acid (P(St-AP-OH)). A successful deprotection reaction was provided by IR measurements. Furthermore, direct evidence for the conversion of phosphonate moiety into phosphonic

acids was proven by ^{31}P -NMR measurements which were conducted before and after deprotection reaction and revealed an obvious peak at 20.8 ppm owing to phosphonates disappeared and a clear peak at 18.8 ppm owing to phosphonic acid developed (see Supporting Information Publication I).

Finally, *sur*-KFR was conducted on the silicon substrate surface and α -aminophosphonic acid moieties were installed on the surface. Based on the deprotection reaction of polymeric α -aminophosphonates, deprotection of polymeric α -aminophosphonates immobilized on a silicon substrate was conducted in acetonitrile in the presence of a large excess amount of TMSBr. The deprotection of phosphonate moieties was confirmed by FT-IR measurements and contact angle measurements (see Figure 10, Publication I). The IR spectra of the silicon surfaces before and after *sur*-KFR confirmed a practically quantitative deprotection of phosphonate moieties.

The measurements of the contact angle after deprotection reaction show that there is a decrease in the CA values of up to 42° after deprotection reaction providing good evidence of structural changes from a non-polar phosphonate ester to a polar zwitterionic α -aminophosphonic acid (Figure 11 and 12, Publication I).

The conversion of aldehyde-functionalized surfaces with amines and dialkyl phosphonates by the Kabachnik-Fields reaction was proven by IR, EDX, and XPS measurements. Afterwards, the deprotection strategy of the obtained α -amino phosphonic acids for zwitterionic functionalized surfaces was demonstrated, opening the possibilities for new anti-fouling surfaces.

9.2.3 Investigation on Antifouling Properties of Zwitterionic α -Aminophosphonic Acid Moieties on Surfaces

Many different polymers have been used as nonfouling materials, such as poly(ethylene glycol) (PEG) and zwitterionic polymers and poly(sulfobetaine methacrylate) (PSBMA) for the reduction of the protein adsorption on the surfaces. The antifouling coatings became more and more important within the last three decades due to their essential role in various medical, biochemical, marine and industrial applications as well as in water purification systems.

The zwitterionic nature has been revealed to play a unique and indispensable role in polymer chemistry due to the anionic and cationic terminal groups which form a hydration

layer during the solvation of the charged groups. Zwitterionic polymers possess two very distinguishing properties for the antifouling property and the silent property as a medium in blood.

An effective two-step approach to integrate zwitterionic α -aminophosphonic acids onto substrate surfaces was investigated. First, aldehyde-functionalized surfaces were treated by *sur*-KFR with amines and dialkyl phosphonates. Subsequently, the deprotection reaction was conducted in order to create zwitterionic- functionalized polymer substrates (Figure 16). The obtained zwitterionic surfaces were characterized by various techniques, for example, IR, CA and surface energy measurements. In addition, the antifouling properties of the resulting films were proven by bacterial cell adhesion assays and blood assays.

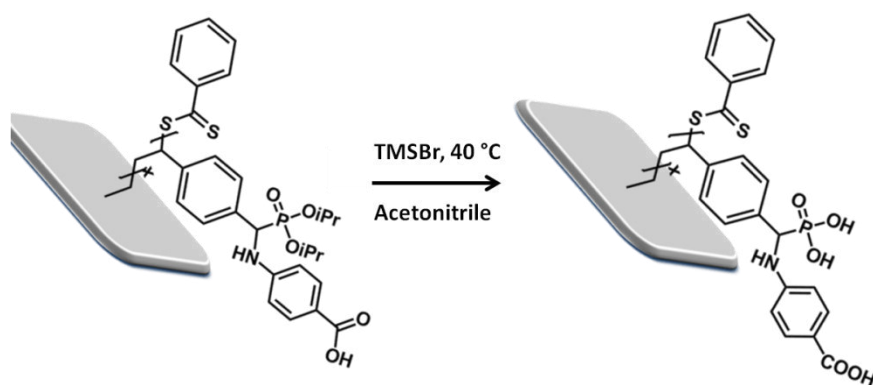


Figure 16 Deprotection reaction of *sur*-KFR modified substrate surfaces.

The water contact angles of PMSSQ-PStCHO-modified silicone substrates decreased after *sur*-KFR and after the subsequent deprotection reaction. This decrease in the CA is a direct consequence of the structural changes from a non-polar phosphonate to a polar zwitterionic α -aminophosphonic acid. The biggest reduction of contact angles of up to 31 ° could be obtained for *sur*-KFR with *p*-aminobenzoic acid and diisopropyl phosphonate (see Paper III).¹⁰⁹

Moreover, a change in surface energy of the functionalized surfaces could be observed. The polar component of silicone substrate surfaces increased moderately after *sur*-KFR, but increased remarkably after deprotection reaction, proving the installation of zwitterionic α -aminophosphonic acid. Figure 17 summarizes the trends of surface energy before and after *sur*-KFR with diisopropyl phosphonates and *p*-aminobenzoic acid, and after deprotection reaction (for more information see Paper III).

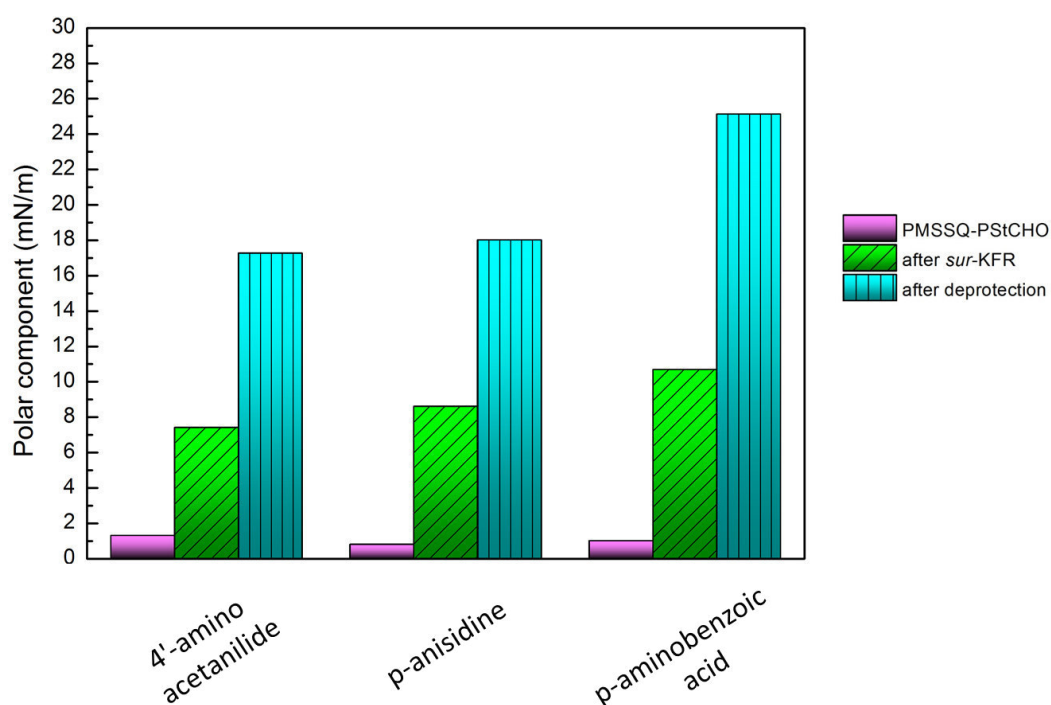


Figure 17 Polar component of PMSSQ-PStCHO-cured silicon surfaces, after *sur*-KFR and after deprotection reaction with various amines and diisopropyl phosphonates. (*Investigation of Antifouling Properties of Surfaces Featuring Zwitterionic α -Aminophosphonic Acid Moieties*, N. Wagner, P. Zimmermann, P. Heisig, F. Klitsche, W. Maison, P. Theato, *Macromolecular Bioscience* **15**, 1673-1678 (2015)).

Further, the antifouling properties were investigated by a protein assay using blood and comparative bacterial cell adhesion tests. The resulting zwitterionic α -aminophosphonic acid moieties exhibit a clear reduction of the adsorption of biomaterial and show a clear antifouling effect with almost no bacterial colonization on the coated silicon substrates after deprotection reaction.¹⁰⁹

10 References

- ¹ L. Ionov, A. Sidorenko, K. Eichhorn, M. Stamm, S. Minko, K. Hinrichs, *Langmuir* **2005**, *21*, 8711.
- ² W. Feng, W. Luo, Y. Feng, *Nanoscale* **2012**, *4*, 6118.
- ³ D. Tian, X. Zhang, Y. Tian, Y. Wu, X. Wang, J. Zhai et al. *J. Mater. Chem.* **2012**, *22*, 19652.
- ⁴ L. Song, Y. Yang, Q. Zhang, H. Tian, W. Zhu, *J. Phys. Chem. B* **2011**, *115*, 14648.
- ⁵ G. Zhang, X. Zhu, F. Miao, D. Tian, H. Li, *Org. Biomol. Chem.* **2012**, *10*, 3185.
- ⁶ J. Lutz, S. Liu, B. Sumerlin, J.G. Ray, S.S. Naik, E.A. Hoff et al. *Macromol. Rapid Commun.* **2012**, *33*, 819.
- ⁷ B. Thieke, *Makromolekulare Chemie*, 2th ed, Wiley-VCH, Weinheim, **2005**.
- ⁸ M. Schönhoff, *Current Opinion in Colloid & Interface Science* **2003**, *8*, 86–95.
- ⁹ J.S. Wang, K. Matyjaszewski, *J. Am. Chem. Soc.* **1995**, *117*, 561.
- ¹⁰ T. Grimaud, K. Matyjaszewski, *Macromolecules* **1997**, *30*, 2216.
- ¹¹ M. Sawamoto, *Macromolecules* **1996**, *29*, 1070.
- ¹² V. Percec, H.J. Kim, B. Barboiu, *Macromolecules* **1995**, *28*, 7970.
- ¹³ K. Matyjaszewski, J. Xia, *Chem. Rev.* **2001**, *101*, 2921.
- ¹⁴ K. Matyjaszewski, T.E. Patten, J. Xia, *J. Am. Chem. Soc.* **1997**, *119*, 674.
- ¹⁵ W. Tang, Y. Kwak, W. Braunecker, N.V. Tsarevsky, M.L. Coote, K. Matyjaszewski, *J. Am. Chem. Soc.* **2008**, *130*, 10702.
- ¹⁶ C. Barner-Kowollik, *Handbook of RAFT Polymerization*, Wiley-VCH, Weinheim, Germany, **2008**.
- ¹⁷ R.T.A. Mayadunne, E. Rizzardo, J. Chiefari, Y.K. Chong, G. Moad, S.H. Thang, *Macromolecules* **1999**, *32*, 6977–6980.
- ¹⁸ T.M. Legge, A.T. Slark, S. Perrier, *Journal of Polymer Science Part A: Polymer Chemistry* **2006**, *44*, 6980–6987.
- ¹⁹ Y.K. Chong, T.P.T. Le, G. Moad, E. Rizzardo, S.H. Thang, *Macromolecules* **1999**, *32*, 2071–2074.
- ²⁰ S. Perrier, P. Takolpuckdee, *Journal of Polymer Science Part A: Polymer Chemistry* **2005**, *43*, 5347–5393.
- ²¹ G. Moad, E. Rizzardo, S. Thang, *Polymer* **2008**, *49*, 1079.

-
- ²² J. Chiefari, Y. Chong, F. Ercole, J. Krstina, J. Jeffery, T. Le, R. Mayadunne, G. Meijs, C. Moad, G. Moad, E. Rizzardo, S. Thang, *Macromolecules* **1998**, *31*, 5559.
- ²³ J.M. O'Donnell, *Chem. Soc. Rev.* **2012**, *41*, 3061–3076.
- ²⁴ M. Vallet-Regi, D. A. Navarrete, *Biomimetic nanoceramics in clinical use from materials to applications*, RSC Publishing, **2008**.
- ²⁵ G. Kickelbick, *Hybrid materials: synthesis, characterization, and applications*, ed. Wiley-VCH, Weinheim, **2006**.
- ²⁶ R. Gupta, N.K. Chaudhury, *Biosens Bioelectron* **2007**, *22*, 2387.
- ²⁷ E.P. Plueddemann, *Prog. Org. Coat.* **1983**, *11*, 297.
- ²⁸ M.N.Sathyanaarayana, M. Yassen, *Prog. Org. Coat.* **1995**, *26*, 275.
- ²⁹ T. Gunji, Y. Iizuka, K. Arimitsu, Y. Abe, *J. Poly. Sci.: Part A: Polym. Chem.* **2004**, *42*, 3676.
- ³⁰ D.A. Loy, K.J. Shea, *Chem. Rev.* **1995**, *95*, 1431.
- ³¹ K.J. Shea, D.A. Loy, *Chem. Mater.* **2001**, *13*, 3306.
- ³² K. Matyjaszewski, P.J. Miller, N. Shukla, B. Immaraporn, A. Gelman, B.B. Luokala, T.M. Siclovan, G. Kickelbick, T. Vallant, H. Hoffmann, T. Pakula *Macromolecules* **1999**, *32*, 8716.
- ³³ R. Vasita, D.S. Katti, *Int. J. Nanomed.* **2006**, *1*, 15.
- ³⁴ H. Wu, W. Pan, D. Lin, H. Li, *J. Adv. Ceram.* **2012**, *1*, 2.
- ³⁵ A. Greiner, J.H. Wendorff, *Angew. Chem. Int. Ed.* **2007**, *46*, 5670.
- ³⁶ K. Sarkar, C. Gomez, S. Zambrano, M. Ramirez, E. de Hoyos, H. Vasquez, K. Lozano, *Mater. Today* **2010**, *13*, 12.
- ³⁷ J. Drelich, A. Marmur, *SURF*, **2013**, *2*, 211.
- ³⁸ L. Xu, Z. Chen, W. Chen, A. Mulchandani, Y. Yan, *Macromol. Rapid Commun.* **2008**, *29*, 832.
- ³⁹ C. Simão, M. Mas-Torrent, J. Veciana, C. Rovira, *Nano Lett.* **2011**, *11*, 4382.
- ⁴⁰ A.K. Sinha, M. Basu, M. Pradhan, S. Sarkar, Y. Negishi, T. Pal, *Langmuir* **2011**, *27*, 11629.
- ⁴¹ Y. Pei, J. Travas-Sejdic, D.E. Williams, *Langmuir* **2012**, *28*, 8072.
- ⁴² E. Spruijt, E. Choi, W.T.S. Huck, *Langmuir* **2008**, *24*, 11253.
- ⁴³ D. Tian, X. Zhang, J. Zhai, L. Jiang, *Langmuir* **2011**, *27*, 4265.
- ⁴⁴ J. Wang, B. Mao, J.L. Gole, C. Burda, *Nanoscale* **2010**, *2*, 2257.
- ⁴⁵ D. Wang, X. Wang, X. Liu, F. Zhou, *J. Phys. Chem. C* **2010**, *114*, 9938.
- ⁴⁶ M. Kettunen, R.J. Silvennoinen, N. Houbenov, J. Ruokolainen, J. Sainio, N. Pore et. al. *Adv. Funct. Mater.* **2011**, *21*, 510.
- ⁴⁷ S. Liu, G. Han, M. Shu, L. Han, S. Che, *J. Mater. Chem.* **2010**, *20*, 10001.

- ⁴⁸ J. Drelich, E. Chibowski, D.D. Meng, K. Terpilowski, *Soft Matter*. **2011**, 7, 9804.
- ⁴⁹ H.G. Schild, *Prog. Polym. Sci.* **1992**, 17, 163.
- ⁵⁰ X. Zhao, Y. Liu, J. Lu, J. Zhou, J. Li, *Chem. Eur. J.* **2012**, 18, 3687.
- ⁵¹ H. Kuroki, I. Tokarev, S. Minko, *Annu. Rev. Mater. Res.* **2012**, 42, 343.
- ⁵² O. Azzaroni, *J. Polym. Sci. A Polym. Chem.* **2012**, 50, 3225.
- ⁵³ B. Xin, J. Hao, *Chem. Soc. Rev.* **2010**, 39, 769.
- ⁵⁴ E. Svetushkina, N. Puretskiy, L. Ionov, M. Stamm, A. Synytska, *Soft Matter*. **2011**, 7, 5691.
- ⁵⁵ N.C. Estillore, J.Y. Park, R.C. Advincula, *Macromolecules* **2010**, 43, 6588.
- ⁵⁶ E. Turan, S. Demirci, T. Caykara, *Thin Solid Films* **2010**, 518, 5950.
- ⁵⁷ S.L. Gras, T. Mahmud, G. Rosengarten, A. Mitchell, K. Kalantar-zadeh, *Chem. Phys. Chem* **2007**, 8, 2036.
- ⁵⁸ P. Muthiah, S.M. Hoppe, T.J. Boyle, W. Sigmund, *Macromol. Rapid Commun.* **2011**, 32, 1716.
- ⁵⁹ T. Sun, G. Qing, *Adv. Mater.* **2011**, 23, H57-H77.
- ⁶⁰ H.J. Moon, D.Y. Ko, M.H. Park, M.K. Joo, B. Jeong, *Chem. Soc. Rev.* **2012**, 41, 4860.
- ⁶¹ J. Das, J.M.J. Frechet, A.K. Chakraborty, *J. Phys. Chem. B* **2009**, 42, 13768.
- ⁶² T. Chen, I. Amin, R. Jordan. *Chem. Soc. Rev.* **2012**, 41, 3280.
- ⁶³ J. Choi, P. Schattling, F.D. Jochum, J. Pyun, K. Char, P. Theato, *Chem. Soc. Rev.* **2013**, 42, 7468.
- ⁶⁴ K. Ichimura, *Science* **2000**, 288, 1624.
- ⁶⁵ L.F.V. Pinto, S. Kundu, P. Brogueira, C. Cruz, S.N. Fernandes, A. Aluculesei, M.H. Godinho, *Langmuir* **2011**, 27, 6330.
- ⁶⁶ C. Jin, R. Yan, J. Huang, *J. Mater. Chem.* **2011**, 21, 17519.
- ⁶⁷ K. Matyjaszewski, P.J. Miller, N. Shukla, B. Immaraporn, A. Gelman, B.B. Luokala, T.M. Siclovan, G. Kickelbick, T. Vallant, H. Hoffmann, T. Pakula, *Macromolecules* **1999**, 32, 8716.
- ⁶⁸ D.J. Chung, Y. Ito, Y. Imanishi, *J. Appl. Polym. Sci.* **1994**, 51, 2027.
- ⁶⁹ L.M. Siewierski, W.J. Brittain, S. Petrash, M.D. Foster, *Langmuir* **1996**, 12, 5838.
- ⁷⁰ K. Ichimura, Y. Akita, H. Akiyama, K. Kudo, Y. Hayashi, *Macromolecules* **1997**, 30, 903.
- ⁷¹ A.A. Brown, O. Azzaroni, W.S. Huck, *Langmuir* **2009**, 25, 1744.
- ⁷² A. Blanc, C.G. Bochet, *J. Org. Chem.* **2002**, 67, 5567.
- ⁷³ S.P.J. Higson, *Analytical Chemistry*, Oxford University Press, **2004**.

-
- ⁷⁴ J.F. Moulder, W.F. Stickle, P.E. Sobol, K.D. Bomben, *Handbook of X-ray Photoelectron Spectroscopy*, Perkin-Elmer Corp., Eden Prairie, MN, USA, **1992**.
- ⁷⁵ C.D. Wagner, W.M. Riggs, L.E. Davis, J.F. Moulder, G.E. Mullenberger, *Handbook of X-ray Photoelectron Spectroscopy*, Perkin-Elmer Corp., Eden Prairie, MN, USA, **1979**.
- ⁷⁶ L.E. Davis, *Modern Surface Analysis: Metallurgical Applications of Auger Electron Spectroscopy (AES) and X-ray Photoelectron Spectroscopy (XPS)*, The Metallurgical Society of AIME, Warrendale, USA, **1980**.
- ⁷⁷ F. Giessibl, *Rev. Modern Phys.* **2003**, 75, 949.
- ⁷⁸ H.U. Gremlich, *IR-Spektroskopie*, Wiley-VCH, Weinheim, Germany, **2003**.
- ⁷⁹ H.U. Gremlich, *IR-Spektroskopie*, Wiley-VCH, Weinheim, Germany, **2003**.
- ⁸⁰ D.S. Kendall, *Infrared Spectroscopy of Coatings*, in Tracton, A. A. (Ed.), *Coatings Technology. Fundamentals, Testing, and Processing Techniques*, CRC Press, Boca Raton, FL, USA, **2007**.
- ⁸¹ H.J. Butt, K. Graf, M. Kappl, Chapter 7 „Contact Angle Phenomena and Wetting“, *Physics and Chemistry of Interfaces*, Wiley-VCH, Weinheim, Germany, **2006**.
- ⁸² D.K. Owens, R.C. Wendt, *J. Appl. Polym. Sci.* **1969**, 13, 1741.
- ⁸³ Y.Q. Zhu, C.X. Yu, Y. Li, Q.Q. Zhu, L. Zhou, C. Cao, T.T. Yu, F.P. Du, *Pest Manag. Sci.* **2014**, 70, 462.
- ⁸⁴ R.N. Wenzel, *Ind. Eng. Chem.* **1936**, 28, 988.
- ⁸⁵ A.B.D. Cassie, S. Baxter, *Trans. Faraday Soc.* **1944**, 40, 546.
- ⁸⁶ A.B.D. Cassie, *Discus. Faraday Soc.* **1948**, 3, 11.
- ⁸⁷ T. Onda, S. Shibuichi, N. Satoh, K. Tsujii, *Langmuir* **1996**, 12, 2125.
- ⁸⁸ G. Li, H.-J. Butt, K. Graf, *Langmuir* **2006**, 22, 11395.
- ⁸⁹ K.L. Mittal, (Ed.) *Contact Angle, Wettability and Adhesion*, VSP: Leiden, The Netherlands, **2006**.
- ⁹⁰ D. Kessler, C. Teutsch, P. Theato, *Macromol. Chem. Phys.* **2008**, 209, 1437.
- ⁹¹ D. Kessler, M.C. Lechmann, S. Noh, R. Berger, C. Lee, J.S. Gutmann, P. Theato, *Macromol. Rapid Commun.* **2009**, 30, 1238.
- ⁹² K.T. Wiss, D. Kessler, T.J. Wendorff, P. Theato, *Macromol. Chem. Phys.* **2009**, 210, 1201.
- ⁹³ D. Kessler, H. Löwe, P. Theato, *Macromol. Chem. Phys.* **2009**, 210, 807.
- ⁹⁴ D. Kessler, P. Théato, *Macromolecules* **2008**, 41, 5237.
- ⁹⁵ D. Kessler, P. Théato, *Chemistry and Physics* **2009**, 210, 807.
- ⁹⁶ D. Kessler, P. Théato, *Langmuir* **2009**, 25, 14200.

- ⁹⁷ N. Wagner, L. Schneider, M. Michelswirth, K. Küpper, P. Théato, *Macromol. Chem. Phys.* **2015**, *7*, 783.
- ⁹⁸ N. Wagner, P. Zimmermann, P. Heisig, F. Klitsche, W. Maison, P. Théato, *Macromol. Biosci.* **2015**, *15*, 1673.
- ⁹⁹ N. Wagner, D. Kessler, P. Théato, *Macromol. Chem. Phys.* **2015**, *217*, 92.
- ¹⁰⁰ N. A. Plate, T. L. Lebedeva, L. I. Valuev, *Polym. J.* **1999**, *31*, 21.
- ¹⁰¹ I. Idziak, D. Avoce, D. Lessard, D. Gravel, X. X. Zhu, *Macromolecules* **1999**, *32*, 1260.
- ¹⁰² G. Li, H.-J. Butt, K. Graf, *Langmuir* **2006**, *22*, 11395.
- ¹⁰³ A. Strecker. *Ann. Chem. Pharm.* **1850**, *75*, 27.
- ¹⁰⁴ F. Moldenhauer, P. Théato *Adv. Polym. Sci.* **2015**, *269*, 133.
- ¹⁰⁵ K.A. Günay, P. Théato, H.A. Klok *Functional polymers by post-polymerization modification*, Wiley-VCH, New York, **2012**.
- ¹⁰⁶ R. Kakuchi, *Angew. Chem.* **2014**, *126*, 48.
- ¹⁰⁷ R. Kakuchi, *Angew. Chem. Int. Ed.* **2014**, *53*, 46.
- ¹⁰⁸ R. Kakuchi, P. Théato *Polym. Chem.* **2014**, *5*, 2320.
- ¹⁰⁹ F. Khalil, E. Franzmann, J. Ramcke, O. Dakischew, K.S. Lips, A. Reinhardt, P. Heisig, W. Maison, *Colloids Surf. B*, **2014**, *117*, 185.

Appendix

Copyright WILEY-VCH Verlag GmbH & Co. KGaA, 69469 Weinheim, Germany, 2015.



Supporting Information

for *Macromol. Chem. Phys.*, DOI: 10.1002/macp.201500324

Reactive Coatings in Glass Capillaries: Preparation of
Temperature- and Light-Responsive Surfaces and Accurate
Determination of Wettability Switching

Natalie Wagner, Daniel Kessler, Patrick Theato*

Reactive Coatings in Glass Capillaries: Preparation of Temperature- and Light-Responsive Surfaces and Accurate Determination of Wettability Switching

Natalie Wagner¹, Daniel Kessler², Patrick Theato^{1*}

Supporting information

Table S1. Equilibrium contact angles obtained by the sessile drop method and the capillary rise method on different temperature-responsive surface coatings.

entry	coating with	conversion with	T [°C]	sessile drop method			capillary rise method		
				Θ_a [°]	Θ_r [°]	Θ_{equi} [°]	x [mm]	Θ_{equi} [°] ¹	error range [°]
#1	PMSSQ-PNIPAM		15	78	66	72	15	78.8	79.5-77.9
			60	103	90	97	-7	94.8	95.6-94.2
#2	PMSSQ-PPFPA	IPA	15	77	67	72	20	73.7	75.5 – 74.2
			60	100	92	96	-5	93.4	94.0 – 92.8
#3	PMSSQ-PPFPA	MEA	15	82	77	79	19	75.3	76.4 – 74.9
			60	110	101	105	-9	96.3	97.0 – 95.6
#4	PMSSQ-PPFPA	CPA	15	75	69	72	21	74.2	74.9 – 73.4
			60	105	98	102	-8	95.6	96.3 – 94.9
#5	PMSSQ-PPFPA	DEA	15	89	75	72	8	84.0	84.8 – 83.3
			60	117	102	109	-10	97.0	97.9 – 96.3
#6	PMSSQ-PPFPA	no conversion	15	96	82	89	-3	92.4	92.8– 91.4
			60	98	84	91	-3	92.4	92.8 – 91.4
#7	P2 ²		15	77	65	71	15	78.8	79.5-77.9
			60	99	85	92	-5	93.4	94.0-92.8

¹ Θ_{equi} in the sessile drop method was calculated using equation 3; x: meniscus height; the error range was calculated from $x \pm 1$ mm.

² measured before UV irradiation

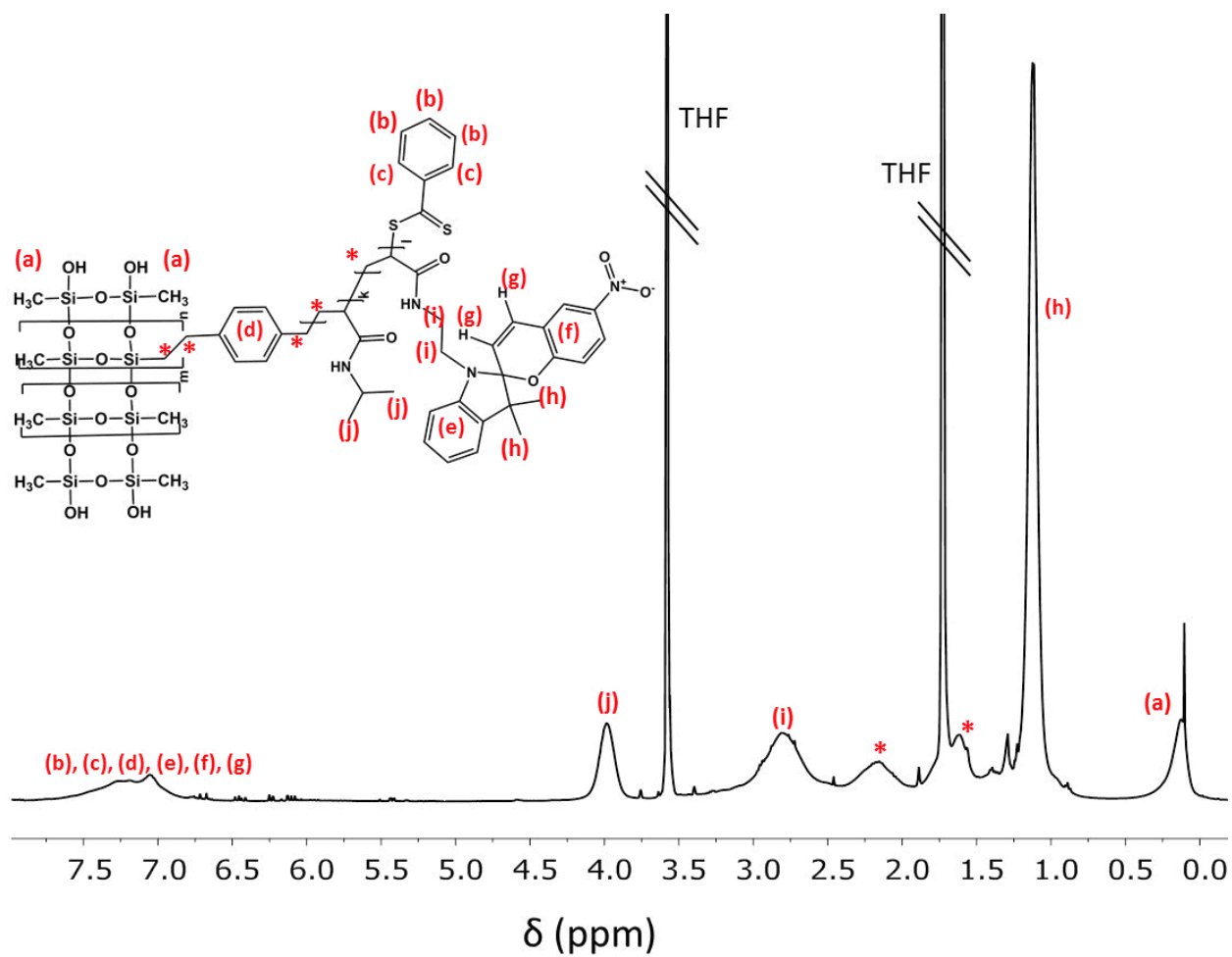


Figure S1. ^1H NMR spectra of purified PMSSQ-PNIPAM-PSpAM (P2).

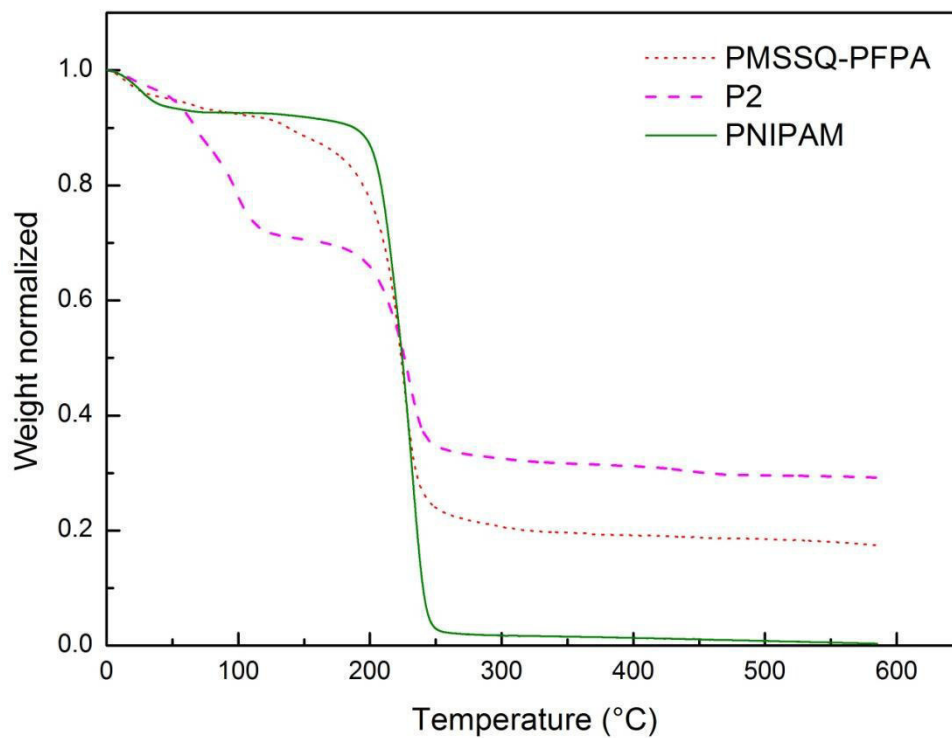


Figure S2. TGA

Figure S2. Thermogravimetric analysis of PNIPAM, PMSSQ-PFPA and P2.

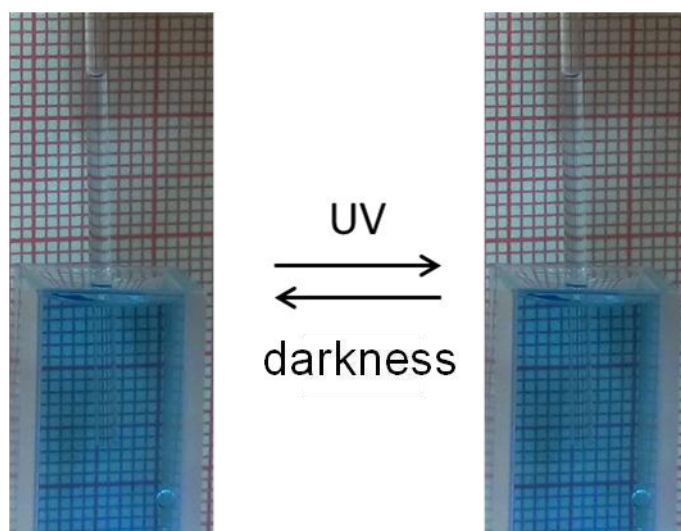


Figure S3. Meniscus heights in glass capillaries coated with P2 before and after UV light irradiation at 15°C.

Installation of Zwitterionic α

-Amino Phosphonic Acid Moieties on Surfaces via a Kabachnik-Fields Post-Polymerization Modification

Natalie Wagner¹, Lilli Schneider², Martin Michelswirt³,

Karsten Küpper² and Patrick Theato^{1}*

Supporting information

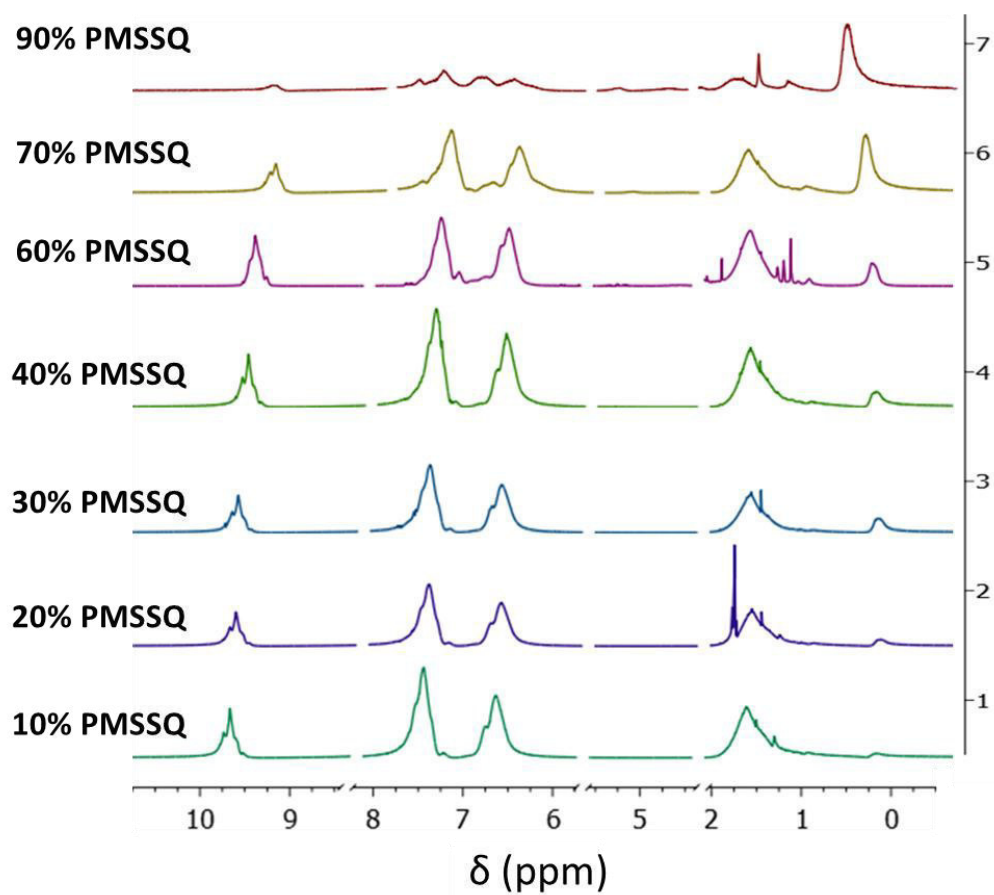


Figure S1. ^1H -NMR spectra of synthesized PMSSQ-PSStCHO with different ratios of inorganic and organic moieties.

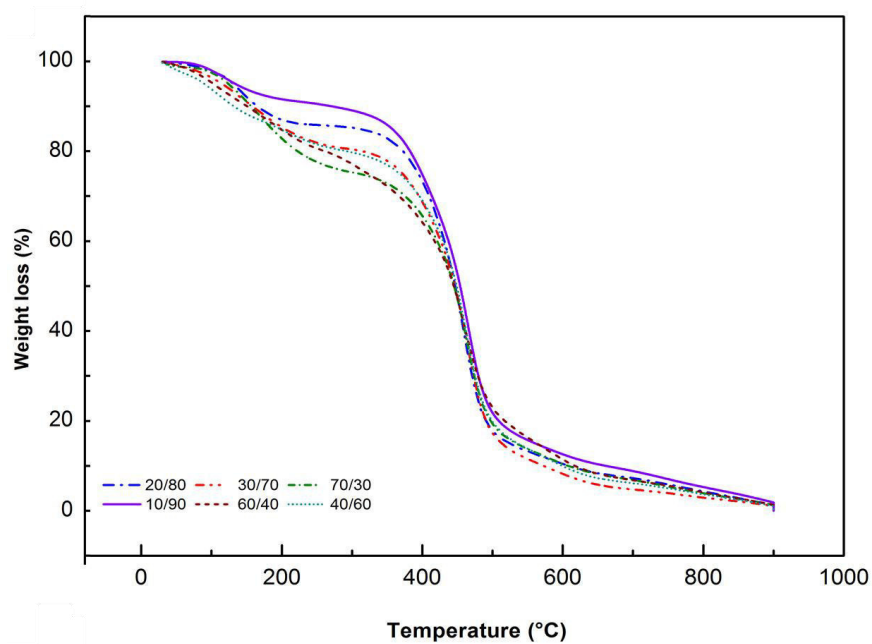


Figure S2. Thermogravimetric analyses of PMSSQ-PSiCHO with expected weight ratio Inorganic/Organic: 70/30, 60/40, 40/60, 30/70, 20/80, 10/90.

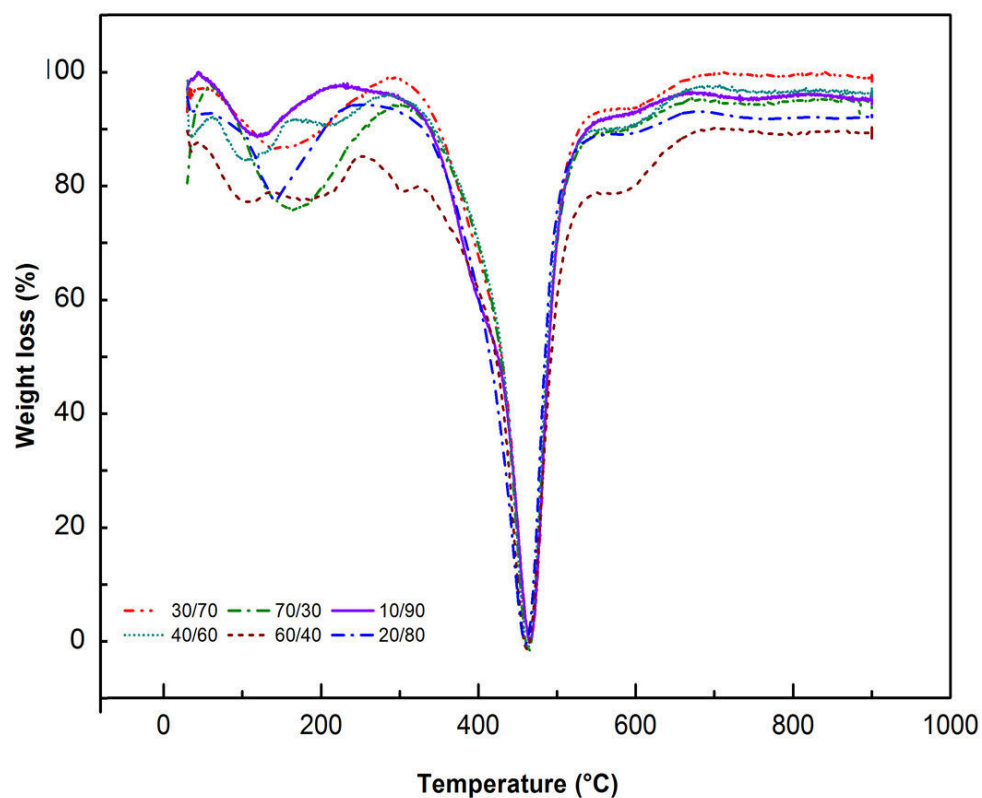


Figure S3. The corresponding 1st derivative of the thermogravimetric curves of PMSSQ-PSiCHO with expected weight ratio Inorganic/Organic: 70/30, 60/40, 40/60, 30/70, 20/80, 10/90.

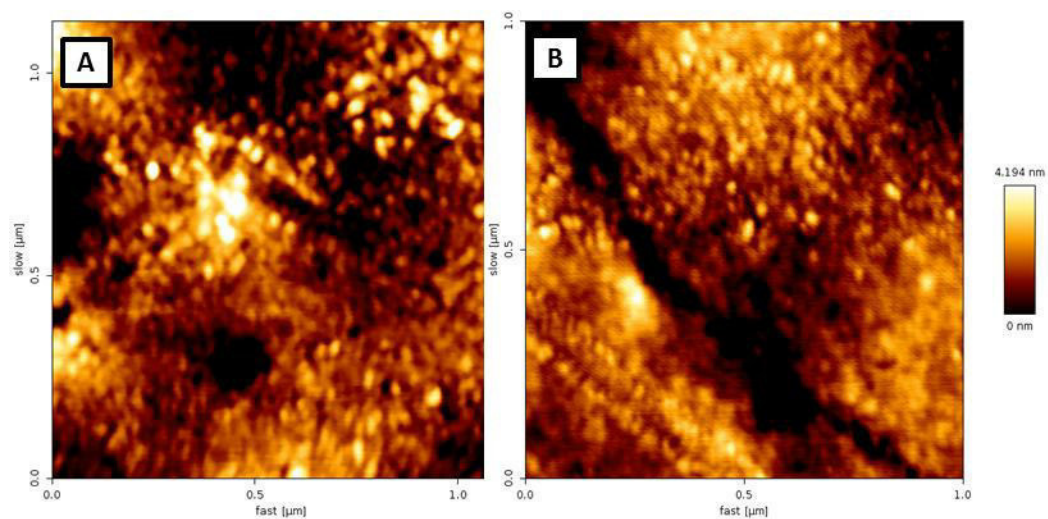


Figure S4. AFM height image of Si-surfaces before (A) and after functionalization by Kabachnik-Fields reaction R1 (B).

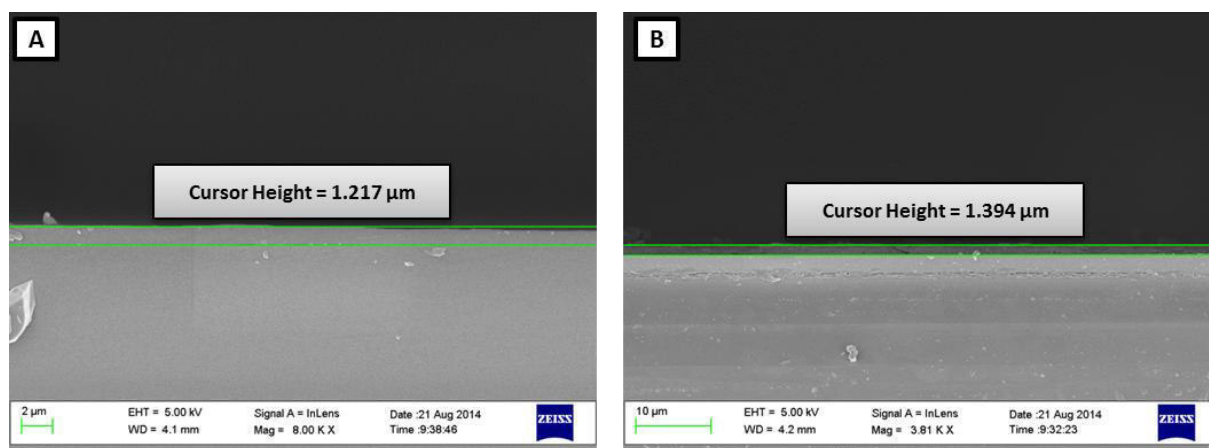


Figure S5. SEM image of Si-surfaces before (A) and after functionalization by Kabachnik-Fields reaction R1 (B).

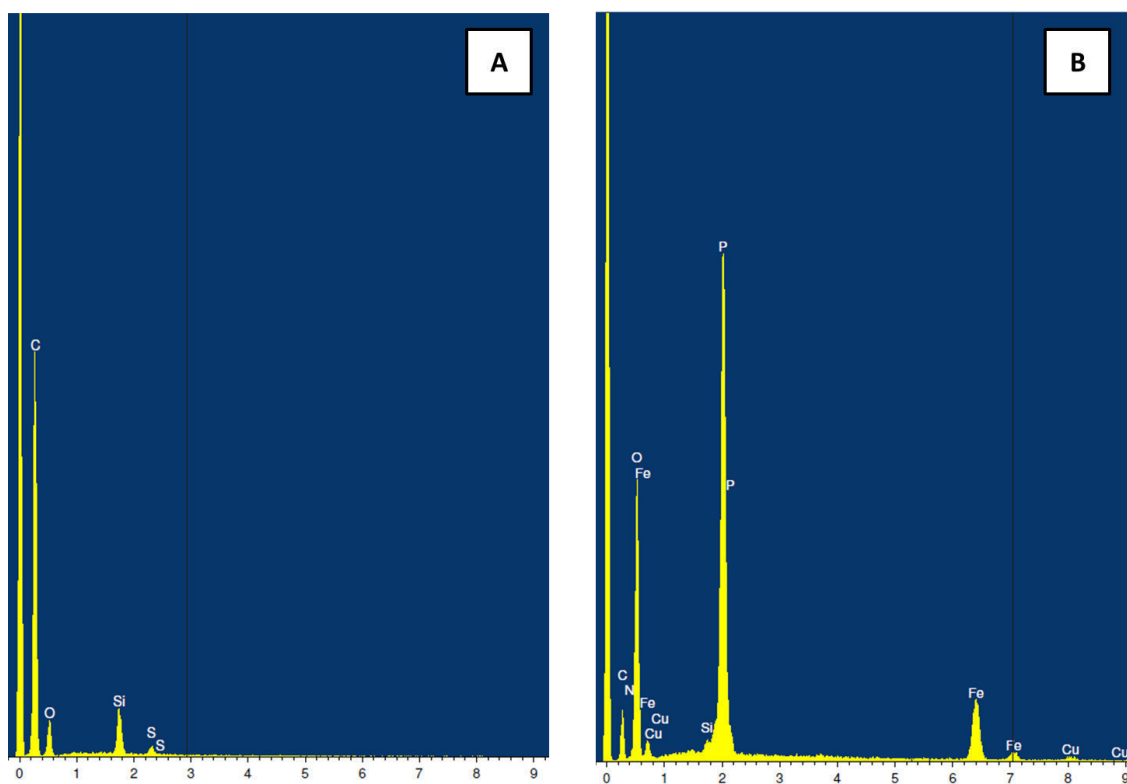


Figure S6. EDX measurements on Cu-surfaces before (A) and after functionalization by Kabachnik-Fields reaction R1 (B).

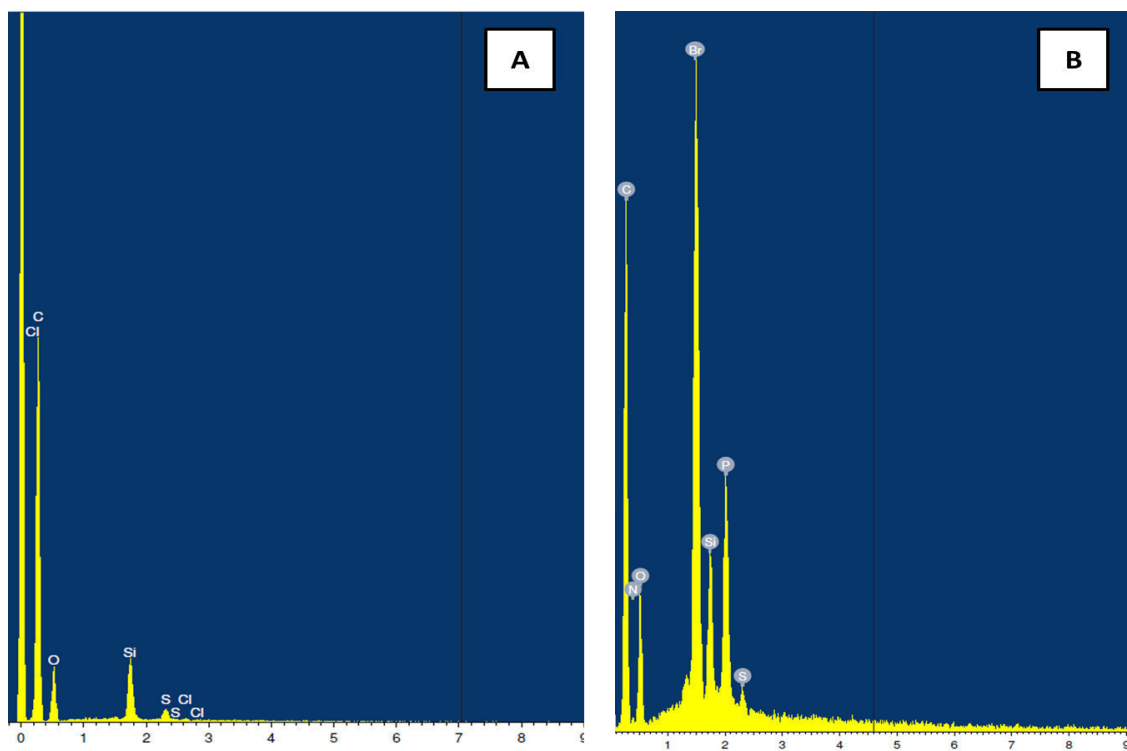


Figure S7. EDX measurements on Al-surfaces before (A) and after functionalization by Kabachnik-Fields reaction R6 (B).

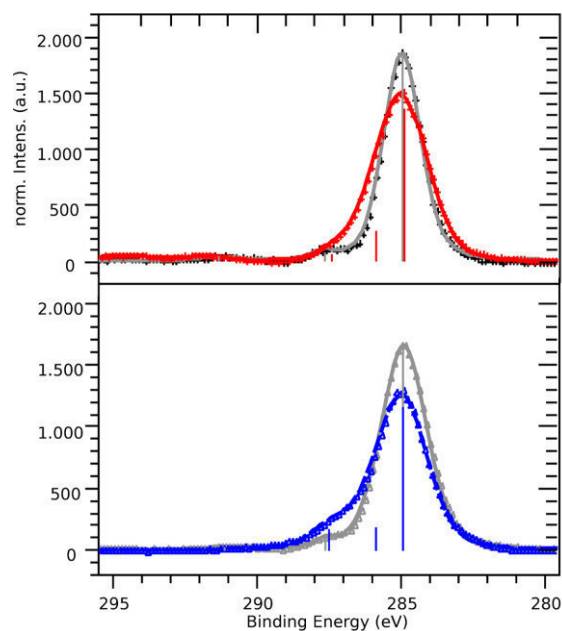


Figure S8. C_{1s} spectra of P1 modified substrates with R13 (red curve) and R17 (blue curve) in comparison to the non-functionalized by sur-KFR substrates (gray curves) respectively. Localization and amplitudes of the spectroscopic species features of the spectra were revealed by fit. They are given to the diagrams by use of vertical lines.

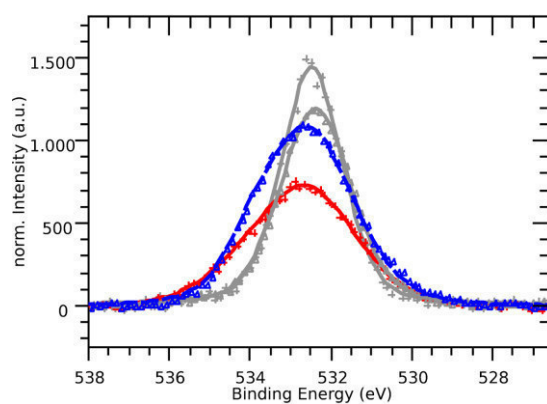


Figure S9. Si_{2p} spectra of P1 modified substrates with R13 (red curve) and R17 (blue curve). Localization and amplitudes of the spectroscopic species features of the spectra were revealed by fit. They are given to the diagrams by use of vertical lines.

Synthesis of diisopropyl [(4-methyphenyl) amino-phenyl-methyl]phosphonate (AP-ⁱPr)

Under Ar atmosphere at 80 °C, diisopropyl phosphonate (4.70 mL, 28.2 mmol) was added to a dry 1,4-dioxane solution (10 mL) of benzaldehyde (2.20 g, 20.5 mmol), and *p*-toluidine (2.0 g, 18.7 mmol). After the reaction mixture was stirred for 20 hours at 80 °C, the reaction mixture was directly purified by column chromatography (silica gel, eluent; ethyl acetate/petro ether = 1/2) to give diisopropyl [(4-methyphenyl)amino-phenyl-methyl]phosphonate (**AP-ⁱPr**) as a white solid.

Yield, 5.98 g (16.5 mmol, 88.5 %). ¹H NMR (300 MHz, CDCl₃) δ; 7.60 – 7.13 (m, 5H), 6.91 (d, *J* = 7.7 Hz, 2H), 6.53 (d, *J* = 8.4 Hz, 2H), 4.83 – 4.59 (m, 2H), 4.48 (dp, *J* = 7.0, 6.1 Hz, 1H), 2.19 (s, 3H), 1.43 – 1.13 (m, 9H), 0.95 (dd, *J* = 6.3, 0.7 Hz, 3H). ¹³C NMR (75 MHz, CDCl₃) δ; 144.33, 144.13, 136.40, 129.63, 128.40, 128.36, 128.05, 127.97, 127.67, 127.63, 127.39, 113.92, 71.98, 71.93, 71.89, 71.83, 57.78, 55.77, 24.26, 23.82, 23.75, 23.28, 23.20, 20.36. ³¹P NMR (162 MHz, CDCl₃) δ; 20.49. Anal. Calcd for C₂₀H₂₈NO₃P (361.41): C, 66.46; H, 7.81; N, 3.88. Found: C, 66.46; H, 7.87; N, 3.74. ESI-MS; Calcd for C₂₀H₂₈NO₃P, [M+Na⁺]; 384.17; Found for [M+H⁺]; 384.1703.

Synthesis of [(4-methyphenyl) amino-phenyl-methyl]phosphonic acid (AP-OH)

Under Ar atmosphere at room temperature, trimethylsilyl bromide (2.20 mL, 16.8 mmol) was added to a dry 1,4-dioxane solution (10 mL) of **AP-ⁱPr** (1.0 g, 2.8 mmol). After the reaction mixture was stirred for 6 hours at 60 °C, 10 mL of methanol was added to the reaction mixture under open condition. After stirring for another 30 minutes, the reaction mixture was evaporated under vacuum condition to give [(4-methyphenyl)amino-phenyl-methyl]phosphonate (**AP-OH**) as a pale yellow solid.

Yield, 690 mg (2.5 mmol, 88.9 %). ¹H NMR (300 MHz, CD₃OD) δ; 7.63 – 7.12 (m, 9H), 4.96 (d, *J* = 17.2 Hz, 1H), 2.31 (s, 3H). ¹³C NMR (75 MHz, CD₃OD) δ; 141.12, 133.43, 133.32, 131.35, 131.18, 131.10, 130.77, 130.01, 124.61, 68.10, 65.45 (d, *J* = 147.1 Hz), 20.98. ³¹P

NMR (162 MHz, CD₃CN) δ ; 9.25. ESI-MS; Calcd for C₁₄H₁₆NO₃P, [M-(P(O)(OH)₂+H⁺]; 196.11; Found for [M-(P(O)(OH)₂+H⁺]; 196.1125.

In order to guarantee the successful deprotection processes, the Kabachnik-Fields reaction and subsequent deprotection with low molecular weight model compounds were monitored by using ¹H and ³¹P NMR and ATR-mode IR measurements. In this context, diisopropyl [(4-methyphenyl)amino-phenyl-methyl]phosphonate (**AP-ⁱPr**) was prepared and deprotected in the presence of excess amount of TMSBr in 1,4-dioxane to afford the corresponding α -amino phosphonic acid, namely [(4-methyphenyl)amino-phenyl-methyl]phosphonic acid (**AP-OH**). The isopropyl protons of **AP-ⁱPr** were observed in the region ranging from 0.9 to 1.4 ppm in the ¹H NMR spectrum of **AP-ⁱPr**, whereas the peaks owing to the isopropyl protons completely disappeared for **AP-OH**. The ATR-mode IR measurements of the model compounds before and after the deprotection reaction revealed that strong absorption at 1370 cm⁻¹ clearly disappeared (Figure S10). Furthermore, in the ³¹P NMR spectra of **AP-ⁱPr** and **AP-OH**, an obvious peak at 20.5 ppm owing to phosphonates of **AP-ⁱPr** clearly shifted to a peak at 9.3 ppm owing to phosphonic acid of **AP-OH**, giving a reasonable agreement with the spectral changes in the case of polymeric α -amino phosphonates. Therefore, we fully confirmed a facile conversion of polymeric α -amino phosphonates into polymeric α -amino phosphonic acids by simple treatment with TMSBr.

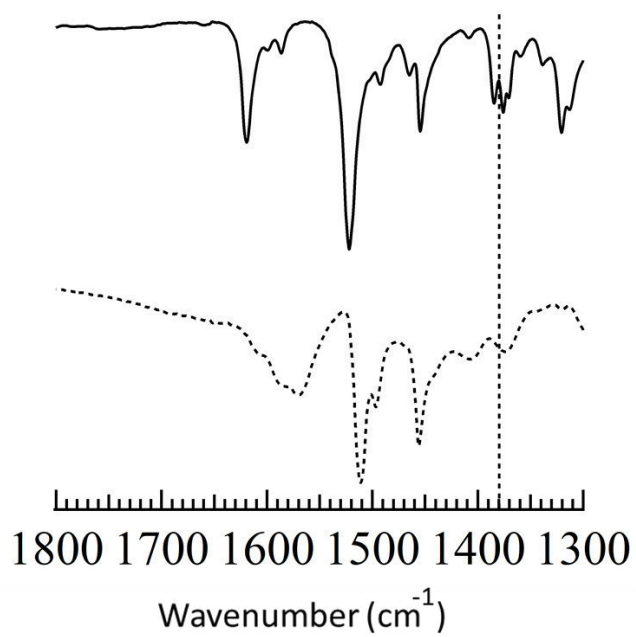


Figure S10. ATR-mode IR spectra of AP-ⁱPr before (solid line) and after (dashed line) deprotection reaction on AP-ⁱPr with TMSBr.

Investigation of Antifouling Properties of Surfaces Featuring Zwitterionic α -

Aminophosphonic Acid Moieties

*Natalie Wagner¹, Phyllis Zimmermann², Peter Heisig², Franziska Klitsche³, Wolfgang
Maison³ and Patrick Theato^{1*}*

Supporting information

Synthesis of PMSSQ Macro-CTA. A preparation of inorganic macro-RAFT CTA was conducted by slightly modifying a previously reported method³³ and the typical procedure was as follows: A dry THF solution (15 mL) containing dithio benzoic acid 4-ethyltrimethoxy-silylester (0.98 g, 2.5 mmol) was placed in a round bottomed flask. The reaction mixture was cooled to 0 °C and methyltrimethoxysilane (MTMS, 3.47 g, 25 mmol) and 500 mmol water and 10 mmol HCl were added and stirred for 3 hours at 0 °C. Afterwards, the reaction mixture was dissolved in diethyl ether, washed with water. After drying organic phase over MgSO₄, ether was removed and the product was dried in high vacuum. Yield 3.32 g (1.46 mmol, 58%). ¹H-NMR (CDCl₃) δ: 7.99 (br, 1H); 7.36 (br, 8H); 5.80 (br, 8H); 4.55 (br, 2H); 3.48 (br, 2H); 2.71 (br, 2H); 0.99 (br, 2H); 0.17 (br, 69.1H). M_n = 2279 g/mol, PDI = 1.6

Synthesis of PMSSQ-PStCHO: A DMSO solution (4 mL) of PMSSQ macro RAFT agent (0.5 g, 219.4 μmol), AIBN (10 mg, 60.89 μmol), and 4-vinylbenzaldehyde (1.0 g, 7.56 μmol) was placed in a Schlenk flask and degassed by freeze-thaw cycles. The degassed reaction mixture was stirred at 80 °C for 4 hours and afterwards precipitated into methanol to afford a pale colored powder. Yield 0.91 g (0.042 mmol, 82%). ¹H-NMR (300 MHz, DMSO-d₆) δ: 9.92 (br); 8.13-7.93 (br, 2H); 7.39-7.82 (br, 2H); 7.30-6.90 (br); 6.37-6.80 (br); 5.18-5.42 (br, 1H); 0.7-1.85 (br); 0.10 (br, H). M_n=21400 g/mol, PDI=1.63

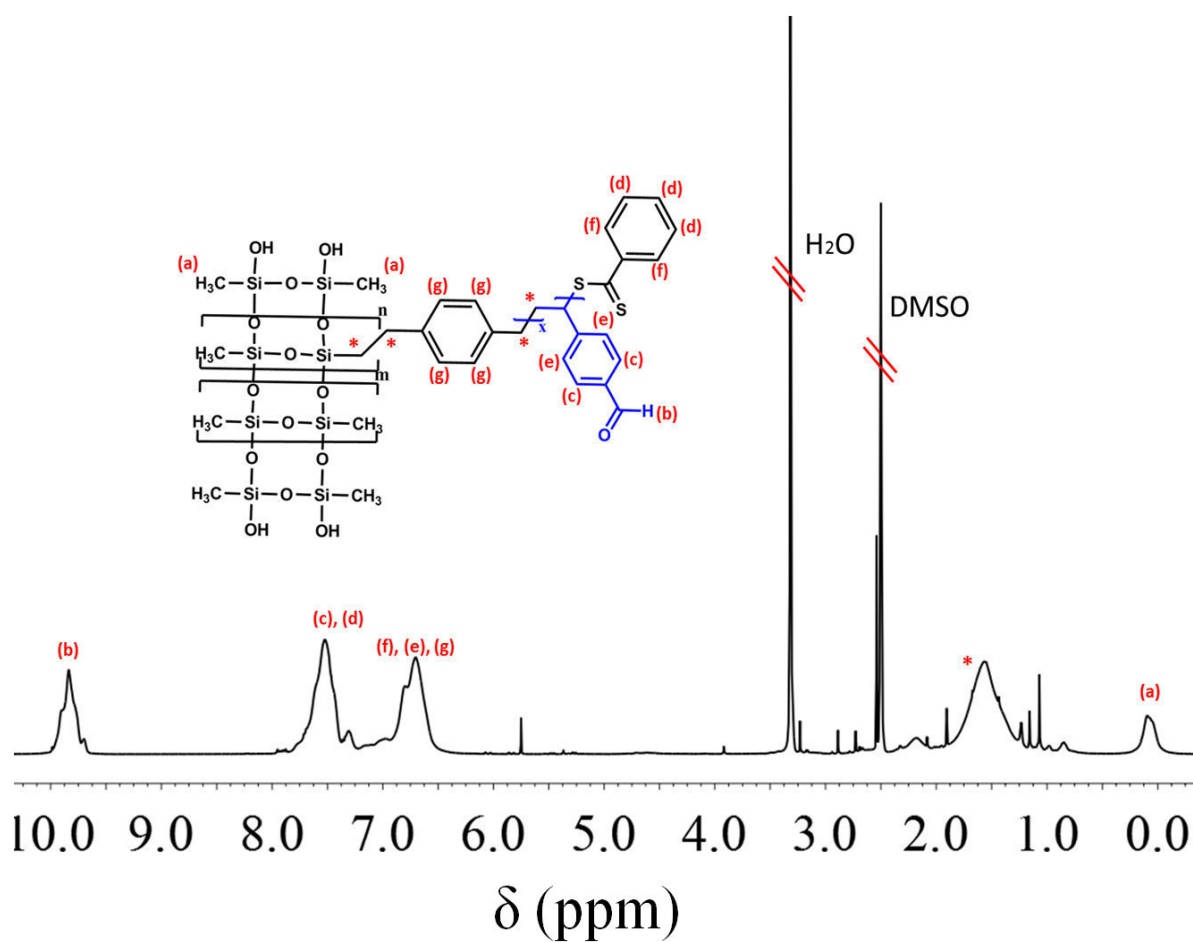


Figure S1. ^1H NMR spectra of purified PMSSQ-PStCHO.

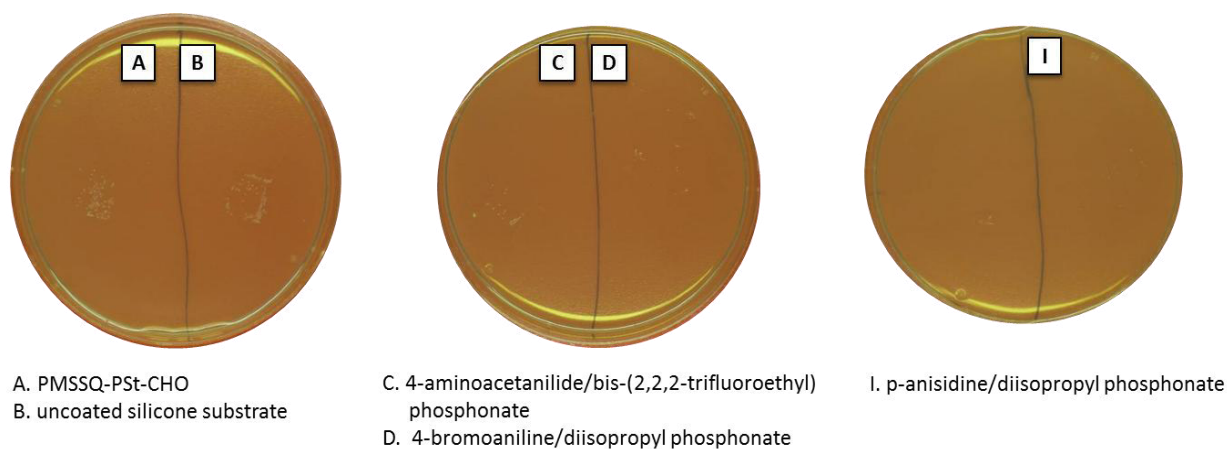


Figure S2. Antifouling assay on silicone substrates. Uncoated silicon substrate (B), PMSSQ-PStCHO modified surfaces (A). Surfaces functionalized by *sur*-KFR with 4-

aminoacetanilide/bis-(2,2,2-trifluoroethyl) phosphonate (C), 4-bromoaniline/diisopropyl phosphonate (D), p-anisidine/diisopropyl phosphonate (E) after deprotection reaction with TMSBr.

Table 1. Growth of Staphylococcus epidermidis DSM20044 / ATCC 14990.

t	Time [min]	OD 550	CFU/mL	logCFU
0	0		200000	5,30
1	48	0,0015	220000	5,34
2	80	0,0015	580000	5,76
3	115	0,0168	620000	5,79
4	184	0,0038	1040000	6,02
5	260	0,0175	1560000	6,19
6	289	0,0284	2580000	6,41
7	320	0,0597	3400000	6,72
8	351	0,0137	4000000	6,60
9	378	0,2095	20000000	7,30
10	414	0,3595	50000000	7,70
11	446	0,4842	104000000	8,01
12	471	0,5445	140000000	8,15
13	505	0,6352	180000000	8,26
14	535	0,7212	246000000	8,39
15	560	0,7913	288000000	8,46
16	595	0,9099	400000000	8,60

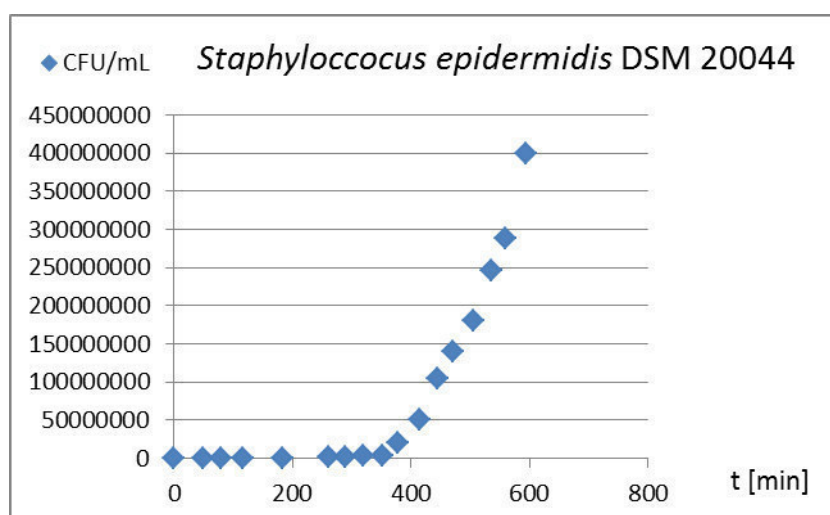
































































Figure S3. Viable cell count (CFU/ml) of S. epidermidis plotted against time.








Chemicals

Chemicals CAS number	Hazard symbol	H-phrases	P-phrases
Acetone (67-64-1)	  GHS02, GHS07	H225-H319-H336	P210-P261- P305+P351+P338
Acetonitrile (75-05-8)	  GHS02, GHS07	H225-H302+H312 + H332-H319	P210-P280- P305+P351+P338
Azobisisobutyronitrile (78-67-1)	  GHS02, GHS07	H242-H332-H302-H412	P210-P240-P403+P235
<i>p</i> -Anisidine (67-66-3)	   GHS08, GHS09, GHS06	H301-H310-H330- H350-H373-H400	P201-P260-P273— P280-P284-P301+P310
Benzene (71-43-2)	   GHS02, GHS08, GHS07	H225-H350-H340- H372-304-319-315	P201-P210-P308+P313- P301+P310-P331- P305+P351+P338- P302+P352
Chloroform (67-66-3)	  GHS08, GHS07	H225-H302+H332- H315-H319-H335	P210-P261- P305+P351+P338
Cyclopropylamine (765-30-0)	   GHS02, GHS05, GHS07	H225-H302-H314	P210-P280- P305+P351+P338-P310
Dichlormethane (75-09-2)	  GHS07, GHS08	H315-H319-H335- H336-H351-H373	P261-P281- P305+P351+P338
Diethylether (60-29-7)	  GHS02, GHS07	H224-H302-H336	P210-P261
Dimethyl sulfoxid (67-68-5)	This substance is not classified as hazardous according to directive 67/548/EWG		
Dioxane (123-91-1)	   GHS02, GHS08, GHS07	H225-H319-H335-H351	P210-P261-P281- P305+P351+P338
Ethanol (64-17-5)	 GHS02	H225	P210
Ethyl acetate (141-78-6)	  GHS02, GHS07	H225-H319-H336	P210-P261- P305+P3+P338
2-Ethyl-1-Hexylamine (104-75-6)	   GHS02, GHS05, GHS06	H226-H302- H311+H331-H314	P261-P280- P305+P351+P338-P310
Hexane (110-54-3)	    GHS02, GHS08, GHS07,	H225-H304-H315- H336-H361f-H373-	P210-P261-P273-P281- P301+P310-P331

Chemicals

	GHS09	H411	
Isopropanol (67-63-0)	  GHS02, GHS07	H225-H319-H336	P210-P261- P305+P351+P338
Isopropylamine (75-31-0)	   GHS02, GHS05, GHS06	H224- H301+H311+H331- H314-H335	P210-P261-P280- P301+P310- P305+P351+P338-P310
Carbon disulfide (75-15-0)	   GHS02, GHS07, GHS08	H225-H361fd-H372- H319-H315	P210-P281-P305 +P351+P338-P314
Magnesium sulfate (7487-88-9)	This substance is not classified as hazardous according to directive 67/548/EWG		
Methanol (67-56-1)	   GHS02, GHS06 GHS08	H225- H301+H311+H331- H370	P210-P260-P280- P301+P310-P311
<i>N,N</i> -Dimethylformamide (68- 12-2)	   GHS02, GHS07, GHS08	H226-H312+H332- H319-H360D	P201-P280- P305+P351+P338- P30+P313
<i>N,N'</i> -Dicyclohexylcarbodiimide (538-75-0)	  GHS05, GHS06	H302-H311-H317-H318	P280-P305+P351+P338- P312
<i>N,N</i> -Dimethylethylenediamine (108-00-9)	   GHS02, GHS05, GHS07	H225-H302-H312-H314	P210-P280- P305+P351+P338-P310
Sodium bicarbonate (144-55-8)	This substance is not classified as hazardous according to directive 67/548/EWG		
Sodium hydroxide (1310-73-2)	 GHS05	H290-H314	P280-P305+P351+P338- P310
Sodium sulfate (7757-82-6)	This substance is not classified as hazardous according to directive 67/548/EWG		
Pentafluorophenol (771-61-9)	  GHS05, GHS06	H301-H311-H314-H318	P260-P301+P310- P303+P361+P353- P305+P351+P338-P361- P405
Pentafluorophenyl acrylate (71195-85-2)	 GHS07	H315-H319-H335	P261-P305+351+338
Hydrochloric acid (7647-01-0)	  GHS05, GHS07	H290-H314-H335	P261-P280- P305+P351+P338-P310
Tetrahydrofuran (109-99-9)	   GHS02, GHS07, GHS08	H225-H260-H351- H319-H335	P210-P231+P232- P303+P361+P353-

Chemicals

			P305+P351+P338-P405-P501A
Triethylamine (121-44-8)	   GHS02, GHS05, GHS06	H225-H302-H312-H314-H332	P210-P280-P305+P351+P338-P310
Trifluoroacetic acid (76-05-1)	  GHS05, GHS07	H314-H332-H412	P273-P280-P305+P351+P338-P310
Trimethylsilyl bromide (2857-97-8)	  GHS02, GHS05	H226-H314	P280-P305+P351+P338-P310

Acknowledgements

I would like to thank everyone who helped and assisted me during my PH.D. studies.

In particular I would like to thank my advisor Prof. Patrick Theato for giving me an interesting topic, valuable comments and suggestions.

Moreover, I wish to express my gratitude to Prof. Hans-Ulrich Moritz for his financial support and helpful advice.

I would also like to thank all my collaborators who directly contributed to the success of the presented thesis:

Phyllis Zimmermann (University of Hamburg)

Franziska Klitsche (University of Hamburg)

Lilli Schneider (University of Osnabrück)

Martin Michelswirth (University of Hamburg)

In addition, I would like to thank all the academic and non-academic staff of the Institute for Technical and Macromolecular Chemistry for their kindness and availability: thank you Mrs. Khenkhar; thank you Mrs. Zhu; thank you Mrs. Pruntsch; thank you Mrs Kloodt.

My sincere thanks also go to the NMR team, to the Institute of Physical Chemistry and to all the technicians who helped me do my analyses and measurements: Dr. Hauke Heller, Dr. Haupt and his team, Michael Gröger, Stefan Bleck, Katrin Rehmke, Petra Borbe and Renate Walter of the Institute of Geology.

I am also grateful to Dr. Ryohei Kakuchi for the support and valuable scientific discussion during the preparation of my paper "**Installation of Zwitterionic α -Amino Phosphoric Acid Moieties on Surfaces via a Kabachnik-Fields Post-Polymerization Modification**", N. Wagner, L. Schneider, M. Michelswirth, K. Küpper, P. Théato, *Macromolecular Chemistry and Physics* **216**, 783-793 (2015).

Furthermore, I would like to thank the bachelor students Sven Petersen, Magdalena Bozek and the RISE student Daniel Brauer for their fruitful collaboration.

Finally, I wish to thank all colleagues of the AK Théato: Denis, Fenja, Sven, Julia, Hanju, Tim, Ilona, Heba, Michael, Alexander, Shaojian, Jiaojiao, Anindita.

Acknowledgements

And last but not least, I wish to thank my family, and especially my husband Viktor, for the immense support they have given me during my study period and during my scientific work.

Declaration about previous Ph.D. attempts

I herewith declare that I, Natalie Wagner, have not made any previous attempts to write a doctoral thesis, neither with the present nor with any other doctoral thesis. Merely an application to open a doctoral examination procedure had been submitted.

Natalie Wagner

Hamburg, the 03.03.2016

Affidavit

I herewith declare that I have written the present doctoral thesis on my own and that I have not used other than the acknowledge resources and aids. This doctoral thesis has never been submitted to any examination authority, neither in the similar form.

Natalie Wagner

Hamburg, the 03.03.2016